

Catalytic oxidation of lignin model compounds

by
Emile Darron Maggott

*Thesis presented in fulfilment of the requirements for the degree
of Masters of Science in the Faculty of Chemistry and Polymer
Science at Stellenbosch University*



Supervisor: Prof Selwyn Frank Mapolie

April 2019

Declaration

By submitting this thesis electronically, I declare that the entirety of the work contained therein is my own, original work, that I am the sole author thereof (save to the extent explicitly otherwise stated), that reproduction and publication thereof by Stellenbosch University will not infringe any third party rights and that I have not previously in its entirety or in part submitted it for obtaining any qualification.

.....

Emile Darron Maggott

January 2019

Copyright © 2019 Stellenbosch University

All rights reserved

Abstract

This thesis pertains to the synthesis of a range of model and siloxane functionalized complexes containing salicylaldehyde ligands. The functionalized complexes were immobilized onto two types of mesoporous silica viz. MCM-41 and SBA-15 which were employed in the oxidation of veratryl alcohol.

Both model (**L1**) and functionalized (**L2**) were fully characterized by a range of analytical techniques such as FT-IR (ATR) and ¹H NMR spectroscopy. The model and siloxane functionalized salicylaldehyde ligands were complexed to metal precursors based on copper, cobalt and palladium salts in a bis-bidentate fashion. Full characterization of the model (**MC1-MC3**) and functionalized (**FC1-FC3**) complexes was achieved by mass spectrometry, FT-IR (ATR) spectroscopy, ¹H NMR spectroscopy (**MC3** and **FC3**), UV-Vis spectroscopy, EPR spectroscopy (**MC1**, **MC2**, **FC1** and **FC2**), single crystal X-ray diffraction (**MC3**), elemental analysis and melting point determinations.

The native silica supports, MCM-41 and SBA-15 and the functionalized complexes were reacted with each other to afford the immobilized complexes (**IC1-IC6**). The immobilization process involves a condensation reaction between the surface silanol groups of the support and the siloxane functionality of the complexes. These complexes are covalently bound to their respective supports, which ultimately led to “heterogenized” catalysts. The immobilized complexes (**IC1-IC6**) were fully characterized by a range of solid-state analytical techniques which include FT-IR (ATR) spectroscopy, low angle powder X-ray diffraction, thermal gravimetric analysis (TGA), solid state ²⁹Si NMR spectroscopy, nitrogen adsorption/desorption (BET) surface analysis, scanning and transmission electron microscopy (SEM and TEM). Inductive coupled plasma optical emission spectroscopy (ICP-OES) was used to quantitatively determine the metal loading of the immobilized complexes.

Both the model (**MC1-MC3**) and immobilized (**IC1-IC6**) complexes were evaluated in the oxidation of veratryl alcohol. A comparison of the effect of different oxidants on the activity was investigated using either molecular oxygen, hydrogen peroxide or tert-butyl hydroperoxide (TBHP). Model complex, **MC1**, exhibited better activity than the other model catalysts (**MC2** and **MC3**) in the oxidation of veratryl alcohol at 25 °C under 1 atm oxygen pressure. This catalyst managed to selectively produce veratrylaldehyde. Amongst the three oxidants,

Abstract

hydrogen peroxide exhibited the least activity when used in conjunction with **MC1**, which was used to optimize reaction conditions. Experiments with catalyst, **MC1**, were also conducted in the absence of oxygen, which resulted in only moderate activity of about 20% with 100% aldehyde formation. This most likely suggests that the reaction undergoes a β -hydride elimination reaction with subsequent generation of molecular hydrogen. The use of tert-butyl hydroperoxide as oxidant in the oxidation of veratryl alcohol, exhibited relatively high activity compared when molecular oxygen is used. The high activity can be attributed to the higher stability of TBHP as well as its solubility in the reaction mixture. This suggests that the active species forms faster with TBHP as oxidant. The best conversion was obtained for the cobalt catalyst, **MC2**, which was 85% followed by **MC1** and **MC3** respectively. The higher activity of TBHP resulted in higher veratrylaldehyde yield but unfortunately it also led to over-oxidation to veratric acid.

The immobilized catalysts, **IC1-IC6**, were also evaluated in the oxidation of veratryl alcohol using TBHP as oxidant. These catalysts generally exhibited moderate activity although the cobalt analogues (**IC3** and **IC4**) showed moderate conversion of up to 65%. Molecular oxygen when used as oxidant with the immobilized catalysts seemed to be ineffective in the oxidation of veratryl alcohol. All the immobilized catalysts except **IC5** were recycled and reused for up to five catalytic runs. **IC3** and **IC4** exhibited moderate activity over the five cycles with only a slight decrease in activity. The nature of the support had an effect on the activity as well as the selectivity. The immobilized catalysts based on MCM-41 supports, showed enhanced activity. The selectivity was slightly altered when using SBA-15 as a support.

Overall, the immobilized catalysts exhibited reasonable to moderate activity in the presence of TBHP while no activity is observed when using molecular oxygen as oxidant. However, the immobilized catalysts were outclassed by their model counterparts when employing both oxidants.

Opsomming

Hierdie proefskrif behels die sintese van 'n verskeidenheid model- en siloksaan gefunksionaliseerde komplekse wat salisielaldemien ligande bevat. Die gefunksionaliseerde komplekse is geïmmobiliseer op twee tipes mesoporeuse silika draers, naamlik, MCM-41 en SBA-15 wat daarna in die oksidasie van veratryl alkohol geëvalueer was.

Beide model (**L1**) en siloksaan gefunksionaliseerde (**L2**) ligande is ten volle gekarakteriseer deur middel van 'n reeks analitiese tegnieke soos FT-IR (ATR) en ¹H KMR spektroskopie gebruik te maak. Die model- en siloksaan gefunksionaliseerde salisielaldemien ligande was met metaalvoorlopers gebaseer op koper-, kobalt- en palladiumsoute in 'n bis-bidentate wyse gereageer. Volle karakterisering van die model (**MC1-MC3**) en gefunksionaliseerde (**FC1-FC3**) komplekse is bereik deur massa spektrometrie, FT-IR (ATR) spektroskopie, ¹H KMR spektroskopie (**MC3 en FC3**), UV-Sig spektroskopie, EPR spektroskopie (**MC1 , MC2, FC1 en FC2**), enkel kristal X-straal diffraksie (**MC3**), elementêre analise en smeltpunt bepaling.

Die onveranderde-silika draers, MCM-41 en SBA-15 en die gefunksionaliseerde komplekse is met mekaar gereageer om die geïmmobiliseerde komplekse (**IC1-IC6**) te vorm. Die immobiliserings proses behels 'n kondensasie reaksie tussen die oppervlaksilanol groepe van die draers en die siloksaanfunktionaliteit van die komplekse. Hierdie komplekse word op 'n kovalente manier aan hul onderskeie draers gebind, wat uiteindelik lei tot die vorming van "heterogeniseerde" katalisators. Die geïmmobiliseerde komplekse (**IC1-IC6**) is ten volle gekarakteriseer deur 'n verskeidenheid analitiese tegnieke in die vaste toestand wat FT-IR (ATR) spektroskopie, laë-hoek poeier X-straal diffraksie, termiese gravimetriese analise (TGA), vaste toestand ²⁹Si KMR spektroskopie, stikstof adsorpsie/ desorpsie (BET) oppervlakanalise, skandeer en transmissie-elektron mikroskopie (SEM en TEM) insluit. Induktiewe gekoppelde plasma optiese emissie spektroskopie (ICP-OES) was gebruik om die metaal inhoud van die geïmmobiliseerde komplekse te bepaal.

Beide die model (**MC1-MC3**) en geïmmobiliseerde (**IC1-IC6**) komplekse was geëvalueer in die oksidasie van veratryl alkohol. 'n Vergelyking van die effek van verskillende oksideermiddels op die aktiwiteit is ondersoek deur gebruik te maak van molekulêre suurstof, waterstofperoksied of *tert*-butielhidroperoksied as oksideermiddels. Model kompleks, **MC1**, het beter aktiwiteit getoon as die ander model katalisators (**MC2 en MC3**) in die oksidasie van

Opsomming

veratryl alkohol by 25 °C onder 1 atm atmosferiese druk. Hierdie katalisator het selektief veratryl aldehid geproduseer. Van die drie oksideermiddels, het waterstof peroksied die laagste aktiwiteit getoon wanneer dit gebruik word in samewerking met **MC1** gebruik was. Die laasgenoemde is gebruik om die reaksietoestande te optimaliseer. Eksperimente met katalisator, **MC1**, was ook in die afwesigheid van suurstof uitgevoer, wat slegs matige aktiwiteit van ongeveer 20% met 100% aldehid selektiwiteit getoon het. Dit stel waarskynlik voor dat die reaksie 'n β -hidried eliminasiereaksie ondergaan met daaropvolgende vorming van molekulêre waterstof. Die gebruik van *tert*-butielhidroperoksied as oksideermiddel in die oksidasie van veratryl alkohol het hoër aktiwiteit getoon in vergelyking met die gebruik van molekulêre suurstof. Die hoër aktiwiteit kan toegeskryf word aan die hoër stabiliteit van TBHP sowel as die oplosbaarheid daarvan in die reaksiemengsel. Dit dui daarop dat die aktiewe spesie vinniger met TBHP as oksideermiddel vorm. Die beste omsetting van substraat was verkry vanaf die kobalt katalisator, **MC2**, met 'n waarde van 85%. Dit is dan gevolg deur **MC1** en **MC3**. Die hoër aktiwiteit van TBHP, het tot hoër aldehid opbrengs gelei, maar dit het ongelukkig ook tot oor-oksidasie van veratrylaldehyd na veratriese suur gelei.

Die geïmmobiliseerde katalisators, **IC1-IC6**, was ook geëvalueer in die oksidasie van veratryl alkohol met behulp van TBHP as oksideermiddel. Hierdie katalisators het oor die algemeen redelik tot matige aktiwiteit vertoon, terwyl die kobalt analoë (**IC3** en **IC4**) matige omsetting van tot 65% getoon het. Die gebruik van molekulêre suurstof as oksideermiddel tesame met die geïmmobiliseerde katalisators was ondoeltreffend in die oksidasie van veratryl alkohol. Al die geïmmobiliseerde katalisators behalwe **IC5** was herwinbaar en hergebruik vir vyf katalitiese lopies. **IC3** en **IC4** het matige aktiwiteit oor die vyf siklusse vertoon met slegs 'n effense afname in aktiwiteit. Die aard van die silika draers het 'n uitwerking op die aktiwiteit sowel as die selektiwiteit gehad. Die geïmmobiliseerde katalisators gebaseer op MCM-41 draers, het beter aktiwiteit getoon. Die selektiwiteit was effens verandered toe SBA-15 as draer gebruik word.

In die algeheel het die geïmmobiliseerde katalisators redelik tot matige aktiwiteit getoon in die teenwoordigheid van TBHP, terwyl geen aktiwiteit waargeneem is nie wanneer molekulêre suurstof as oksideermiddel gebruik word. Die geïmmobiliseerde katalisators was egter deur hul model-analoë oortref wanneer beide oksideermiddels aangewend was.

Acknowledgements

Firstly, I would like to thank the heavenly father for giving me the strength throughout my career.

I would also like to thank my supervisor, Prof Selwyn Mapolie, for affording me the opportunity to have done this MSc and for providing me with his wisdom and guidance.

To my colleagues from the Organometallic Research Group at Stellenbosch University, special thanks for their friendship, guidance and support within the academic environment: Ene Storm, Annick Van Niekerk, Nicole Visagie, Sean O'Kennedy, Derik Wilbers as well as Joshua Hensburg and Hezron Ogutu.

Special thanks to Jacquin October, Cassiem Joseph and Laura Leckie, aka die manne + Laura, for being great friends and colleagues and for guiding me during this process.

I would like to thank the technical staff at the Inorganic Chemistry building for their assistance: Sylete, Peta, Moebarick, Chalon, Ayanda, Kwezi and Malcolm. Thanks to the CAF staff for assisting with various analytical techniques especially Elsa Malherbe at the NMR facility and Charney Small at the ICP-OES facility. Special thanks to Malcolm Taylor for his assistance with HPLC troubleshooting. Thanks to Hanlie Botha for the BET surface analysis and also to Dr Remi Bucher for powder XRD analysis.

I would like to thank Alicia Kriel and Eric Shandu from Council of Scientific and Industrial Research (CSIR) Pretoria for my electron microscopy analysis as well as Professor Koch and Doctor Arnot for their assistance with HPLC. Thanks to Dr. Peter Makgwane for hosting me at his research facility and allowing me to get a feel for the industry. I would also like to thank CSIR for financial support.

Thanks to Sameera for playing a pivotal role during this difficult journey.

Lastly, I would like to express my gratitude to my family, especially my brother Isadore and mother Ursula, for their patience and support throughout my studies.

Conference contributions

Emile Maggott and Prof S.F. Mapolie

Poster presentation titled: *Schiff-base complexes as catalyst precursors in lignin valorisation via oxidation reactions.*

Catalysis Society of South Africa (CATSA), Pilanesberg (Kwa-Maritane Bush lodge), South Africa, 2017.

Table of contents

Declaration.....	I
Abstract	II
Opsomming	IV
Acknowledgements	VI
Conference Contributions	V
Table of Content	VIII
List of Figures	XIII
List of Schemes.....	XVII
List of Tables.....	XIX
List of Abbreviations.....	XXI

Chapter 1: Literature review of immobilized catalysts in the oxidation of lignin model compounds

1.1 Introduction.....	1
1.1.1 Different types of biomass as potential renewable resources	2
1.2 Oxidation of lignin and model compounds	5
1.2.1 Lignin valorization using different protocols and application.....	5
1.2.1.1 Acid mediated depolymerisation of lignin	5
1.2.1.2 Base mediated depolymerisation of lignin	6
1.2.1.3 Lignin depolymerisation via biochemical processes.....	7
1.2.1.4 Metal catalysed lignin depolymerization	8
1.2.1.5 The use of ionic liquids & supercritical fluids in lignin depolymerization	9
1.2.1.6 Application of photocatalysis in lignin depolymerization	9
1.2.2 Lignin model compounds	10

1.3	Oxidation of lignin model compounds	11
1.3.1	Transition metals used for oxidation of lignin model compounds	11
1.4	Heterogeneous systems employed for oxidation reactions of lignin model compounds.	14
1.5	Aims and objectives	18
1.6	Outline of the thesis.....	18
1.7	References	19

Chapter 2: Preparation and Characterization of Schiff-base ligands and complexes

2.1	Introduction.....	24
2.1.1	Metals used for oxidation	25
2.1.2	Immobilization of catalyst	25
2.2	Synthesis and characterization of model salicylaldimine ligands and siloxane-functionalized salicylaldimine ligands.....	26
2.2.1	Characterization of model and functionalized 2-((propylimino)methyl) phenol ligands	26
2.2.1.1	Characterization of ligands by means of FT-IR (ATR) spectroscopy	26
2.2.1.2	Characterization of 2-((propylimino)methyl)phenol ligand via ¹ H NMR spectroscopy	27
2.3	Synthesis and characterization of model and siloxane -functionalized salicylaldimine copper complexes	29
2.3.1	Characterization of model and functionalized salicylaldimine Cu(II) complexes	30
2.4	Synthesis and characterization of cobalt (II) 2-((propylimino)methyl) phenolate complexes.....	34
2.4.1	Characterization of model and functionalized salicylaldimine Co(II) complexes	34
2.5	Synthesis and characterization of palladium (II) 2 ((propylimino)methyl) phenolate complex	36
2.5.1	Characterization of model and functionalized salicylaldimine Pd(II) complexes	36
2.6	Concluding remarks	41
2.7	Experimental section	42
2.7.1	General remarks and instrumentation.....	42
2.7.2	Materials.....	42
2.7.3	Synthesis of salicylaldimine model and functionalized Schiff base ligands	42

2.7.4	Synthesis of model and functionalized Cu(II) complexes	43
2.7.5	Synthesis of model and functionalized Co(II) complexes	44
2.7.6	Synthesis of model and functionalized Pd(II) complexes	45
2.8	References	46

Chapter 3: Preparation and Characterization of immobilized catalysts IC1-IC6.

3.1	Introduction.....	49
3.2	Results and discussion.....	50
3.2.1	Synthesis and characterization of mesoporous silica, MCM-41 and SBA-15.....	50
3.3.1.1	Characterization of the native material SBA-15 and MCM-41 by FT-IR spectroscopy.	51
3.3.1.2	Characterization of MCM-41 and SBA-15 via BET analysis.	52
3.3.1.3	Characterization of MCM-41 and SBA-15 via thermal gravimetric analysis (TGA).....	54
3.3.1.4	Characterization of MCM-41 and SBA-15 by means of ²⁹ Si nuclear magnetic resonance (NMR) spectroscopy.	55
3.3.1.5	Characterization of MCM-41 and SBA-15 by means of Powder X-Ray Diffraction (XRD)	56
3.3.1.6	Characterization of MCM-41 and SBA-15 by means scanning electron microscopy (SEM) and transmission electron microscopy (TEM).	57
3.3	Synthesis and characterization of immobilized catalysts	58
3.3.1	Characterization of immobilized catalysts, IC1-IC6	58
3.4	Concluding Remarks	69
3.5	Experimental section	69
3.5.1	General remarks and instrumentation.....	69
3.5.2	Materials.....	70
3.5.3	Synthesis of silica native material (MCM-41).....	70
3.5.4	Synthesis of silica native material (SBA-15)	70
3.5.5	Synthesis of immobilized catalysts.....	70
3.6	References	71

Chapter 4: Model and immobilized catalysts as precursors in the oxidation of veratryl alcohol.

4.1	Introduction.....	72
4.2	Preliminary reaction conditions employed in the oxidation of veratryl alcohol.....	73
4.3	Optimizing catalytic conditions for the oxidation of veratryl alcohol.....	74
4.3.1	Typical oxidation reaction conditions.....	75
4.3.1.1	Control reactions.....	75
4.3.1.2	Catalyst concentration.....	76
4.3.1.3	Effect of base concentration.....	77
4.3.1.4	Effect of temperature.....	78
4.3.1.5	Effect of reaction time.....	79
4.3.1.6	Effect of oxidant.....	80
4.3.1.7	Model complexes in the absence of oxygen.....	82
4.4	Comparative study of model catalysts (MC1-MC3) against immobilized catalysts (IC1-IC6).....	85
4.4.1	Model catalysts in presence of oxygen.....	85
4.4.2	Model catalysts in presence of TBHP.....	87
4.4.3	Immobilized catalyst applied in the oxidation of veratryl alcohol.....	88
4.4.3.1	The nature of the support on activity and selectivity.....	89
4.5	Recyclability of catalysts.....	90
4.6	Concluding remarks.....	93
4.7	Experimental section.....	93
4.7.1	General remarks and instrumentation.....	94
4.7.2	General catalysis procedure using Oxygen.....	94
4.7.3	General catalysis procedure using Peroxides (H ₂ O ₂ or TBHP) as oxidants.....	94
4.7.4	Recycling experiments.....	94
4.8	References.....	95

Chapter 5: Thesis summary and future recommendations.

5.1 Thesis summary.....	97
5.2 Recommendations for further studies	98

List of figures

Chapter 1: Literature review of immobilized catalysts in the oxidation of lignin model compounds

Figure 1.1: Schematic representation of biomass. ²⁷	3
Figure 1.2: Representation of the complex polymer structure of lignin containing β -O-4 linkages.	3
Figure 1.3: Product obtained from aldol-condensation reaction. ^{38,39}	6
Figure 1.4: The formation of a six-membered transition state during depolymerization. ⁴¹	7
Figure 1.5: Biochemical funneling using <i>Pseudimonas putida</i> . ⁴³	7
Figure 1.6: Lignin model compounds.	10
Figure 1.7: Two types of lignin model compounds, phenolic and non-phenolic. ²⁸	11
Figure 1.8: Catalyst used for oxidation of veratryl alcohol. ⁵⁵	12
Figure 1.9: Representation of the β -O-4 linkages in lignin model compounds. ⁵⁸	13
Figure 1.10: Co(salen) immobilized onto graphene oxide. ¹⁹	15
Figure 1.11: Reduced palladium catalyst used in acceptor-free dehydrogenation reactions. ¹⁸	16
Figure 1.12: Structure of cobalt Schiff-base ionic liquid bearing different counter ions. ⁶⁶	17

Chapter 2: Preparation and Characterization of Schiff-base ligands and complexes

Figure 2.1: FT-IR (ATR) spectrum of functionalized ligand (L2) as a neat yellow oil.	27
Figure 2.2: Labelled structure of ligand for ¹ H NMR assignment.....	27
Figure 2.3: ¹ H NMR spectrum of functionalized ligand (L2) in deuterated chloroform.	28
Figure 2.4: UV-Vis spectrum of the model and functionalized complex in ethanol.....	31
Figure 2.5: EPR spectrum of the model complex (MC1) recorded in dry dichloromethane at 25 °C. .	33
Figure 2.6: EPR spectrum of functionalized complex (FC1) as a neat powder sample at 25 °C.	33
Figure 2.7: UV-Vis Spectrum of the Cobalt metal complex (MC2).	35

Figure 2.8: ¹ H NMR Spectrum of the Pd-salicylalimine-Complex (MC3) recorded in CDCl ₃	38
Figure 2.9: Molecular structure of palladium (II) 2-((propylimino)methyl)phenolate (MC3) complex with atomic numbering, drawn at 50% probability ellipsoids. Hydrogen atoms are omitted for clarity.	39
Figure 2.10: Palladium complex (MC3) alkylchain protruding from metalloring.	39
Figure 2.11: Mass Spectrum of the Pd-salicyl-aldimine-complex MC3	41

Chapter 3: Preparation and Characterization of immobilized catalysts IC1-IC6.

Figure 3.1: FT-IR (ATR) of the native silica materials (SBA-15 & MCM-41).	51
Figure 3.2: Type of BET isotherms. ¹⁴	52
Figure 3.3: N ₂ adsorption-desorption isotherms of native materials.	53
Figure 3.4: TGA analysis of MCM-41.....	54
Figure 3.5: TGA analysis of SBA-15.	55
Figure 3.6: Deconvoluted ²⁹ Si Nuclear Magnetic resonance spectrum of native silica material MCM-41(left) and SBA-15(right).	55
Figure 3.7: Powder X-ray diffraction of the native silica materials.	56
Figure 3.8: SEM micrographs of native silica materials, MCM-41(left) and SBA-15(right).....	57
Figure 3.9: TEM micrographs of native silica materials, SBA-15(left) and MCM-41(right).	57
Figure 3.10: FT-IR(ATR) spectra of immobilized catalysts based on material SBA-15.....	59
Figure 3.11: FT-IR(ATR) spectra of immobilized catalysts containing silica native material MCM-41.	60
Figure 3.12: BET measurements of immobilized catalysts containing silica native material MCM-41.	61
Figure 3.13: BET measurements of immobilized catalysts containing silica native material SBA-15.	62
Figure 3.14: TGA analysis of immobilized catalyst IC1 supported on MCM-41.	63
Figure 3.15: TGA analysis of immobilized catalyst IC2 containing support material SBA-15.	64
Figure 3.16: Powder X-ray diffraction plots of the immobilized catalyst containing native silica support SBA-15.	65
Figure 3.17: Powder X-ray diffraction plots of the immobilized catalyst containing native silica support MCM-41.....	65

Figure 3.18: SEM micrographs of the immobilized catalysts IC1-IC6 .	66
Figure 3.19: TEM micrographs of the immobilized catalysts IC1-IC6 .	67
Figure 3.20: Selected TEM EDS images of immobilized complexes IC1, IC4 and IC6 .	68

Chapter 4: Model and immobilized catalysts as precursors in the oxidation of veratryl alcohol.

Figure 4.1: Model complexes, MC1-MC3 .	74
Figure 4.2: Representation of immobilized catalysts, IC1-IC6 .	74
Figure 4.3: Influence of main parameters. Reaction conditions: 1.) No catalyst: 1.0 mmol veratryl alcohol, 0.2 mmol NaOH, 25 °C, 6 hours, 10 ml acetonitrile. 2.) No oxidant: 1.0 mmol veratryl alcohol, 0.2 mmol NaOH, 2 mol% catalyst loading, 25 °C, 6 hours, 10 ml acetonitrile, nitrogen atmosphere. 3.) No base (NaOH): 1.0 mmol veratryl alcohol, 2 mol% catalyst loading, 25 °C, 6 hours, 10 ml acetonitrile, 1 atm oxygen pressure.	76
Figure 4.4: Influence of catalyst (MC1) concentration on conversion and selectivity. Reaction conditions: 1.0 mmol veratryl alcohol, 0.2 mmol NaOH, 1 atm oxygen pressure, 60 °C, 24 hours, 10 ml acetonitrile.	77
Figure 4.5: Effect of base concentration on conversion and selectivity. Reaction conditions: 1.0 mmol veratryl alcohol, 2 mol% catalyst (MC1), 1 atm oxygen pressure, 60 °C, 24 hours, 10 ml acetonitrile.	78
Figure 4.6: Influence of temperature on conversion and selectivity. Reaction conditions: 1.0 mmol veratryl alcohol, 2 mol% catalyst loading (MC1), 0.2 mmol NaOH, 1 atm oxygen pressure, 24 hours, 10 ml acetonitrile.	79
Figure 4.7: Influence of time on conversion and selectivity. Reaction conditions: 1.0 mmol veratryl alcohol, 2 mol% catalyst loading (MC1), 0.2 mmol NaOH, 1 atm oxygen pressure, 25°C, 10 ml acetonitrile.	80
Figure 4.8: Influence of oxidant on conversion and selectivity. Reaction conditions: 1.0 mmol veratryl alcohol, 2 mol% catalyst loading (MC1), 0.2 mmol NaOH, 25 °C, 6 hours, 10 ml acetonitrile.	81

Figure 4.9: Influence on conversion and selectivity over time in the absence of oxidant. Reaction conditions: 1.0 mmol veratryl alcohol, 2 mol% catalyst loading (**MC1**), 0.2 mmol NaOH, 25 °C, 6 hours and 12 hours, 10 ml acetonitrile. 83

Figure 4.10: Activity and selectivity of different model catalysts in the presence of oxygen. Reaction conditions: 1.0 mmol veratryl alcohol, 2 mol% catalyst loading (**MC1-MC3**), 0.2 mmol NaOH, 1 atm oxygen pressure, 25 °C, 6 hours, 10 ml acetonitrile. 85

Figure 4.11: Activity of different catalysts on conversion and selectivity in the presence of TBHP. Reaction conditions: 1.0 mmol veratryl alcohol, 2 mol% catalyst loading (**MC1-MC3**), 0.2 mmol NaOH, 2 mmol TBHP, 25 °C, 6 hours, 10 ml acetonitrile. 87

Figure 4.12: Immobilized catalysts **IC1-IC6** and native silica material employed in the oxidation of veratryl alcohol. Reaction conditions: 1.0 mmol veratryl alcohol, 2 mol% catalyst loading, 0.2 mmol NaOH, 2 mmol TBHP, 25 °C, 6 hours, 10 ml acetonitrile. 89

List of schemes

Chapter 1: Literature review of immobilized catalysts in the oxidation of lignin model compounds

Scheme 1.1: Schematic representation of HMF forming after dehydration reaction.	4
Scheme 1.2: Possible products obtained from HMF oxidation reactions.	4
Scheme 1.3: Hydrogenation of levulinic acid using formic acid as hydrogen source. ³³	5
Scheme 1.4: A vanadium catalyst employed in oxidation reactions of lignin model compound, 1,2-diphenyl-2-methoxyethanol. ²⁸	12

Chapter 2: Preparation and Characterization of Schiff-base ligands and complexes

Scheme 2.1: An example of a Schiff base condensation reaction.....	24
Scheme 2.2: Immobilization process	25
Scheme 2.3: General preparation of model and functionalized ligands.	26
Scheme 2.4: General scheme for the preparation of model and functionalized complexes.....	30

Chapter 3: Preparation and Characterization of immobilized catalysts IC1-IC6.

Scheme 3.1: Immobilization process.	50
Scheme 3.2: Preparation of immobilized catalysts IC1-IC6.	58

Chapter 4: Model and immobilized catalysts as precursors in the oxidation of veratryl alcohol.

Scheme 4.1: Typical oxidation reaction of veratryl alcohol to veratrylaldehyde.	75
Scheme 4.2: Metal-hydride pathway for the oxidation of alcohols with peroxides, ROOH as oxidant	82

Scheme 4.3: Currently accepted mechanism for dehydrogenation reactions. ¹⁸	83
Scheme 4.4: Metal-hydride pathway for the oxidation of alcohols with oxygen as oxidant	84
Scheme 4.5: Metal-peroxy pathway for the oxidation of alcohols	86
Scheme 4.6: Metal-hydride pathway for the oxidation of alcohols	86

List of tables

Chapter 2: Preparation and Characterization of Schiff-base ligands and complexes

Table 2.1: Summary of IR vibrations for L1 and L2	27
Table 2.2: Summary of selected ¹ H NMR data of model and functionalized ligands (L1-L2).....	29
Table 2.3: IR shifts of the model (MC1) and functionalized (FC1) complexes.....	30
Table 2.4: Microanalysis of complexes MC1 and FC1	32
Table 2.5: IR shifts of the model (MC2) and functionalized (FC2) complexes.....	34
Table 2.6: Micro-analysis of model and functionalized cobalt complexes.....	36
Table 2.7: IR shifts of the model (MC3) and functionalized (FC3) complexes.....	37
Table 2.8: A summary of the ¹ H NMR data for complexes MC3 and FC3	37

Chapter 3: Preparation and Characterization of immobilized catalysts IC1-IC6.

Table 3.1: Summary of pore volume, surface area and average pore diameter for the native silica materials.	53
Table 3.2: Powder X-ray diffraction data for native silica.	56
Table 3.3: A summary of the metal loading determined by ICP-OES for the immobilized catalysts IC1-IC6 . ^a	61
Table 3.4: A summary of surface area, pore volume and average pore diameter of immobilized catalysts as well as their respective support material.	62

Chapter 4: Model and immobilized catalysts as precursors in the oxidation of veratryl alcohol.

Table 4.1: Conversion, aldehyde yield and turnover numbers at different catalyst loadings using MC1 as catalyst. ^a	77
Table 4.2: Recyclability and reusability pertaining immobilized complexes IC1-IC6. ^a	92

List of abbreviations

δ	chemical shift
Å	angstrom
ATR	attenuated total reflectance
BET	Brunauer Emmett Teller
Bipy	bipyridine
cm^{-1}	wavenumber
comp.	complex (denotes complex pattern of overlapping proton resonances)
CTAB	cetyltrimethylammonium bromide
d	doublet
dd	doublet of doublets
DCM	dichloromethane
DFT	Density Functional Theory
DMSO	dimethyl sulfoxide
DNA	deoxyribonucleic acid
EPR	electron paramagnetic resonance
ESI-MS	electrospray ionization mass spectrometry
FT-IR	Fourier Transform infrared spectroscopy
GC	gas chromatography
HPLC	high performance liquid chromatography
Hz	Hertz
ICP-OES	inductively coupled plasma optical emission spectroscopy
K	Kelvin
LMCT	ligand-to-metal charge transfer
m	multiplet
m/z	mass-to-charge ratio
MCM	Mobil crystalline material
MeOH	methanol
MeCN	acetonitrile
MHz	Megahertz
MLCT	metal-to-ligand charge transfer

List of abbreviations

min	minute(s)
mol	mole
mmol	millimole
MOF	metal–organic framework
NMR	nuclear magnetic resonance
OAc	acetate
ORTEP	Oakridge thermal ellipsoid plot
P/Po	relative pressure
PEG	polyethylene glycol
ph	phenyl
ppm	chemical shift
q	quartet
quin.	quintet
s	singlet
SBA	Santa Barbara amorphous
Sc	supercritical
sept.	septet
sext.	sextet
SEM	scanning electron microscopy
Sol-gel	solution/ gelation
t	triplet
td	triplet of doublets
TBHP	tert-butyl hydroperoxide
TEM	transmission electron microscopy
TEOS	tetraethylorthosilicate
TGA	thermal gravimetric analysis
THF	tetrahydrofuran
TLC	Thin layer chromatography
TON	turn-over number
UV-Vis	ultraviolet-visible
VA	veratryl alcohol
VA-A	veratric acid
VAD	veratrylaldehyde
XRD	X-ray diffraction
ZIF	Zeolitic imidazolate framework

Chapter 1

Literature review of immobilized catalysts in the oxidation of lignin model compounds.

1.1 Introduction

Currently, fossil fuels are one of the fundamental resources to produce energy and fine chemicals including high-value oxygenates. Presently, the continual utilization of fossil fuels is of great concern due to its contribution to pollution of the environment. Not only do fossil fuels have a negative effect on the environment but they are almost at the point where they will be soon depleted, as a result of the increasing world population. The type of pollutants includes fly-ash residues as well as greenhouse gases that are emitted into the atmosphere during combustion processes.¹⁻⁴ These pollutants also play a crucial role in climate change. It also has an impact on our economic development since costs are increasing for the utilization of these fossil fuels. High energy costs can be reduced by simply using biomass which will ultimately increase local economic growth.⁵⁻⁷

There are many sources of renewable energy. These sources include wind energy, hydroelectrical energy, solar energy and biomass valorization.^{8,9} Biomass valorization specifically focusses on the production of fine chemicals which implements green chemistry technologies. In this era, biorefinery technology has emerged as a possible solution to minimize the use of fossil fuels. The use of biomass is a potential renewable resource since it is more environmentally friendly and the fact that it is under-exploited. Biomass valorization has become slightly challenging due to the type of biomass that's available for use, because it should not compete with the necessary food supply. Processes pertaining biomass valorization lack the ability to produce the appropriate conversions of these materials especially in catalytic processes.¹⁰⁻¹² Thus there is a need to develop new catalytic processes to overcome the abovementioned problems.

Many catalytic processes make use of homogeneous catalyst systems instead of heterogeneous catalyst systems to convert hydrocarbons into high-value oxygenates.¹³⁻¹⁵ Homogeneous systems are generally used over heterogeneous systems due to its high activity as well as its high selectivity, forming the desired products. However, homogeneous systems are in general not as sustainable since it does not allow for separation and recovery of the catalysts from the reaction mixture. This thus precludes the re-use of the catalyst.

Chapter 1: Literature review of immobilized catalysts in the oxidation of lignin model compounds.

Another disadvantage, more specifically in oxidation reactions, is the fact that catalysts containing expensive metals are prone to decomposition during the catalytic processes, which results in high catalyst costs.^{16–18}

To create a more environmentally friendly process that implements green chemistry principles, 'heterogenizing' a homogeneous catalyst will open new frontiers in alleviating high cost chemical processes as well as increasing activity in oxidation reactions. The "heterogenizing" process can be initiated by immobilizing homogeneous catalysts onto an inorganic support which will ultimately lead to a "heterogenized" catalyst that could potentially have the same attributes as the homogeneous system and will allow ease of separation of catalyst from the reaction mixture.^{18,19}

Previously, these types of systems have extensively been explored with the use of various support materials. Common supports used in oxidation reactions are mesoporous silicas, graphene oxide, metal organic frameworks, zeolites and boehmite nanoparticles.^{20–23}

In this project, we studied the utilization of mesoporous silica as support since it is cheap and effective in recycling the catalyst which was illustrated by Malumbazo et al.²⁴ These authors reported a comparative study of two mesoporous silica supports MCM-41 and SBA-15. A range of complexes including copper and cobalt salicyldimine analogues were immobilized on these supports. The immobilized catalysts were employed in the oxidation of cyclohexene. All the immobilized catalyst showed moderate activity (between 40 to 84 %) with their respective supports.

1.1.1 Different types of biomass as potential renewable resources

Currently, there are various types of biomass. These include woody and non-woody biomass. Non-woody biomass is derived from a range of crops and garbage waste. The term woody biomass is related to the word woody, material which comprises materials derived from plants, trees and seeds.²⁵ This thesis specifically focuses on woody biomass materials. Woody material from plants, trees and seeds consists of organic extracts, lignocellulose and vital minerals required for the reproduction in plants. Lignocellulose contains cellulose, hemicellulose and lignin.²⁶

Chapter 1: Literature review of immobilized catalysts in the oxidation of lignin model compounds.

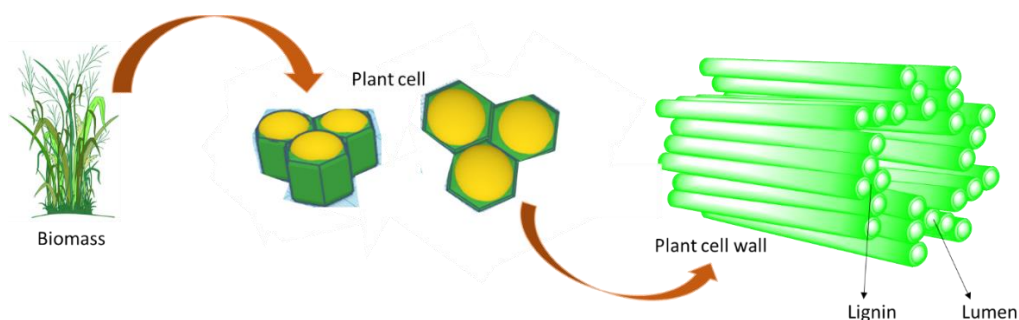


Figure 1.1: Schematic representation of biomass.²⁷

Lignin is a complex naturally occurring organic polymer. This complex polymer plays a vital role in the structure of the cell wall of plants and trees. The polymer structure consists of aromatic subunits that are cross-linked through ether linkages (**Figure 1.2**). These linkages of phenolic units result in the structure of the polymer to be rigid which allows plant cell disintegration to be minimal. Common linkages consists of β -O-4 linkage, 5-5' linkage and β -1 linkages.²⁸ A typical representation of the complex lignin structure can be seen below.

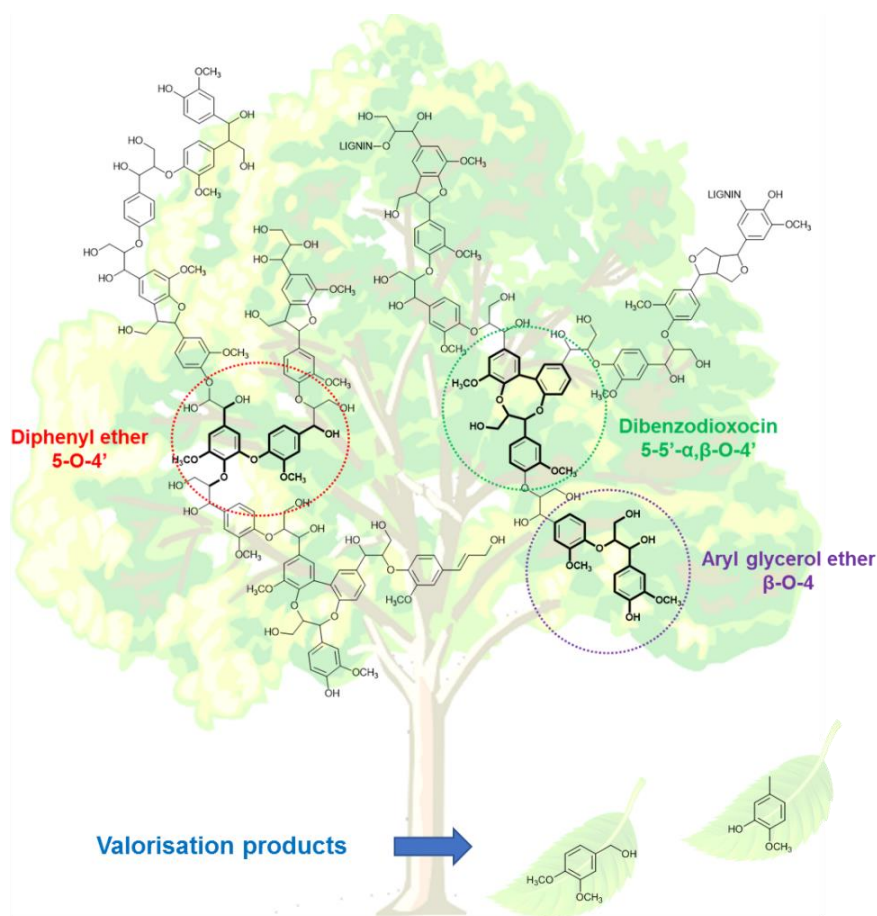
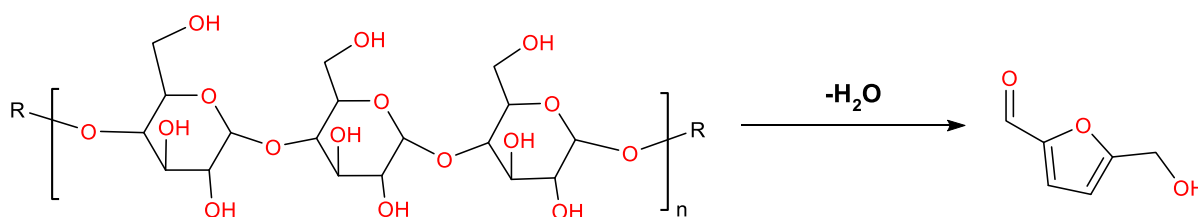


Figure 1.2: Representation of the complex polymer structure of lignin containing β -O-4 linkages.

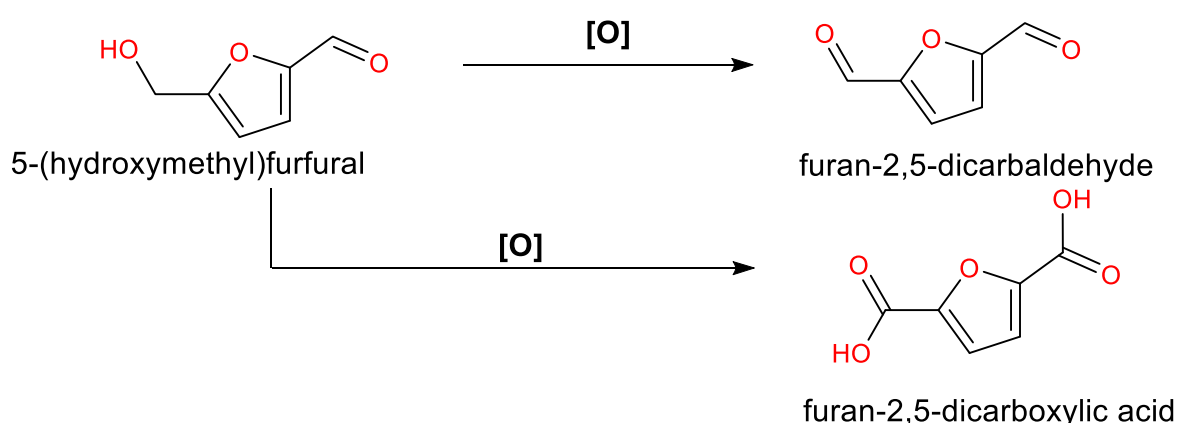
Chapter 1: Literature review of immobilized catalysts in the oxidation of lignin model compounds.

This complex polymer can be depolymerized to produce building blocks for high-end monomers. The monomer building blocks includes p-coumaryl alcohol, synapyl alcohol and coniferyl alcohol.²⁹ This depolymerization process will be discussed in the sections to follow. Cellulose being part of lignocellulose biomass is a polysaccharide that also bears some important characteristic molecules that are useful in the flavourant industry. These materials undergo dehydration reactions to produce high-end chemicals such as 5 hydroxy-methylfurfural (HMF)³⁰⁻³² (**Scheme 1.1**).



Scheme 1.1: Schematic representation of HMF forming after dehydration reaction.

5-Hydroxy-methylfurfural (HMF) consists of a furan ring together with an aldehyde and hydroxyl moiety. Through catalytic oxidation reactions, the 5-hydroxymethylfurfural can be transformed to 2,5 furan dicarbalddehyde (DFF) and 2,5 Furandicarboxylic acid (FDCA) which acts as building blocks for polymer production. These polymers include polyamides and polyesters.³⁰ A typical oxidation route can be seen in **Scheme 1.2**.

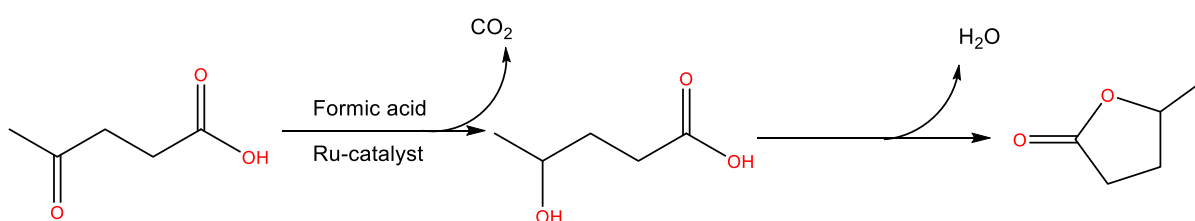


Scheme 1.2: Possible products obtained from HMF oxidation reactions.

Another example of biomass valorization is the hydrogenation of levulinic acid to γ -valerolactone which is potentially the building block for other value-added products such as

Chapter 1: Literature review of immobilized catalysts in the oxidation of lignin model compounds.

polymers and precursors to plasticisers. 5-Hydroxymethylfurfural subjected to hydrolysis results in the formation of levulinic acid which is potentially useful in the production of biofuels and some synthons required in flavourant industry.² γ -Valerolactone production from levulinic acid was illustrated by Amenuvor and co-workers.³³ In this study a ruthenium pyrazolyphosphite complex was employed in hydrogenation reactions of levulinic acid using formic acid or molecular hydrogen as hydrogen source. They illustrated that molecular hydrogen as hydrogen source facilitated the formation of γ -valerolactone selectively. In the current project, only the oxidation of lignin model compounds was investigated.



Scheme 1.3: Hydrogenation of levulinic acid using formic acid as hydrogen source.³³

1.2 Oxidation of lignin and model compounds

1.2.1 Lignin valorization using different protocols and application

Extensive studies were previously conducted on the depolymerization reactions of lignin as well as oxidation reactions of lignin model compounds.³⁴ The cracking of this polyaromatic compound has prompted the use of many organic, inorganic and biological systems to mediate the depolymerisation of this polymer. The systems include the use of sulfuric acid, potassium carbonate, enzymes, transition metal catalysts and photodegradation reagents.³⁵⁻³⁸

1.2.1.1 Acid mediated depolymerisation of lignin

Historically, cracking of the biopolymer was achieved using an acid mediator together with a metal salt such as copper acetate, nickel chloride and metal triflates. Güvenatam et al. demonstrated the use of a Lewis acid in the depolymerisation of lignin. Their approach was to implement a supercritical fluid such as sc-ethanol or sc-water to facilitate the depolymerisation process. Of the two supercritical fluids tested, sc-ethanol exhibited higher monomer yields

Chapter 1: Literature review of immobilized catalysts in the oxidation of lignin model compounds.

compared to sc-water. They also found that the use of sc-water often resulted in the repolymerization of the monomers obtained.³³

In another study conducted by Imai et al. demonstrated that some of the products, more specifically the aldehyde derivatives obtained from the depolymerization of lignin undergo self-condensation reactions. A typical aromatic aldehyde that undergoes self-condensation is shown below.³⁹

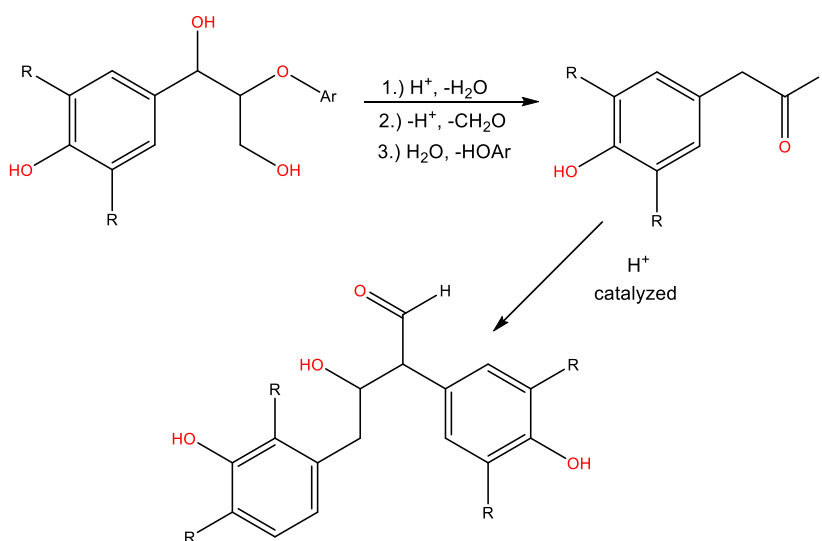


Figure 1.3: Product obtained from aldol-condensation reaction.^{39,40}

1.2.1.2 Base mediated depolymerisation of lignin

Similar to acidolysis reactions, many depolymerisation processes occurs via base mediated reactions. In a typical depolymerisation reaction, organic or inorganic bases promote the β -O-4 cleavage, which is required to break down lignin. This process was illustrated by Konnerth et al.⁴¹ Base catalysed depolymerisation reactions of lignin often lead to unwanted side-reactions especially when using strong bases, which could result in repolymerization reactions.

The use of sodium hydroxide in aqueous media have been studied in depolymerisation reactions by Robert et al. Mechanistic details of this reaction were obtained and it was confirmed that a six-membered transition state formed involving some sort of H-bonded adduct between the substrate and a hydroxide ion and sodium cation. This reaction resulted in a plethora of products forming which included guaiacol and vanillin.⁴²

Chapter 1: Literature review of immobilized catalysts in the oxidation of lignin model compounds.

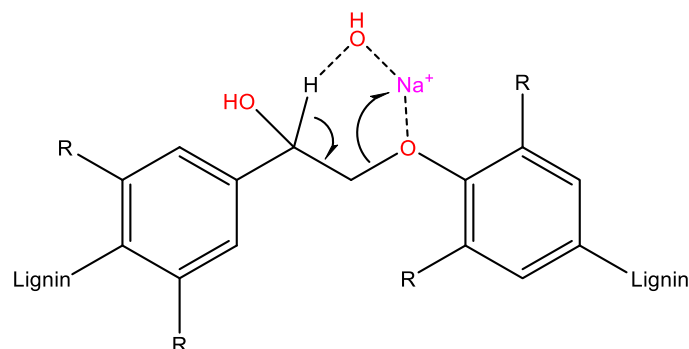


Figure 4: The formation of a six-membered transition state during depolymerization.⁴²

1.2.1.3 Lignin depolymerisation via biochemical processes

Naturally, specific enzymes derived from bacteria and fungi are employed in the depolymerisation of lignin. However, they suffer from a major drawback such as the lack of recyclability that these enzymes exhibit which is a major problem given by its high cost.³ Linger et al. developed a way to oxidatively catabolize lignin and its model compounds into polyhydroxyalkanoates with yields up to 39 % using a natural enzyme, *Pseudomonas putida* KT2440.⁴³

Vardon et al. elaborated on the above by modifying *Pseudimonas putida* to the required specifications. Their catabolic engineered modifications led to the formation of adipic acid from muconic acid through biochemical funnelling.⁴⁴

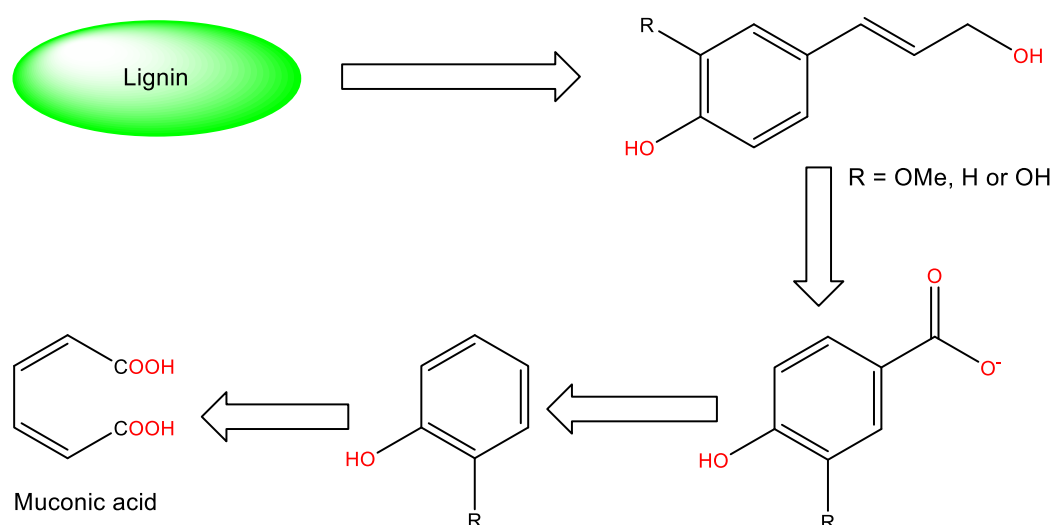


Figure 1.5: Biochemical funnelling using *Pseudimonas putida*.⁴⁴

Chapter 1: Literature review of immobilized catalysts in the oxidation of lignin model compounds.

In a report by Picart et al., a novel biocatalyst was genetically engineered to produce a catalyst system comprising of a laccase-mediator, two β -etherases and a glutathione lyase to depolymerise lignin. This approach gave confirmation that cleavage of the β -O-4 bond of lignin is achieved, which afforded the formation of phenolic monomers. Also, applying this biocatalyst in the oxidation reactions of lignin model compounds resulted in high substrate conversion of 92 % in the presence of an ionic liquid ([EMIM] [EtSO₄]) under mild reaction conditions (pH = 5, 25 °C, 5 days). During the enzymatic cracking of lignin model compounds, β -deoxy- α -veratrylglycerone was obtained in high yields.³⁸

1.2.1.4 Metal catalysed lignin depolymerization

Several transition metal catalysts have been employed in the depolymerization of lignin. These metals include iron, vanadium, manganese, cobalt, copper and ruthenium.^{27,45,46} In-depth studies have been conducted on the utilization of cobalt, copper and vanadium Schiff-base derivatives. These metals showed excellent activity in the oxidation reaction of lignin model compounds. Furthermore, these complexes also exhibited increased regioselectivity that was facilitated by oxidative cleavage. This then produced vanillin and vanillic acid during the depolymerization of lignin.^{11, 28, 46, 47}

Deuss and co-workers explored the use of iron (III) triflate in the depolymerization of lignin. This catalyst together with ethylene glycol gave excellent monomer distribution which include p-hydroxyphenyl, guaiacyl and syringyl units. Furthermore, they studied the use of different types of lignin. In their study they demonstrated that organosolv lignin together with their iron (III) triflate catalyst exhibited better monomer yields of up to 35.5 wt% during the depolymerization process compared to the other type of lignins. Vanillin-acetal exclusively formed during the depolymerization process using pine wood lignin with yields up to 16.5 wt%.¹

An example by Toledano et al. illustrated that nanoparticles of nickel, palladium and ruthenium supported on mesoporous aluminosilicate (Al-SBA-15) displayed activity in depolymerizing lignin. This was done using a microwave irradiation method which afforded the formation of syringe aldehyde as well as mesitol. In this report, different products were obtained to what was expected due to the irradiation of microwaves as well as the catalyst being used. The nickel heterogeneous catalyst used in depolymerization reactions displayed better activity compared to the other catalysts. A decrease in monomer distribution was observed which is due to a repolymerization process taking place.³⁵

Chapter 1: Literature review of immobilized catalysts in the oxidation of lignin model compounds.

1.2.1.5 The use of ionic liquids & supercritical fluids in lignin depolymerization

Ionic liquids and supercritical fluids are also used in the valorization of lignin. These systems are sustainable since it allows catalyst recovery by simple phase separations. It also allows operation at elevated temperatures. In a report by Cox et al. they demonstrated that the ionic liquid 1-H-3-methylimidazolium chloride [HMIM] [Cl] is active in breaking the β -O-4 linkage. It is also selective towards guaiacol at a temperature of 150 °C.⁴⁹

Similarly, supercritical fluids exhibit good solubility as illustrated in a study by Gosselink et al. They explored the difference between organosolv and wheat straw lignins using a CO₂/acetone/water supercritical fluid mixture under extreme conditions (Temperatures between 300-370 °C, 10 MPa). Syringol and guaiacol were selectively obtained after the depolymerisation process. The difference in product distribution (monomers) can be attributed to the diverse nature of the polymer linkages from the two types of lignins.⁵⁰ Despite supercritical fluids showing high activity, good selectivity and the ability to separate mixtures, it is not feasible to invest in this type of research due to the high costs involved in these processes.²⁵

1.2.1.6 Application of photocatalysis in lignin depolymerization

Graphitic carbon nitride (g-C₃N₄) has become one of the more interesting materials used as catalyst supports due to its inert nature in oxidation reactions as well as the ability to separate the material from the reaction mixture. Liu et al. reported that the utilization of metal oxides such as CuO and TiO₂ together with g-C₃N₄ as support, facilitates oxidation reactions of lignin by using visible light (455 nm). This afforded reaction mixtures containing a plethora of products from which benzaldehyde and phenyl formate could predominantly be isolated. Yields of 96 % were obtained at ambient conditions using oxygen as oxidant.³⁷

Another example of photocatalysis in oxidation reactions of lignin and its model compounds was illustrated by Machado et al. In this study they demonstrated that hydroxyl radicals formed during hydroxylation of lignin using TiO₂ and H₂O₂ under UV irradiation. They also observed an electron transfer between the phenolate anion and oxygen. This electron transfer occurred in the absence of TiO₂ and H₂O₂ while irradiating the lignin solution with a mercury lamp between 280 nm - 350 nm. This resulted in the formation of phenolic monomers such as vanillin alcohol.⁵¹

Chapter 1: Literature review of immobilized catalysts in the oxidation of lignin model compounds.

1.2.2 Lignin model compounds

Since lignin exhibits such a complex structure, a large body of research has been conducted on more simple lignin model compounds. These model compounds consist of low molecular weight monomeric compounds and is very useful for the study of catalytic pathways. These monomers are simpler representations of the complex structure of lignin since it contains similar linkages found in lignin. Catalytic degradation on these linkages in the model compounds provides insight to the depolymerisation/ delignification process of lignin. The utilization of these model compounds also helps developing methods for the production of value-added products from lignin. A few of these model compounds are given below (Figure 1.6)

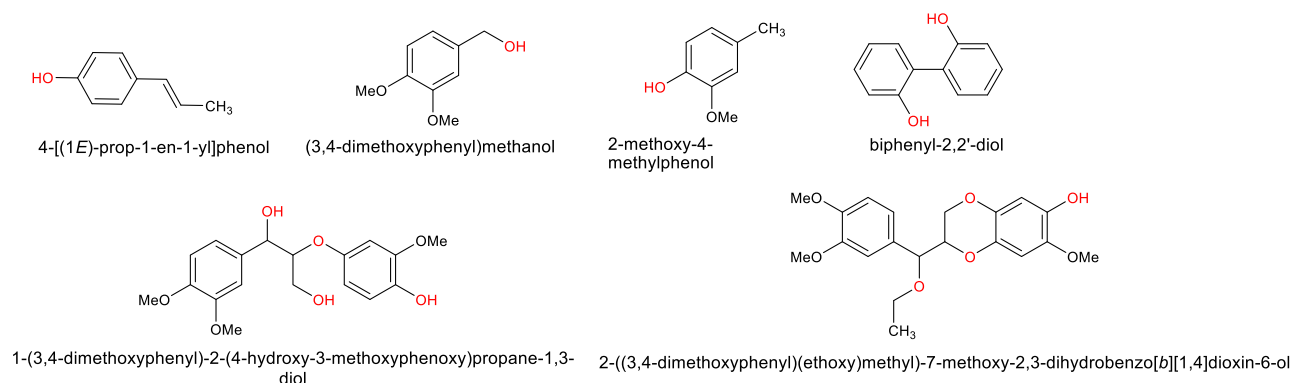


Figure 1.6: Lignin model compounds.

The oxidation/ depolymerisation process of lignin results in a large number of different types of products being formed. This is problematic because it necessitates elaborate separation processes which can be time-consuming. In contrast, the utilization of model compounds in oxidation reactions provides less challenges when it comes to separating products due to the fact that the number of products obtained is limited to a maximum of two. A phenolic type and a non-phenolic type of model compound can be obtained which is representative of the complex polymer structure. Both phenolic and non-phenolic model compounds consist of a phenyl ring bearing different moieties such as methoxy and hydroxyl groups. Phenolic compounds consist of an aryl ring bearing methoxy or hydroxyl moieties together with primary alcohol moiety. These compounds are susceptible for oxidation reactions whereas non-phenolic compounds bear an inert type of moiety such as methyl/ethyl/vinyl moiety instead of the primary alcohols. Examples discussed in literature of these type of model compounds are

Chapter 1: Literature review of immobilized catalysts in the oxidation of lignin model compounds.

given in **Figure 1.7**.^{12,51} Catalytic transformations of these types of compounds are discussed in the sections to follow.

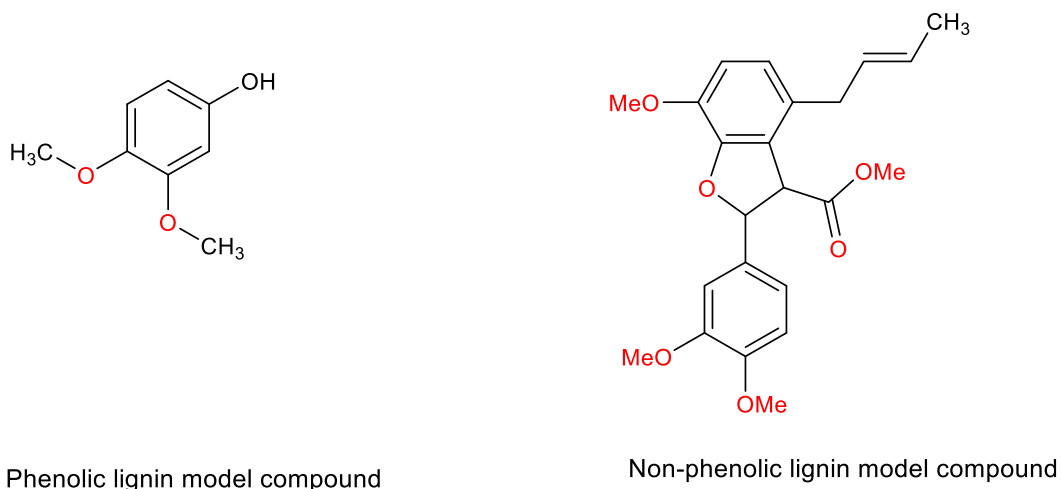


Figure 1.7: Two types of lignin model compounds, phenolic and non-phenolic.²⁸

1.3 Oxidation of lignin model compounds

1.3.1 Transition metals used for oxidation of lignin model compounds

Several transition metals have been employed in oxidation reactions of lignin model compounds. The metals employed range from first row transition metals to platinum group metals. Since the platinum group metal can operate at elevated temperatures, the first-row transition metals are still dominant in these oxidations reactions since they conform to green chemistry principles due to relative abundance thereof as well as the low cost of these metals.

53–55

Recently, Sippola et al. studied the oxidation of the non-phenolic lignin model compound, veratryl alcohol using a cobalt-sulphosalen homogeneous catalyst. Their catalyst was found to be stable in an aqueous alkaline medium (pH = 12). Their catalyst design consists of a bifunctional salicylaldimine ligand and an ethylene bridge resulting in a bidentate system. The employment of cobalt-sulphosalen catalyst in the oxidation of veratryl alcohol to veratraldehyde, lead to relatively low veratryl alcohol conversion (15 %) under moderate conditions (p (O₂) = 1 bar, T= 80 °C, pH = 12, 24 hours, 10 eq pyridine). UV-Vis studies revealed that the base (pyridine) coordinates to the metal center.⁵⁶ From previous work done by Meguro and co-workers, it is expected that a new band in the UV-vis spectrum would mean a new species is being formed.⁵⁷ A typical cobalt-sulphosalen complex used in this study is shown in **Figure 1.8**.

Chapter 1: Literature review of immobilized catalysts in the oxidation of lignin model compounds.

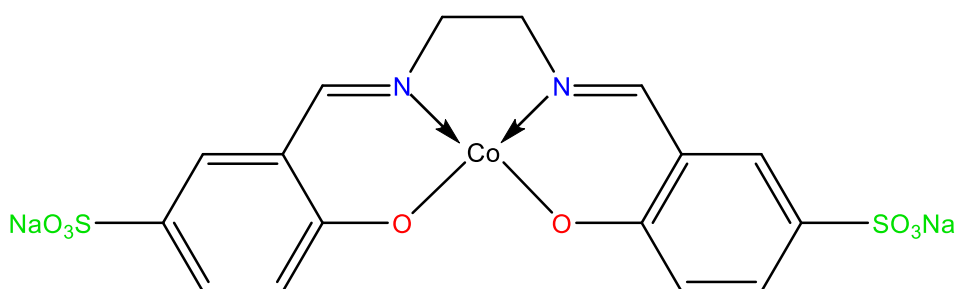
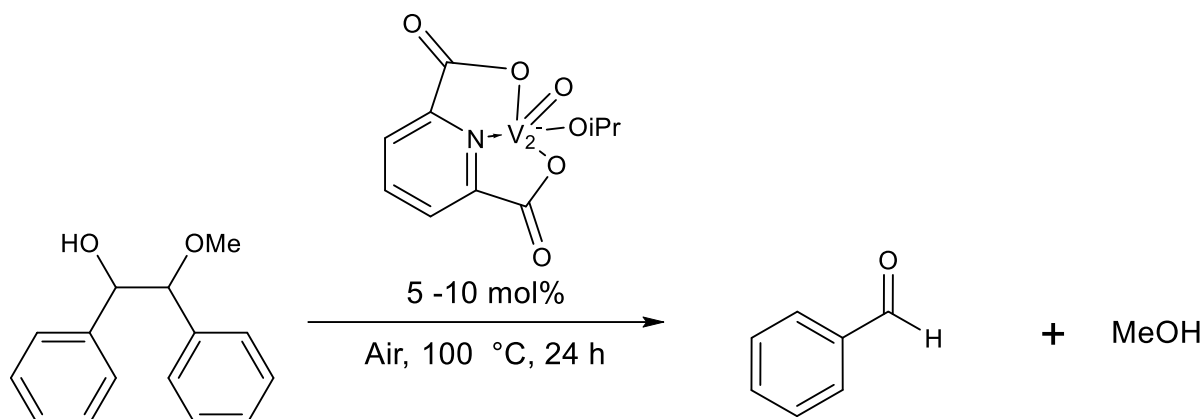


Figure 1.8: Catalyst used for oxidation of veratryl alcohol.⁵⁶

A series of vanadium complexes were prepared by Hanson et al. bearing N^O chelating ligands.²⁸ They employed pinacol derivatives to bond to the metal center in chelating fashion. The evaluation of these catalysts was conducted in oxidative C-C bond cleavage with simple lignin model compounds. Hanson and co-workers reported that using dimethyl sulfoxide (DMSO) as solvent under moderately harsh conditions ($T = 100\text{ }^{\circ}\text{C}$, 5-10 mol %, Air as oxidant), rapid oxidation was achieved which lead to benzaldehyde forming predominantly and methanol as by product. The major product yield is reported to be 73 % while the 27 % is achieved for methanol. An example of one of the vanadium complexes employed in oxidation reactions of 1,2-diphenyl-2-methoxyethanol to produce benzaldehyde and methanol are shown in **Scheme 1.4**.



Scheme 1.4: A vanadium catalyst employed in oxidation reactions of lignin model compound, 1,2-diphenyl-2-methoxyethanol.²⁸

Vanillin is one of the most sought-after aromatic compounds, more specifically in the pharmaceutical, perfume and flavourant industries. However, producing vanillin is quite challenging specifically when it comes to substrate conversion. In addition, selectively producing a particular product as well as separating it from other by-products can also be problematic. Thus, plenty of research has been devoted to simplifying the production of this

Chapter 1: Literature review of immobilized catalysts in the oxidation of lignin model compounds.

fine chemical. Hu and co-workers designed a cobalt Schiff base catalyst that was active in the oxidation reaction of 4-methyl guaiacol to produce vanillin. The oxidation reactions were done in air or using molecular oxygen as oxidant. Water was used as a solvent at 110 °C for 18 hours. The reactions resulted in 100 % substrate conversion with 84 % selectivity towards the aldehyde (vanillin).⁵⁸

Deciding on using the appropriate lignin model compound can be difficult because having a plethora of products can increase the cost for separating these compounds. The development of catalytic processes needs to be as efficient as possible to selectively form the desired products as well as the use of first-row transition metals. To make the process as green as possible, Springer et al. made use of a manganese (III) salen derivative catalyst which is known as the Jacobson's catalyst to oxidize the β -O-4 model compound, 1-(4-hydroxy-3-methoxyphenyl)-2-(2-methoxyphenoxy)propane-1,3-diol.⁵⁹ This manganese salen catalyst displayed high substrate conversions of 91 %. However, only three products formed with product 3 (**Figure 1.9**) forming predominantly. These oxidation reactions were performed in ethanol:water (1:1 ratio) at room temperature and using hydrogen peroxide as oxidant. The catalyst, substrate and oxidant concentration were modified until optimum conditions were achieved.⁶⁰

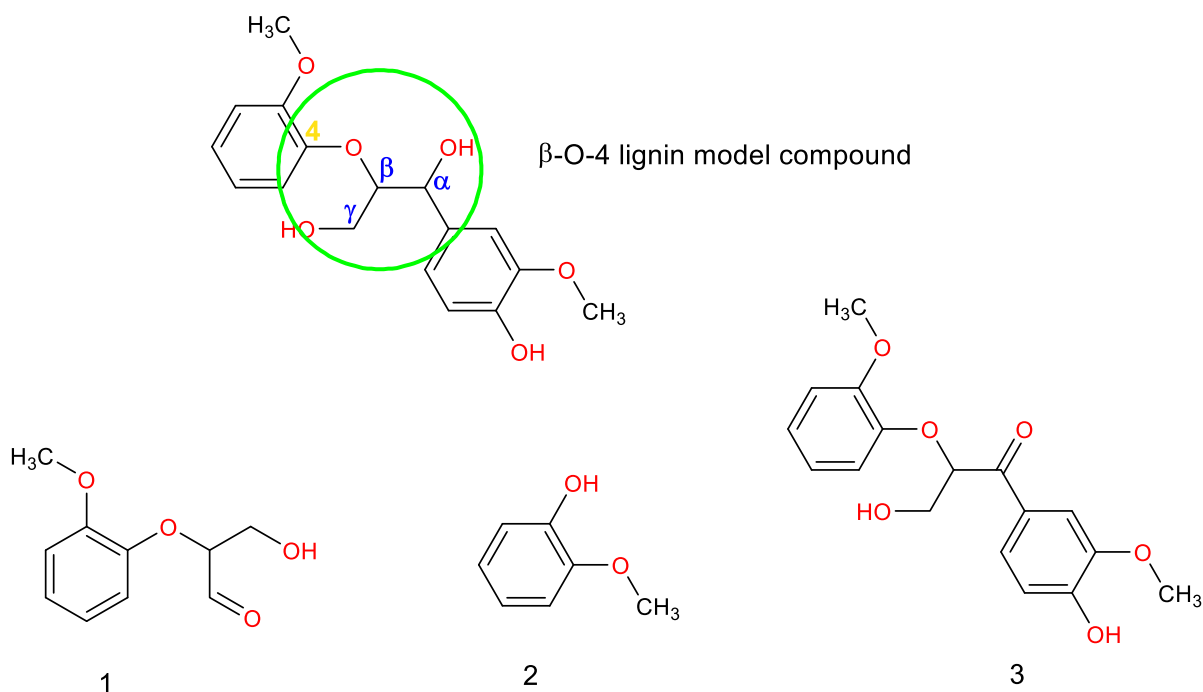


Figure 1.9: Representation of the β -O-4 linkages in lignin model compounds.⁶⁰

Chapter 1: Literature review of immobilized catalysts in the oxidation of lignin model compounds.

As previously discussed in this chapter, complexes of first-row transition metals are being employed as catalyst precursors in oxidation reactions of lignin model compounds, which lower the cost due to their abundance in nature compared to the platinum group metals. The dominance of cobalt and copper being employed was illustrated by Kervinen et al. and Sippola et al.¹³⁻¹⁴ In both cases molecular oxygen is used as oxidant. Kervinen et al. prepared a series of cobalt Schiff base complexes that showed great promise due to the fact it can operate under environmentally friendly conditions. They initially evaluated these catalysts in the oxidation of veratryl alcohol under ambient oxygen pressure in deionised water. Pyridine was introduced to serve as a base but complexed to the metal centre in an axial position. Furthermore, sodium hydroxide was added to these reactions as it should facilitate the abstraction of the hydroxyl hydrogen on the substrate as well as ensuring that the solution is more alkaline (pH = 12). A substrate conversion of 92 % was achieved with selectivity to veratraldehyde being 80 %. Overoxidation was accounted for since veratric acid is highly soluble in water, which remained in the aqueous layer during the extraction of the veratryl alcohol and veratraldehyde with ethyl acetate.

Sippola and Krause explored the selectivity of a bis(o-phenanthroline) copper catalyst in oxygen bleaching of pulp. They studied the simultaneous oxidation of veratryl alcohol and 2,2-biphenol in the presence of dextran. However, they observed that the catalyst is able to depolymerise dextran and thus leading to inadequate selectivities.⁶²

In a report by Kervinen et al. they made use of in-situ infrared spectroscopy to demonstrate the formation of these products. This technique was used to thoroughly study the mechanism of these oxidation reactions. They showed the formation of a cobalt hydroxy bridge intermediate formed during the catalytic cycle as well as the product distribution of the lignin model compounds.⁶³

1.4 Heterogenized systems employed for oxidation reactions of lignin model compounds.

Despite the fact that homogeneous catalysts tend to show high activity in oxidative chemical processes, they are normally outclassed by heterogeneous catalysts due to their poor recyclability. In contrast, the homogeneous catalysts can be immobilized on supports which will have characteristics of both homogeneous and heterogeneous catalysts. This was achieved by immobilizing ruthenium onto a metal oxide as reported by Melián-Rodríguez et

Chapter 1: Literature review of immobilized catalysts in the oxidation of lignin model compounds.

al.⁶⁴ They prepared the metal oxide catalyst by simply using a wet impregnation method using either alumina or silica as supports. The supported ruthenium catalysts exhibited excellent activity of about 99 % conversion of veratryl alcohol. Both catalysts selectively produced veratrylaldehyde (69 %) and veratrole as by-products. The formation of veratrole is due to extended reaction time applied. In the case of the alumina supported catalyst, veratrol was formed in 27 % yield whereas with silica supported catalyst, the yield was less than 1 %. In this report they also prepared copper, cobalt, manganese and silver analogues supported on alumina. These analogues exhibited moderate substrate conversions but were unable to selectively form veratrylaldehyde. A crucial part of their research was the recyclability and durability of the catalysts. Malián and co-workers managed to recycle their catalyst for three catalytic runs with the activity being over 60 % however the catalyst still managed to form veratrylaldehyde.

Zhou and co-workers immobilized a cobalt salen complex on a graphene oxide support. This graphene oxide supported catalyst was employed in the oxidation of lignin model compounds (**Figure 1.10**). These reactions were conducted using air as oxidant at 80 °C for 24 hours. The catalyst exhibited good activity of about 90 % which resulted in producing a mixture of products. They also studied the depolymerization of lignin using this cobalt salen graphene oxide catalyst. This reaction resulted in the formation of various products including vanillin, vanillic acid, 1-(4-hydroxy-3-methoxyphenyl) ethanol and other aromatic compounds. From their study, vanillin predominantly formed during the depolymerization process with vanillic acid being second in line. They managed to recycle their catalyst for 10 catalytic runs with no significant drop in the activity as well as in product selectivity.¹⁹

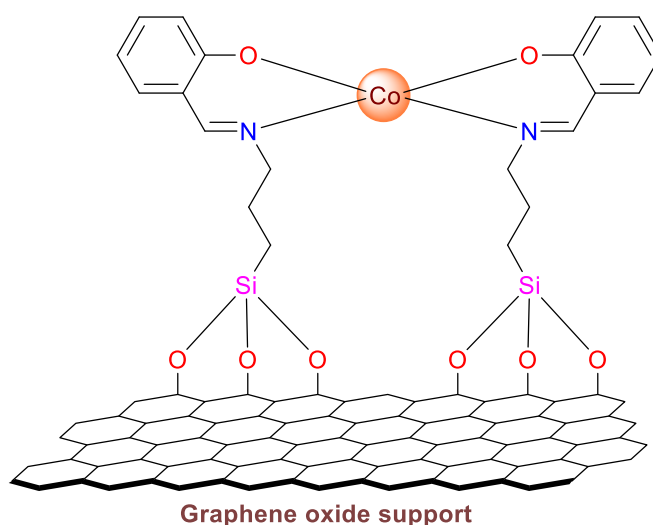


Figure 1.10: Co(salen) immobilized onto graphene oxide.¹⁹

Chapter 1: Literature review of immobilized catalysts in the oxidation of lignin model compounds.

Many oxidation reactions require stoichiometric amounts of oxidants such as periodic acid, which results in toxic by-products forming. Vanillin being the most useful aromatic compound in the flavourant industry raises issues in separating the products from toxic by-products. This problem was alleviated by Yue et al. when they designed an acceptor-free dehydrogenation catalyst immobilized on silica (SBA-15) for the production of vanillin from 4-methyl guaiacol (**Figure 1.11**).¹⁸ They illustrated that the catalyst is active under aerobic (air) and anaerobic (nitrogen) conditions with a conversion of 99 % which indicates that the reaction proceeds via a hydrogen acceptor-free oxidation process. They also studied the catalytic performance of a reduced palladium (Pd^0) catalyst as well as a palladium(II) catalyst system. These experiments revealed that the reduced palladium(0) catalyst exhibited higher activity compared to palladium(II) catalyst. However after adding potassium carbonate as base to the mixture containing the palladium(II) catalyst, a dramatic increase in activity was observed.

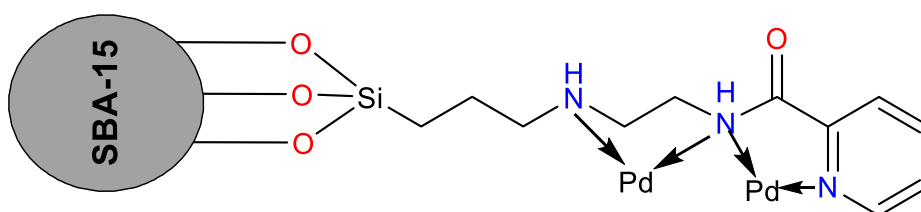


Figure 1.11: Reduced palladium catalyst used in acceptor-free dehydrogenation reactions.¹⁸

The utilization of metal organic framework as a possible support to immobilize homogeneous systems has resulted in increased attention due to the inert nature of carbon materials in oxidation reactions. Lin et al. explored cobalt supported on a Zeolitic Imidazolate Framework (ZIF-67) in oxidation reactions of vanillyl alcohol to produce vanillin. This supported cobalt catalyst together with hydrogen peroxide exhibited good activity in the production of vanillin. The substrate conversion reported, was about 50 % after one hour with the selectivity of vanillin being 100 %.⁶⁵

Olmos et al. explored selective oxidation of veratryl alcohol using a gold: palladium bimetallic catalyst supported on ceria-zirconium which was prepared by sol-gel immobilization. They investigated the efficiency of a monometallic system compared to that of a bimetallic system. In this report they illustrate that the bimetallic system is more active than the monometallic system. Therefore it was implied that in the bimetallic system some sort of a synergistic effect is operative forming veratrylaldehyde selectively.⁶⁶

Chapter 1: Literature review of immobilized catalysts in the oxidation of lignin model compounds.

Recently, Wu and co-workers reported on the oxidation of veratryl alcohol using gold nanoparticles supported on graphene quantum dots (Au/GQD). This heterogeneous catalyst together with hydrogen peroxide was capable of converting the veratryl alcohol to the oxygenate (veratrylaldehyde) with yields up to 99 %. The durability of the catalyst was tested by recycling the catalyst for 6 catalytic runs. This resulted in only a 5 % drop in substrate conversion but remained above 80 % during the course of 6 runs.⁶⁷

Biphasic catalysis using ionic liquids has become one of the most widely used systems in chemical processes due to the higher thermal stability of ionic liquids. Fan et al. studied the oxidation of veratryl alcohol catalysed by ruthenium-zeolitic imidazole framework (Ru@ZIF-8) together with copper-oxide. This ionic liquid-based system showed promising results in converting veratryl alcohol to veratrylaldehyde with yields up to 95 %. Furthermore, addition of acetone to veratrylaldehyde afforded the formation of 3,4-dimethoxybenzylideneacetone via an aldol condensation reaction.¹⁷

Another example in which a cobalt Schiff-base ionic liquid (**Figure 1.12**) was employed as catalyst precursors in the oxidation of veratryl alcohol to produce veratrylaldehyde was explored by Ambrose and co-workers. They demonstrated that the cobalt catalyst selectively oxidized veratryl alcohol to veratryldehyde at optimum reaction conditions without observing the formation of veratric acid. The two versions of the catalysts containing different counter ions both exhibited moderate yields of veratrylaldehyde of up to 82 %. Both catalysts were recycled and reused for 3 catalytic runs, however a drop in activity of about 18 % was observed during the first two runs. Thereafter, a slight drop in activity was observed of about 3 % for catalytic runs 2 and 3.⁶⁸

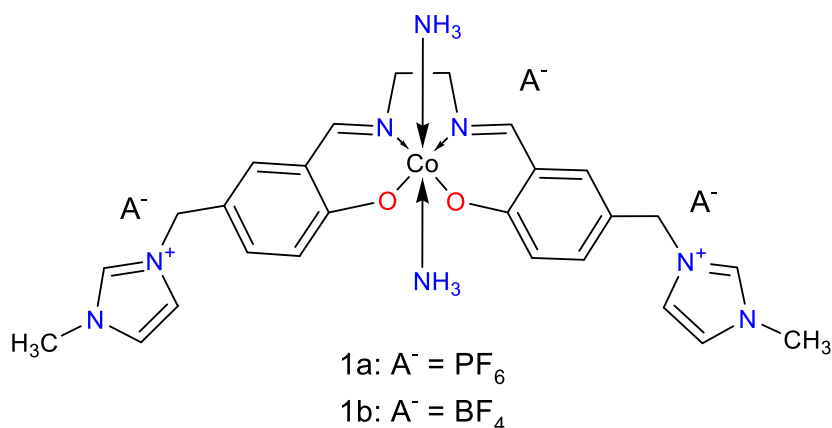


Figure 1.12: Structure of cobalt Schiff-base ionic liquid bearing different counter ions.⁶⁸

Chapter 1: Literature review of immobilized catalysts in the oxidation of lignin model compounds.

1.5 Aims and objectives

The aim of this project is to design model and immobilized catalysts bearing N^o-donor Schiff base ligands for the oxidation of lignin model compounds. Promising catalysts were immobilized on organic/inorganic supports such as SBA-15 and MCM-41. This was done to 'heterogenize' the homogeneous systems. This allowed recovery and reusability of the catalysts. These heterogenized catalysts were tested in oxidation reactions and compared to the model catalysts.

In light of the afore-mentioned the objectives of this project are:

1. To synthesize and characterize model and siloxane functionalized N^o salicylaldimine ligands.
2. To synthesize and characterize copper, cobalt and palladium complexes derived from the above-mentioned ligands.
3. To use the siloxane-functionalized complexes to produce mesoporous silica /metal-organic hybrid materials (composites) which are catalytically active.
4. To study the physical and chemical properties of the hybrid materials produced in 3 using various solid state analytical techniques such as solid state FTIR and solid state NMR spectroscopy, elemental analysis, BET surface analysis, thermal gravimetric analysis, electron microscopy (SEM, TEM) and powder x-ray diffraction (PXRD).
5. To evaluate the composite materials as catalysts in the oxidation of lignin model compounds. A range of co-oxidants such as oxygen, H₂O₂, tert-Butyl hydroperoxide (TBHP) will be screened. A comprehensive study of reaction parameters on the nature of the product stream will be conducted with the aim of tweaking the selectivity of the catalyst system. Investigation into the reusability and recyclability of these catalyst systems were evaluated.

1.6 Outline of the thesis

Chapter one is a brief overview of the biomass as a potential renewable resource to produce value-added products. In addition, this chapter reviews the type of oxidation and depolymerization of lignin as well as the valorization of lignin model compounds.

Chapter two describes the synthesis and characterization of Schiff base ligands as well as their siloxane-functionalized counterparts. This chapter also contains the synthesis and characterization of the model catalysts as well as the siloxane-functionalized catalysts. The

Chapter 1: Literature review of immobilized catalysts in the oxidation of lignin model compounds.

model and functionalized ligands were characterized by FT-IR (ATR) and ^1H NMR spectroscopy. The characterization of the model complexes as well as the functionalized complexes were achieved by FT-IR (ATR) spectroscopy, UV-Vis spectroscopy, mass spectrometry, EPR spectroscopy, ^1H NMR spectroscopy and elemental analysis.

Chapter three covers the preparation and characterization of support materials as well as the immobilization of functionalized complexes onto these supports. These silica supports include MCM-41 and SBA-15. The support material and immobilized complexes were subjected to various solid-state characterization techniques which include FT-IR (ATR) spectroscopy, BET surface analysis, Powder X-ray diffraction, SEM, TEM, TGA and ICP-AES.

Chapter four covers the evaluation of model and immobilized catalyst in the oxidation of veratryl alcohol to veratraldehyde and veratric acid. These oxidation reactions were monitored by TLC and FT-IR. Conversions and yields were quantified using HPLC and GC-FID.

Chapter five contains a summary of all the relevant results obtained in this project. Furthermore, it contains possible suggestions for future studies to further advance the project.

1.7 References

- 1 P. J. Deuss, C. S. Lancefield, A. Narani, J. G. De Vries, N. J. Westwood and K. Barta, *Green Chem.*, 2017, **19**, 2774–2782.
- 2 A. S. Piskun, J. Ftouni, Z. Tang, B. M. Weckhuysen, P. C. A. Bruijninx and H. J. Heeres, *Appl. Catal. A Gen.*, 2018, **549**, 197–206.
- 3 Z. Sun, B. Fridrich, A. De Santi, S. Elangovan and K. Barta, *Chem. Rev.*, 2018, **118**, 614–678.
- 4 S. Stiefel, C. Marks, T. Schmidt, S. Hanisch, G. Spalding and M. Wessling, *Green Chem.*, 2016, **18**, 531–540.
- 5 E. de Jong, A. Higson, P. Walsh and M. Wellisch, *A Rep. Prep. IEA Bioenergy-Task*, 2011, 36.
- 6 T. Werpy and G. Petersen, *U.S. Dep. energy*, 2004, **1**, 76.
- 7 P. Bruijninx, G.-J. Gruter, A. Westenbroek and E. Engelen-Smeets, *Lignin Valorisation THE IMPORTANCE OF A FULL VALUE CHAIN APPROACH*, 2016.
- 8 A. K. Akella, R. P. Saini and M. P. Sharma, *Renew. Energy*, 2008, **34**, 390–396.

Chapter 1: Literature review of immobilized catalysts in the oxidation of lignin model compounds.

- 9 S. Adams, E. K. M. Klobodu and A. Apio, *Renew. Energy*, 2018, **125**, 755–767.
- 10 R. Chaudhary and P. L. Dhepe, *Green Chem.*, 2017, **19**, 778–788.
- 11 K. Kervinen, *Studies on Veratryl Alcohol Oxidation Catalyzed by Co(salen) Type Complexes and Molecular Oxygen in Aqueous Solution*, 2005.
- 12 V. Sippola, *TRANSITION METAL-CATALYSED OXIDATION OF LIGNIN MODEL COMPOUNDS FOR OXYGEN DELIGNIFICATION OF PULP* Väinö Sippola
Distribution : Helsinki University of Technology Laboratory of Industrial Chemistry FIN-02015 TKK Otamedia Oy Espoo 2006, 2006.
- 13 V. M. Roberts, *Dep. Chemie, Lehrstuhl für Tech. Chemie II*, 2008, 144.
- 14 C. Crestini, M. C. Caponi, D. S. Argyropoulos and R. Saladino, *Bioorganic Med. Chem.*, 2006, **14**, 5292–5302.
- 15 R. Behling, S. Valange and G. Chatel, *Green Chem.*, 2016, **18**, 1839–1854.
- 16 J. Zakzeski, A. Dbczak, P. C. A. Bruijninx and B. M. Weckhuysen, *Appl. Catal. A Gen.*, 2011, **394**, 79–85.
- 17 H. Fan, Y. Yang, J. Song, G. Ding, C. Wu, G. Yang and B. Han, *Green Chem.*, 2014, **16**, 600–604.
- 18 W. Fu, L. Yue, X. Duan, J. Li and G. Lu, *Green Chem.*, 2016, **18**, 6136–6142.
- 19 X. F. Zhou and X. J. Lu, *J. Appl. Polym. Sci.*, 2016, **133**, 1–9.
- 20 S. Bhunia and S. Koner, *Polyhedron*, 2011, **30**, 1857–1864.
- 21 Y. Wang, Z. Wen, H. Zhang, G. Cao, Q. Sun and J. Cao, *Catalysts*, 2016, **6**, 214.
- 22 J. Liang, Z. Liang, R. Zou and Y. Zhao, *Adv. Mater.*, 2017, **29**, 1–21.
- 23 M. Mirzaee, B. Bahramian and M. Mirebrahimi, *Cuihua Xuebao/Chinese J. Catal.*, 2016, **37**, 1263–1274.
- 24 N. Malumbazo and S. F. Mapolie, *Mol. Catal. A*, 2009, **312**, 70–77.
- 25 H. Wang, M. Tucker and Y. Ji, *J. Appl. Chem.*, 2013, **2013**, 1–9.
- 26 K. Wilson and A. F. Lee, *Philos. Trans. R. Soc. A Math. Phys. Eng. Sci.*, 2016, **374**, 20150081.
- 27 A. L. Jongerius, *Catalytic Conversion of Lignin for the Production of Aromatics*, 2013.

Chapter 1: Literature review of immobilized catalysts in the oxidation of lignin model compounds.

- 28 S. K. Hanson and R. T. Baker, *Acc. Chem. Res.*, 2015, **48**, 2037–2048.
- 29 S. R. Collinson and W. Thielemans, *Coord. Chem. Rev.*, 2010, **254**, 1854–1870.
- 30 S. M. McKenna, P. Mines, P. Law, K. Kovacs-Schreiner, W. R. Birmingham, N. J. Turner, S. Leimkühler and A. J. Carnell, *Green Chem.*, 2017, **19**, 4660–4665.
- 31 D. X. Martínez-Vargas, J. Rivera De La Rosa, L. Sandoval-Rangel, J. L. Guzmán-Mar, M. A. Garza-Navarro, C. J. Lucio-Ortiz and D. A. De Haro-Del Río, *Appl. Catal. A Gen.*, 2017, **547**, 132–145.
- 32 S. Xu, P. Zhou, Z. Zhang, C. Yang, B. Zhang, K. Deng, S. Bottle and H. Zhu, *J. Am. Chem. Soc.*, 2017, **139**, 14775–14782.
- 33 G. Amenuvor, B. C. E. Makhubela and J. Darkwa, *ACS Sustain. Chem. Eng.*, 2016, **4**, 6010–6018.
- 34 A. Das, A. Rahimi, A. Ulbrich, M. Alherech, A. H. Motagamwala, A. Bhalla, L. Da Costa Sousa, V. Balan, J. A. Dumesic, E. L. Hegg, B. E. Dale, J. Ralph, J. J. Coon and S. S. Stahl, *ACS Sustain. Chem. Eng.*, 2018, **6**, 3367–3374.
- 35 A. Toledano, L. Serrano, A. Pineda, A. A. Romero, R. Luque and J. Labidi, *Appl. Catal. B Environ.*, 2014, **145**, 43–55.
- 36 B. Güvenatam, E. H. J. Heeres, E. A. Pidko and E. J. M. Hensen, *Catal. Today*, 2016, **259**, 460–466.
- 37 H. Liu, H. Li, J. Lu, S. Zeng, M. Wang, N. Luo, S. Xu and F. Wang, *ACS Catal.*, 2018, **8**, 4761–4771.
- 38 P. Picart, H. Liu, P. M. Grande, N. Anders, L. Zhu, J. Klankermayer, W. Leitner, P. Domínguez de María, U. Schwaneberg and A. Schallmey, *Appl. Microbiol. Biotechnol.*, 2017, **101**, 6277–6287.
- 39 T. Imai, T. Yokoyama and Y. Matsumoto, *J. Wood Chem. Technol.*, 2012, **32**, 165–174.
- 40 P. J. Deuss and K. Barta, *Coord. Chem. Rev.*, 2016, **306**, 510–532.
- 41 H. Konnerth, J. Zhang, D. Ma, M. H. G. Prechtl and N. Yan, *Chem. Eng. Sci.*, 2015, **123**, 155–163.
- 42 V. M. Roberts, V. Stein, T. Reiner, A. Lemonidou, X. Li and J. A. Lercher, *Chem. - A*

Chapter 1: Literature review of immobilized catalysts in the oxidation of lignin model compounds.

- Eur. J.*, 2011, **17**, 5939–5948.
- 43 J. G. Linger, D. R. Vardon, M. T. Guarnieri, E. M. Karp, G. B. Hunsinger, M. A. Franden, C. W. Johnson, G. Chupka, T. J. Strathmann, P. T. Pienkos and G. T. Beckham, *Proc. Natl. Acad. Sci.*, 2014, **111**, 12013–12018.
- 44 D. R. Vardon, M. A. Franden, C. W. Johnson, E. M. Karp, M. T. Guarnieri, J. G. Linger, M. J. Salm, T. J. Strathmann and G. T. Beckham, *Energy Environ. Sci.*, 2015, **8**, 617–628.
- 45 M. Wang, L. Li, J. Lu, H. Li, X. Zhang, H. Liu, N. Luo and F. Wang, *Green Chem.*, 2016, **110**, 3552–3559.
- 46 X. F. Zhou, *Polish J. Chem. Technol.*, 2014, **16**, 91–96.
- 47 M. D. Kärkäs, B. S. Matsuura, T. M. Monos, G. Magallanes and C. R. J. Stephenson, *Org. Biomol. Chem.*, 2016, **14**, 1853–1914.
- 48 M. Fache, B. Boutevin and S. Caillol, *ACS Sustain. Chem. Eng.*, 2016, **4**, 35–46.
- 49 A. Toledano, L. Serrano, A. Pineda, A. A. Romero, R. Luque and J. Labidi, *Appl. Catal. B Environ.*, 2014, **145**, 43–55.
- 50 R. J. A. Gosselink, W. Teunissen, J. E. G. van Dam, E. de Jong, G. Gellerstedt, E. L. Scott and J. P. M. Sanders, *Bioresour. Technol.*, 2012, **106**, 173–177.
- 51 A. E. H. Machado, A. M. Furuyama, S. Z. Falone, R. Ruggiero, D. D. S. Perez and A. Castellan, *Chemosphere*, 2000, **40**, 115–124.
- 52 H. Lange, S. Decina and C. Crestini, *Eur. Polym. J.*, 2013, **49**, 1151–1173.
- 53 S. S. Stahl, *Angew. Chemie - Int. Ed.*, 2004, **43**, 3400–3420.
- 54 Y. Wang, J. L. Dubois, B. Hedman, K. O. Hodgson, Y. Wang, J. L. Dubois, B. Hedman, K. Hodgson and T. D. P. Stack, *Science (80-.)*, 2018, **279**, 537–540.
- 55 M. J. Capeness, M. C. Edmundson and L. E. Horsfall, *N. Biotechnol.*, 2015, **32**, 727–731.
- 56 V. O. Sippola and A. O. I. Krause, *J. Mol. Catal. A Chem.*, 2003, **194**, 89–97.
- 57 L. Tolvaj, R. Nemeth, D. Varga and S. Molnar, *Drewno-Wood*, 2009, **52**, 5–17.
- 58 J. Hu, Y. Hu, J. Mao, J. Yao, Z. Chen and H. Li, *Green Chem.*, 2012, **14**, 2894.

Chapter 1: Literature review of immobilized catalysts in the oxidation of lignin model compounds.

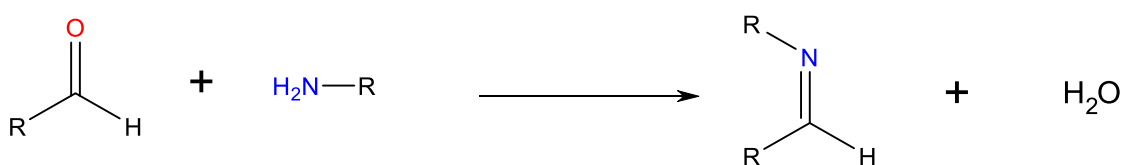
- 59 S. Chang, J. M. Galvin and E. N. Jacobsen, *J. Am. Chem. Soc.*, 1994, **116**, 6937–6938.
- 60 S. D. Springer, J. He, M. Chui, R. D. Little, M. Foston and A. Butler, *ACS Sustain. Chem. Eng.*, 2016, **4**, 3212–3219.
- 61 K. Kervinen, H. Korpi, M. Leskelä and T. Repo, *J. Mol. Catal. A Chem.*, 2003, **203**, 9–19.
- 62 V. O. Sippola and A. O. I. Krause, *Catal. Today*, 2005, **100**, 237–242.
- 63 K. Kervinen, H. Korpi, J. Gerbrand Mesu, F. Soulimani, T. Repo, B. Rieger, M. Leskelä and B. M. Weckhuysen, *Eur. J. Inorg. Chem.*, 2005, **2005**, 2591–2599.
- 64 M. Melián-Rodríguez, S. Saravanamurugan, S. Kegnæs and A. Riisager, *Top. Catal.*, 2015, **58**, 1036–1042.
- 65 K. Y. A. Lin, H. K. Lai and Z. Y. Chen, *J. Taiwan Inst. Chem. Eng.*, 2017, **78**, 337–343.
- 66 C. Olmos, L. Chinchilla, A. Cappella, A. Villa, J. Delgado, A. Hungría, G. Blanco, J. Calvino, L. Prati and X. Chen, *Nanomaterials*, 2018, **8**, 669.
- 67 X. Wu, S. Guo and J. Zhang, *Chem. Commun.*, 2015, **51**, 6318–6321.
- 68 K. Ambrose, B. B. Hurisso and R. D. Singer, *Can. J. Chem.*, 2013, **91**, 1258–1261.

Chapter 2

Preparation and Characterization of Schiff-base ligands and complexes

2.1 Introduction

As a result of environmental concerns linked to the utilization of fossil fuels to produce fine chemicals, investigations have been conducted into the possibility of using alternative renewable resources. These environmental concerns include sustainability surrounding the depletion of fossil fuel reserves as well as harmful gases being emitted into the atmosphere. In the past decade or so, biomass, more specifically lignin has been explored as a possible candidate and a viable source of renewable fuels and fine chemicals. Oxidative transformation of lignin is a potential route to produce value added products. These oxygenates can be useful in the flavourant, pharmaceutical and perfume industry.¹⁻³ Traditional protocols employed to oxidise lignin is both time consuming and energy intensive and often results in large amounts of waste. Thus, there is a need for cheaper and more effective technologies. Catalysts based on earth abundant metals in combination with cheap Schiff base ligands could play a role in developing more effective lignin oxidation systems.⁴⁻⁵ Shifting our attention to designing cheap Schiff base complexes could be an answer to this dilemma. Schiff base ligands/complexes have been around for a few decades now. These Schiff base ligands can be prepared by simple condensation reactions which occur between aldehydes or ketones with amines to form imine moieties (**Scheme 2.1**).⁶⁻⁸



Scheme 2.1: An example of a Schiff base condensation reaction.

Often these Schiff base compounds can be part of bidentate ligands which incorporate N,O and S as other donor sites in addition to the imine functionality.⁶⁻⁷ Moreover, Schiff base ligands renders stability to metal complexes with various oxidation states. Schiff base complexes have a wide variety of applications, which include, metal extraction, catalysis, fire retardants and as biological agents.⁸⁻⁹ The most important application of transition metal complexes is largely in the field of catalysis.

Chapter 2: Preparation and Characterization of Schiff-base ligands and complexes

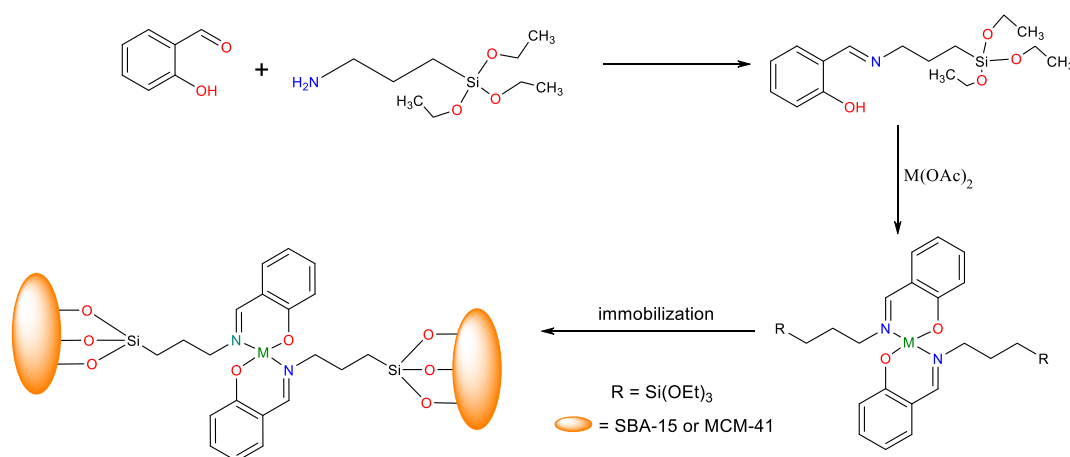
2.1.1 Metals used for oxidation

Copper and cobalt are earth abundant elements that are found in soil and biological systems.¹³⁻¹⁴ These metals are relatively cheap compared to the platinum group metals such as rhodium, platinum and ruthenium to name a few. Salts of these metals are usually employed as precursors to react with organic ligands in the synthesis of coordination complexes, which make the metal centre electron efficient for catalysis purposes.

In a study by Sippola et al.,¹⁵ a method was developed to oxidize lignin model compounds using cobalt salen complexes as catalyst and oxygen as oxidant that gave high catalyst activity and product selectivity. Similar catalytic studies were conducted by Kervinen et al.¹⁶ in which they studied the effect of pH on product formation. It was found that adding moderate amounts of base, led to higher yields of product.

2.1.2 Immobilization of catalyst

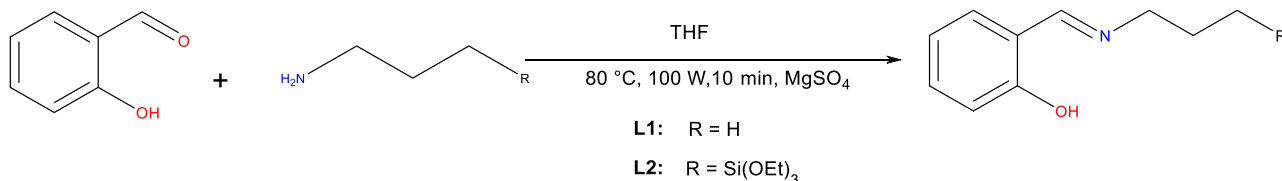
One of the objectives of the current project is to immobilize promising homogeneous catalysts on an organic/inorganic support, which could potentially allow easy separation of the catalyst from the reaction mixture. The Schiff base ligand scaffold incorporating a siloxane group, is an essential part of the synthesis of siloxane functionalized complexes. Inorganic supports, such as silica have surface hydroxyl groups which allow the linkages between the support and siloxane functionalized complexes to be immobilized via covalent bonding through the silicon-oxygen on the functionalized complex. There are two ways in which to immobilize these functionalized complexes on a support. The first method involves preparation of the siloxane functionalized complex to confirm that complexation occurred.¹⁷ The second method involves the prior immobilization of the ligand on the support followed by the complexation of the metal precursor.¹⁸ Although both methods have been reported in the literature, the first method is more effective as the isolation of the complex allows for more structural information to be obtained as illustrated by Vargas et al.¹⁷ (**Scheme 2.2**).



Scheme 2.2: Immobilization process

2.2 Synthesis and characterization of model salicylaldimine ligands and siloxane-functionalized salicylaldimine ligands

The model ligand (**L1**) was prepared using a method adapted from that reported by Guieu et al.¹⁹ This involved a Schiff-base condensation reaction of salicylaldehyde with n-propylamine in a 1:1.5 ratio in tetrahydrofuran (THF) as solvent using a microwave reactor. In addition, MgSO₄ was added to the reaction vessel to remove any water formed during the reaction. The siloxane functionalized ligand (**L2**) was prepared in a similar way by simply replacing the n-propylamine with 3-aminopropyltriethoxysilane. This was done using a 1:1 ratio of salicylaldehyde and 3-aminopropyltriethoxysilane. After the allotted time, excess aldehyde was removed by means of vacuum distillation. All reactions were done under nitrogen using a microwave reactor. The introduction of the siloxane moiety is required to heterogenize the homogeneous complex. Both ligands (**L1-L2**) were obtained as sticky yellow oils. The model ligand appeared to be stable in solution and as the isolated oil in air. As for the functionalized ligand, it was only stable in solution and therefore it was stored in a glovebox under nitrogen. This was done to prevent the siloxane functionality from self-condensing. A general synthetic procedure is shown in **Scheme 2.3** below.



Scheme 2.3: General preparation of model and functionalized ligands.

2.2.1 Characterization of model and functionalized 2-((propylimino)methyl) phenol ligands

Both salicylaldimine ligands were characterized by FTIR (ATR) and ¹H NMR spectroscopy.

2.2.1.1 Characterization of ligands by means of FT-IR (ATR) spectroscopy

The formation of salicylaldimine ligands were confirmed by FTIR (ATR) spectroscopy. The appearance of new imine stretches, and the disappearance of the aldehyde stretch were monitored to determine whether the reaction went to completion. A new imine band appeared around 1631 cm⁻¹ while the aldehyde band around 1666 cm⁻¹ reduced in intensity as the reaction went to

Chapter 2: Preparation and Characterization of Schiff-base ligands and complexes

completion. A $\nu(\text{C-O})$ absorbance around 1276 cm^{-1} is due to the hydroxyl group attached to the aromatic ring. The $\nu(\text{C=C})$ stretches of the aromatic ring can be seen around $1459\text{--}1494\text{ cm}^{-1}$. Furthermore, strong absorbances were observed for the siloxane functionalized ligand (**L2**). These absorbances were seen around $1070\text{--}1099\text{ cm}^{-1}$ and 752 cm^{-1} which is due to the Si-O bond of the functionalized siloxane tail-end. A summary of the important vibrations is given in **Table 2.1** below.

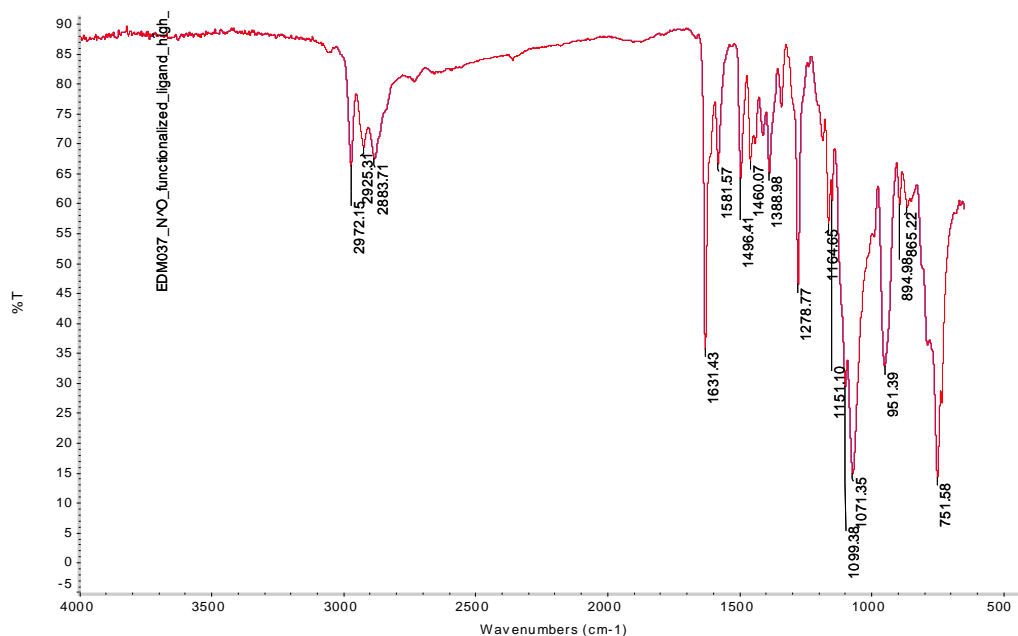


Figure 2.1: FT-IR (ATR) spectrum of functionalized ligand (**L2**) as a neat yellow oil.

Table 2.1: Summary of IR vibrations for **L1** and **L2**.

Ligand	$\nu(\text{C=N})\text{ cm}^{-1}$	$\nu(\text{C=C})\text{ cm}^{-1}$	$\nu(\text{C-O})\text{ cm}^{-1}$	$\nu(\text{Si-O-Si})\text{ cm}^{-1}$	$\nu(\text{Si-OH})\text{ cm}^{-1}$
L1	1630	1493	1275	-	-
L2	1631	1496	1278	1099-1071	751

All ligands were recorded as neat oils using ATR accessory.

2.2.1.2 Characterization of 2-((propylimino)methyl)phenol ligand via ^1H NMR spectroscopy

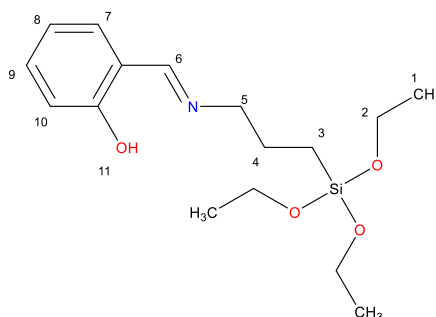


Figure 2.2: Labelled structure of siloxane functionalized ligand (**L2**) for ^1H NMR assignment.

Chapter 2: Preparation and Characterization of Schiff-base ligands and complexes

The expected resonances of the aliphatic (0.67 – 3.88 ppm) and the aromatic (6.85 – 8.67 ppm) regions are observed by ^1H NMR spectroscopy. A broad peak appeared around 13.58 ppm which can be attributed to the hydroxyl group present in the ligand (H-11). The H-1 protons, which constitute 9 protons and can be assigned to the CH_3 groups of the ethyl substituents on the siloxane functionality resonate as a triplet at δ 1.22 ppm. The 6 protons which correspond to the methylene protons (H-2) of the siloxane functionality resonate as a quartet at δ 3.81 ppm. The close proximity of the oxygen atom results in the methylene protons resonating more downfield compared to the methyl protons. The resonances of the methylene protons on the propyl chain are found at δ 0.68 (H-3), δ 1.82 (H-4) and δ 3.59 (H-5) ppm respectively. H-3 resonates as a triplet and due to the proximity of the silicon atom, it is the most upfield. H-4 and H-5 resonate as a multiplet and a triplet respectively. Due to the deshielding effect of nitrogen, H-5 is the most downfield. The most upfield aromatic resonance is the triplet assigned to H-8 at δ 6.86 ppm. H-7 resonates as a doublet at δ 6.95 ppm. H-9 and H-10 overlap and resonate as a “multiplet”. The proton on the imine (H-6) carbon accounts for the singlet found at δ 8.33 ppm. A full ^1H NMR spectrum is shown in **Figure 2.3** and a complete summary of the ^1H NMR data for **L1-L2** is given in **Table 2.2**.

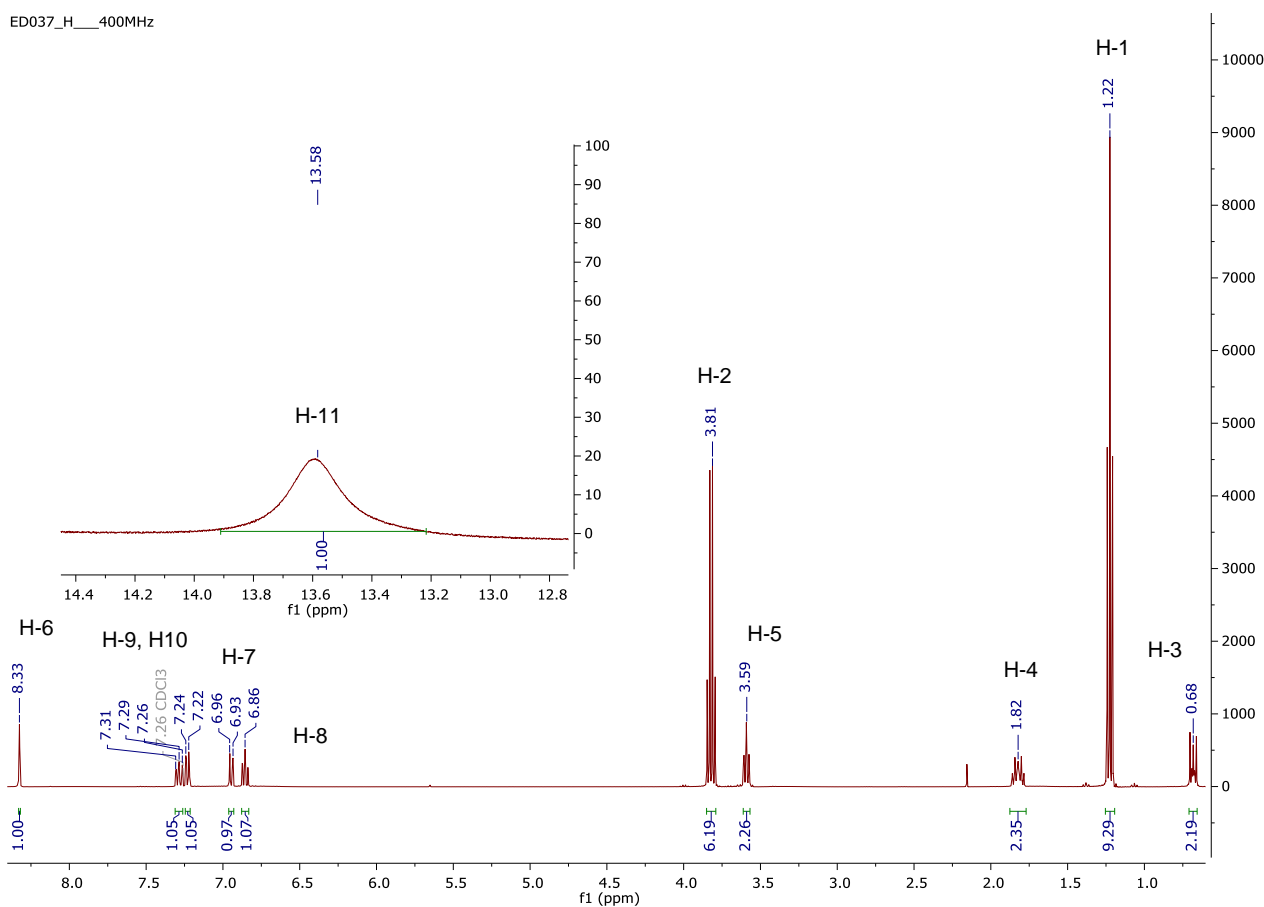


Figure 2.3: ^1H NMR spectrum of functionalized ligand (**L2**) in deuterated chloroform.

Chapter 2: Preparation and Characterization of Schiff-base ligands and complexes**Table 2.2:** Summary of selected ^1H NMR data of model and functionalized ligands (**L1-L2**).^a

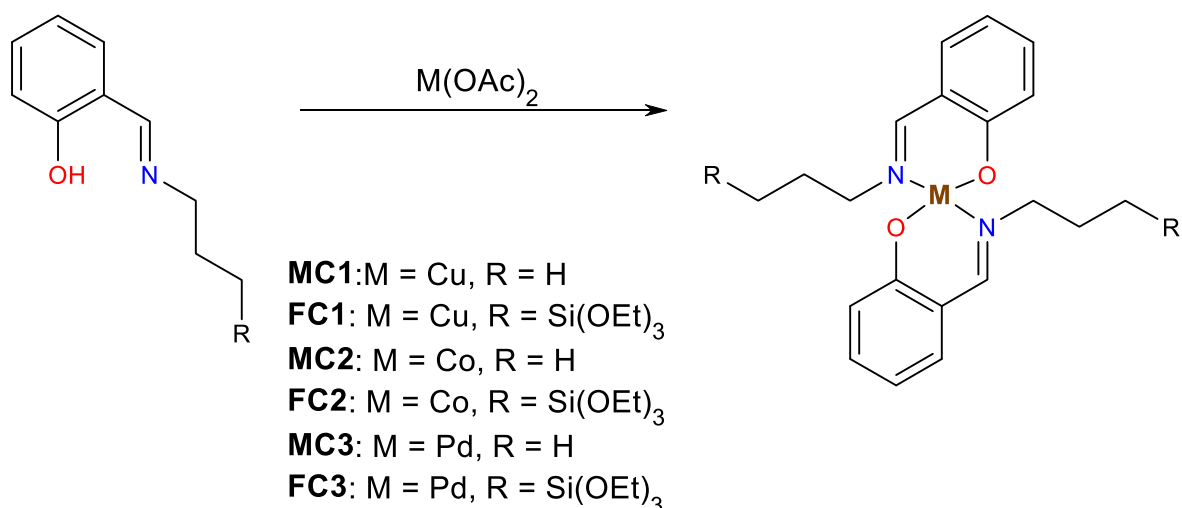
Ligand	Siloxane functionality		Aliphatic Protons	Aromatic Protons (H)	Imine Proton (H)	Hydroxyl proton
	$\text{Si}(\text{OCH}_2\text{CH}_3)_3$	$\text{Si}(\text{OCH}_2\text{CH}_3)_3$				
L1	-	-	0.99 (t, 3H, $^3J=7.4$ Hz), 1.73 (sext, 2H), 3.56 (td, 2H, $^3J=6.8$ Hz, $^4J=1.2$ Hz)	6.86 (td, 1H, $^3J=7.4$ Hz, $^4J=1.1$ Hz), 6.96 (d, 1H, $^3J=8.3$ Hz) 7.25 (dd, 1H, $^3J=7.6$ Hz, $^4J=1.7$ Hz), 7.28-7.31 (m, 1H)	8.33 (s, 1H)	13.65 (s, 1H)
L2	3.81 (q, 6H, $^3J=7.0$ Hz)	1.22 (t, 9H, $^3J=7.0$ Hz)	0.60-0.70 (m, 2H), 1.80-1.83 (m, 2H), 3.59 (td, 2H, $^3J=6.8$ Hz, $^4J=1.1$ Hz)	6.86 (td, 1H, $^3J=7.6$ Hz, $^4J=1.1$ Hz), 6.86 (d, 1H, $^3J=8.3$ Hz) 7.24 (dd, 1H, $^3J=7.6$ Hz, $^4J=1.7$ Hz), 7.29-7.31 (m, 1H)	8.33 (s, 1H)	13.58 (s, 1H)

^a s = singlet, d = doublet, t = triplet, dd = doublet of doublets, td = triplet of doublets, q = quartet, quin. = quintet sext. = sextet, sept. = septet, m = multiplet (denotes complex pattern for a single proton resonance), comp. = complex (denotes complex pattern of overlapping proton resonances)

2.3 Synthesis and characterization of model and siloxane -functionalized bis(salicylaldiminato) copper complexes

The synthesis of the bis(salicylaldiminato)copper(II) complexes were prepared following an adapted procedure reported by Uzman et al.²⁰ The model and functionalized complexes were prepared by simply dissolving copper acetate in dry ethanol and then adding two equivalents of the appropriate salicylaldimine ligand to this solution. The solution was refluxed for 6 hours using Schlenk techniques. Both model and functionalized complexes were recrystallised by slow evaporation of dichloromethane solutions (DCM). Dark green crystals were obtained for the model complex (**MC1**) while an olive-green powder was obtained for the functionalized complex (**FC1**). A general reaction for the formation of a range of salicylaldimine complexes, including of **MC1** and **FC1** is shown in **Scheme 2.4**.

Chapter 2: Preparation and Characterization of Schiff-base ligands and complexes



Scheme 2.4: General scheme for the preparation of model and functionalized complexes.

2.3.1 Characterization of model and functionalized bis(salicylaldiminato)Cu(II) complexes

Complexes **MC1** and **FC1** were characterized by FT-IR (ATR) spectroscopy, UV/vis spectroscopy, EPR spectroscopy, mass spectrometry, elemental analysis and melting point determination.

2.3.1.1 Characterization of model and functionalized bis(salicylaldiminato)Cu(II) complexes by FT-IR spectroscopy

The formation of complexes (**MC1** and **FC1**) were confirmed by FTIR (ATR) spectroscopy. In the IR spectra of the complexes, changes in the imine stretching frequency were used to confirm whether complexation had occurred. The imine band of the ligand appears around 1631 cm⁻¹ while the imine band after complexation shifted to 1620 cm⁻¹, which is an indication that the ligand is coordinated to the metal centre. Strong absorbances were observed for the siloxane functionalized complex (**FC1**). These absorbances were seen around 1047-1099 cm⁻¹ and 755 cm⁻¹ which is due to the Si-O bond of the functionalized siloxane tail-end. A summary of the important vibrations is given in **Table 2.3** below.

Table 2.3: IR shifts of the model (**MC1**) and functionalized (**FC1**) complexes.

Ligand/complex	ν (C=N) cm ⁻¹	
	Ligand	Complex
MC1	1630	1613
FC1	1631	1620

All spectra were recorded as powders using ATR accessory

2.3.1.2 Characterization of model and functionalized bis(salicylaldiminato)Cu(II) complexes by UV-Vis spectroscopy

UV-Vis spectra of the copper complexes were recorded in ethanol at concentration of 10^{-4} M over the range 500 – 200 nm. Both complexes **MC1** And **FC1** were soluble at the abovementioned concentration. **Figure 2.4** depicts the electronic spectra of these complexes (**MC1** and **FC1**). Five peaks are observed in the region 200 nm – 500 nm. Intra-ligand $\pi - \pi^*$ transitions resulted in three peaks being observed between 221 nm and 312 nm. Ligand to metal charge transfer bands can be seen at peak maximum 363 nm and 366 nm for **MC1** and **FC1** respectively. The ligand to metal charge transfer takes place when electrons are transferred from the phenolate into the d-orbitals of the copper (II). This peak can typically be seen with Schiff base copper(II) complexes.^{20, 21}

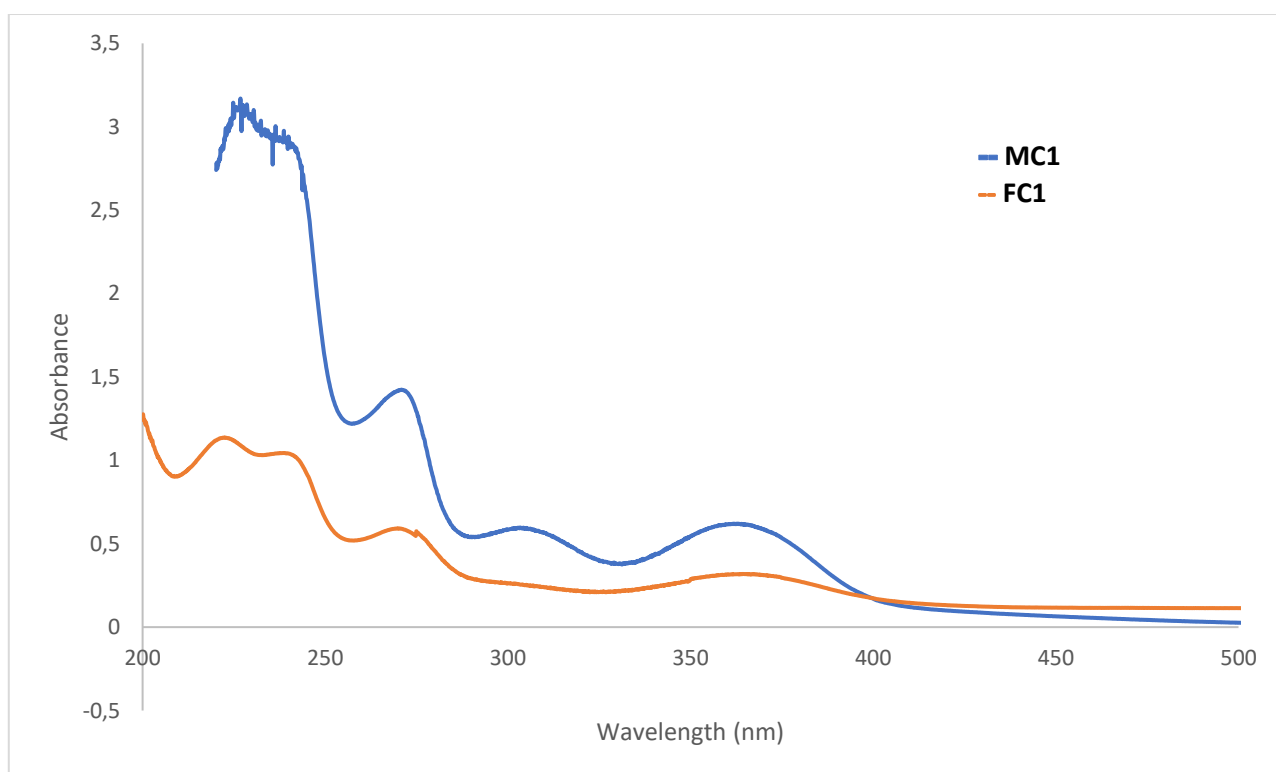


Figure 2.4: UV-Vis spectrum of the model and functionalized complex in ethanol.

2.3.1.3 Characterization of model and functionalized bis(salicylaldiminato)Cu(II) complexes by mass spectrometry, elemental analysis and melting point

All copper complexes were subjected to micro-analysis as the results reported in **Table 2.4**.

Chapter 2: Preparation and Characterization of Schiff-base ligands and complexes**Table 2.4:** Microanalysis of complexes **MC1** and **FC1**.

Complex	ESI-MS (m/Z)	Elemental analysis			Melting point (°C)
	Calculated (Found)	C	H	N	
MC1	388.9(388.1)	61.91(61.69)	6.24(6.86)	7.22(7.17)	124-126
FC1	x	53.94(53.71)	7.36(6.99)	3.93(3.91)	236-239

For **MC1**, a peak at m/z 164.11 can be assigned to the free ligand indicative of ligand dissociation. A peak at m/z 388.12 can be attributed to the copper complex **MC1**. This proves that the ligand is coordinated to the copper metal centre as well as the complex being stable. There is also indication that a sodium adduct formed at m/z ratio 410.10.

2.3.1.4 Characterization of model and functionalized bis(salicylaldiminato)Cu(II) complexes by EPR spectroscopy

The two copper complexes **MC1** and **FC1** were characterised by EPR spectroscopy. Electron paramagnetic resonance spectroscopy was used to study the chemical environment of the model and functionalized complexes. The EPR spectrum of the model complex (**MC1**) was recorded in dry dichloromethane whereas the functionalized complex (**FC1**) was recorded as a solid. The EPR spectrum of complex **MC1** indicated typical tetrahedral signals, which can be seen by the hyperfine splitting consisting of four peaks (**Figure 2.5**). The g -values for **MC1** and **FC1** are 2.17 and 2.20 respectively. These g -values compare well with those of analogous complexes reported in the literature, which is 2.12.²²⁻²³ These results are an indication that copper(II) ion is in a ligand coordination environment in which the two neutral nitrogen atoms as well as two charged oxygen atoms are bound to copper. A broad signal is obtained for the solid-state spectrum of **FC1** (**Figure 2.6**) which is caused by paramagnetic molecules closely packed in the solid-state which causes very short spin-spin relaxation time thus resulting in a broad signal. In contrast, hyperfine splitting is visible for **MC1** (**Figure 2.5**), as expected for paramagnetic molecules in solution.²⁴⁻²⁶

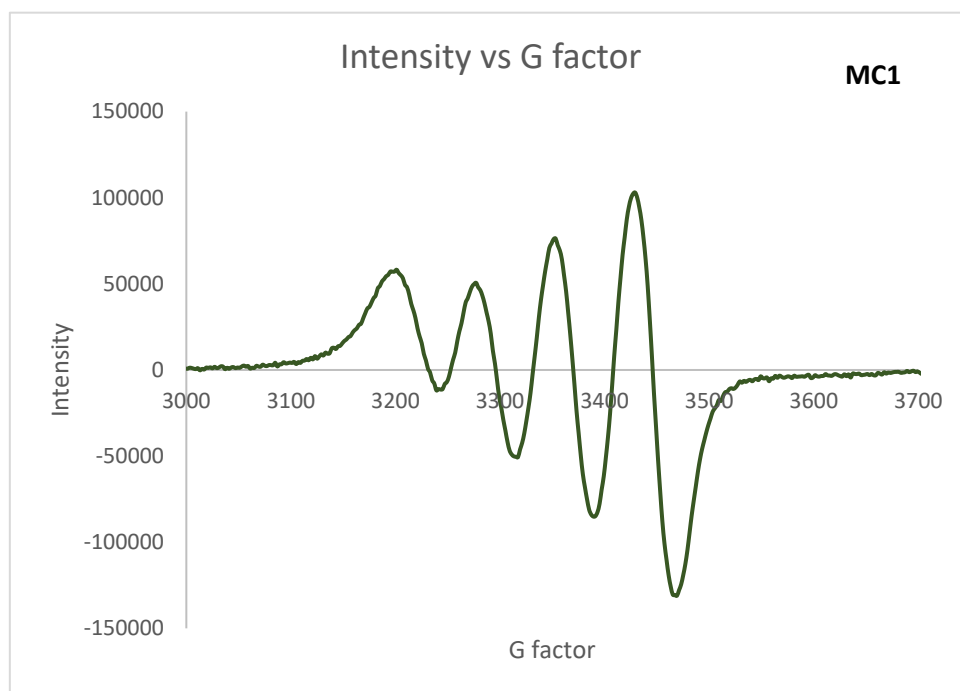
Chapter 2: Preparation and Characterization of Schiff-base ligands and complexes

Figure 2.5: EPR spectrum of the model complex (**MC1**) recorded in dry dichloromethane at 25 °C.

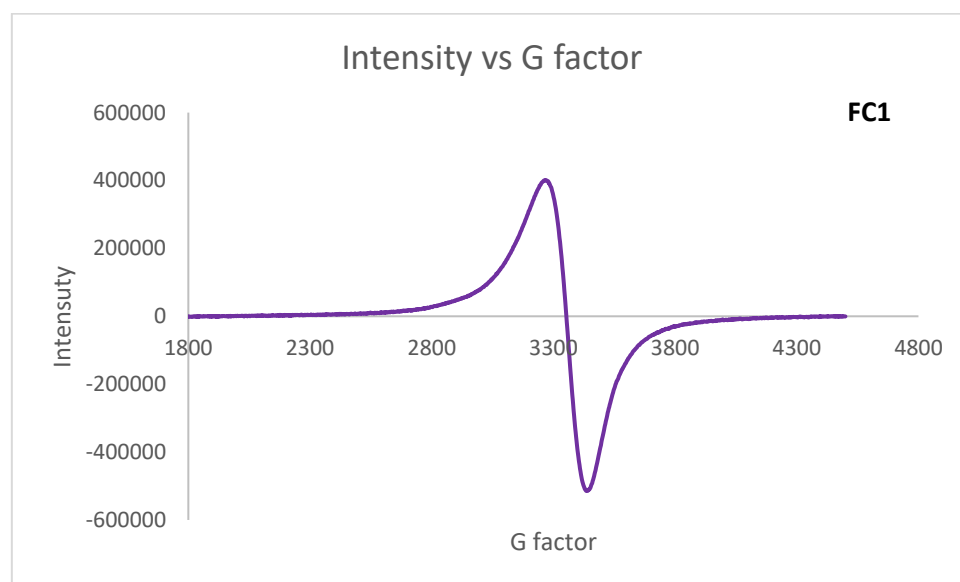


Figure 2.6: EPR spectrum of functionalized complex (**FC1**) as a neat powder sample at 25 °C.

2.4 Synthesis and characterization of bis(salicylaldiminato)cobalt (II) complexes

The synthesis of the bis(salicylaldiminato)cobalt (II) complexes was performed using an adapted procedure reported by Uzman et al.²⁰ The model and functionalized complexes were prepared by simply dissolving cobalt acetate in dry ethanol and then adding two equivalents of the appropriate salicylaldimine ligand to this solution. The solution was refluxed for 6 hours using Schlenk techniques. Only the model complex was recrystallised by slow evaporation from DCM. The functionalized complex is highly insoluble and was purified by decanting the ethanol solution. Dark green crystals were obtained for the model complex (**MC2**) while a brown powder was obtained for the functionalized complex (**FC2**). A general reaction for the complexation of **MC2** and **FC2** is shown in **Scheme 2.4**.

2.4.1 Characterization of model and functionalized bis(salicylaldiminato)Co(II) complexes

Both complexes were characterized by FT-IR (ATR) spectroscopy, UV-Vis spectroscopy, EPR spectroscopy, mass spectrometry, elemental and melting point analysis.

2.4.1.1 Characterization of model and functionalized bis(salicylaldiminato)Co(II) complexes by FT-IR spectroscopy

The formation of complexes (**MC2-FC2**) was monitored by FTIR (ATR) spectroscopy. The imine band shifted between 9-18 wavenumbers for both complexes. Shifting of the imine band indicated that complexation occurred. The imine band of **MC2** appeared around 1612 cm⁻¹ which is a clear indication that the ligand is coordinated to the metal centre. Furthermore, strong absorbances were observed for the siloxane functionalized complex (**FC2**). These absorbances remained around the same region and can be observed around 1070-1099 cm⁻¹ and 755 cm⁻¹ which is due to the Si-O bond of the functionalized siloxane tail-end. A summary of the important vibrations is given in **Table 2.5**.

Table 2.5: IR shifts of the model (**MC2**) and functionalized (**FC2**) complexes.

Ligand/complex	ν (C=N) cm ⁻¹	
	Ligand	Complex
MC2	1630	1612
FC2	1631	1622

All complexes were recorded as powders using ATR accessory

2.4.1.2 Characterization of model and functionalized bis(salicylaldiminato)Co(II) complexes by UV/vis spectroscopy

UV-Vis spectrum of the cobalt complex **MC2** was recorded in ethanol at a concentration of 10^{-4} M over the range 600 – 200 nm. **Figure 2.7** depicts the electronic spectrum of this complex. Two peaks were observed in the region 200 nm – 600 nm. The peak at 260 nm can be assigned to intra-ligand $\pi - \pi^*$ transitions, while the peak at 397 nm can be assigned to the ligand to metal charge transfer.^[27] Unfortunately, an electronic spectrum could not be obtained for the functionalized complex (**FC2**) due to the material being highly insoluble.

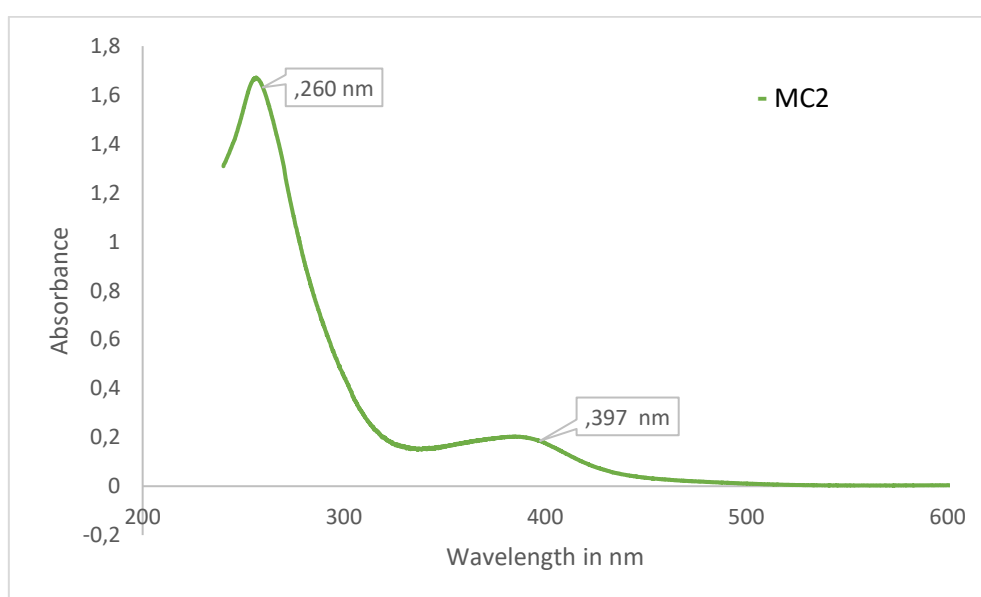


Figure 2.7: UV-Vis Spectrum of the cobalt metal complex (**MC2**).

2.4.1.3 Characterization of model and functionalized bis(salicylaldiminato)Co(II) complexes by EPR spectroscopy

An attempt was made to characterize the cobalt complexes by EPR spectroscopy. However, suitable spectra could not be obtained due to low signal to noise ratios.

2.4.1.4 Characterization of model and functionalized bis(salicylaldiminato)Co(II) complexes by mass spectrometry, elemental analysis and melting point

All complexes were subjected to micro-analysis as can be seen in **Table 2.6**. Further characterization using ESI-MS revealed the molecular ion at m/z 383.1 which proves that the ligand is coordinated to the metal and corresponds with the calculated isotopic pattern.

Chapter 2: Preparation and Characterization of Schiff-base ligands and complexes**Table 2.6:** Micro-analysis of model and functionalized cobalt complexes.

Complex	ESI-MS (m/Z)	Elemental analysis			Melting point (°C)
	Calculated (Found)	C	H	N	
MC2	383.9(383.1)	61.91(61.69)	6.24(6.86)	7.22(7.17)	124-126
FC2	x	54.29(53.97)	7.40(6.93)	3.96(3.78)	>300

2.5 Synthesis and characterization of bis(salicylaldiminato)palladium(II) complex

The synthesis of the bis(salicylaldiminato)palladium(II) complexes followed an adapted procedure reported by Fu et al.²⁸ Both the model and functionalized complexes were prepared by simply dissolving palladium acetate in dry acetone and then adding two equivalents of the appropriate salicylaldimine ligand to this solution. The solution was refluxed for 3 hours using Schlenk techniques. Both model and functionalized complexes were recrystallised from DCM and hexane, which resulted in brown-orange crystals for **MC3** and a yellow powder for **FC3**. A general reaction for the complexation of **MC3** and **FC3** is shown in **Scheme 2.4**.

2.5.1 Characterization of model and functionalized bis(salicylaldiminato)Pd(II) complexes

All complexes were characterized by FT-IR (ATR) spectroscopy, ¹H NMR spectroscopy, mass spectrometry, elemental and melting point analysis. Only **MC3** could be characterized by single crystal X-ray diffraction.

2.5.1.1 Characterization of model and functionalized bis(salicylaldiminato)Pd(II) complexes by FT-IR spectroscopy

The formation of complexes (**MC3** and **FC3**) were monitored by FTIR (ATR) spectroscopy. The imine stretch shifted between ~12-18 wavenumbers for both complexes. Shifting of the imine stretch indicated that complexation had occurred. The imine band of **MC3** appeared around 1612 cm⁻¹ which is a clear indication that the ligand is coordinated to the metal centre. Furthermore, strong absorbances were observed for the siloxane functionalized complex (**FC3**). These absorbances remained around the same region, which can be observed around 1070-1099 cm⁻¹ and 750 cm⁻¹ which is due to the Si-O bond of the functionalized siloxane tail-end. This is also proof that the siloxane moiety remained intact. A summary of the important vibrations are given in **Table 2.7**.

Chapter 2: Preparation and Characterization of Schiff-base ligands and complexes**Table 2.7:** IR shifts of the model (**MC3**) and functionalized (**FC3**) complexes.

Ligand/complex	ν (C=N) cm^{-1}	
	Ligand	Complex
MC3	1630	1612
FC3	1631	1619

All spectra were recorded as powders using an ATR accessory

2.5.1.2 Characterization of bis(salicylaldiminato)palladium(II) via ^1H NMR spectroscopy

The palladium complex **MC3** was characterized by ^1H NMR spectroscopy. The peak of importance is found at δ 7.62 ppm which is due to the imine peak which can be seen in **Figure 2.8**. The corresponding imine peak is found in the ligand ^1H NMR spectrum at δ 8.33 ppm. The OH resonance of the ligand appears around δ 13.62 ppm. This OH resonance disappeared upon coordination of the oxygen to the metal centre. Therefore, disappearance of this resonance confirms coordination of the oxygen to the metal centre and the fact that the ligand is coordinated to the metal centre. A summary of the ^1H NMR data of the palladium complexes (**MC3** and **FC3**) are given in **Table 2.8**.

Table 2.8: A summary of the ^1H NMR data for complexes **MC3** and **FC3**.^a

Complex	Siloxane functionality		Aliphatic Protons	Aromatic Protons	Imine Protons
	$\text{Si}(\text{OCH}_2\text{CH}_3)_3$	$\text{Si}(\text{OCH}_2\text{CH}_3)_3$			
			$\text{NCH}_2\text{CH}_2\text{CH}_2\text{Si}$	Ar-H	N=CH
MC3	-	-	0.98 (t, 3H, $^3J = 7.4$ Hz), 1.83 (sext., 2H), 3.97 (t, 2H, $^3J = 7.3$ Hz)	6.60 - 6.54 (m, 1H), 6.86 (d, 1H, $^3J = 8.4$ Hz) 7.18 (dd, 1H, $^3J = 7.9$ Hz, $^4J = 1.9$ Hz), 7.27-7.22 (m, 1H)	7.62 (s, 1H)
FC3	3.80 (q, 6H, $^3J = 7.0$ Hz)	1.19 (t, 9H, $^3J = 7.0$ Hz)	0.69 (m, 2H), 1.92 (q, 2H, $^3J = 8.1$ Hz), 3.71 (td, 2H, $J = 7$ Hz)	6.54-6.57 (m, 1H), 6.86 (d, 1H, $^3J = 8.4$ Hz) 7.17 (dd, 1H, $^3J = 7.9$ Hz, $^4J = 1.75$ Hz), 7.20-7.23 (m, 1H)	7.64 (s, 1H)

^a s = singlet, d = doublet, t = triplet, dd = doublet of doublets, td = triplet of doublets, q = quartet, quin. = quintet sext. = sextet, sept. = septet, m = multiplet (denotes complex pattern for a single proton resonance), comp. = complex (denotes complex pattern of overlapping proton resonances)

Chapter 2: Preparation and Characterization of Schiff-base ligands and complexes

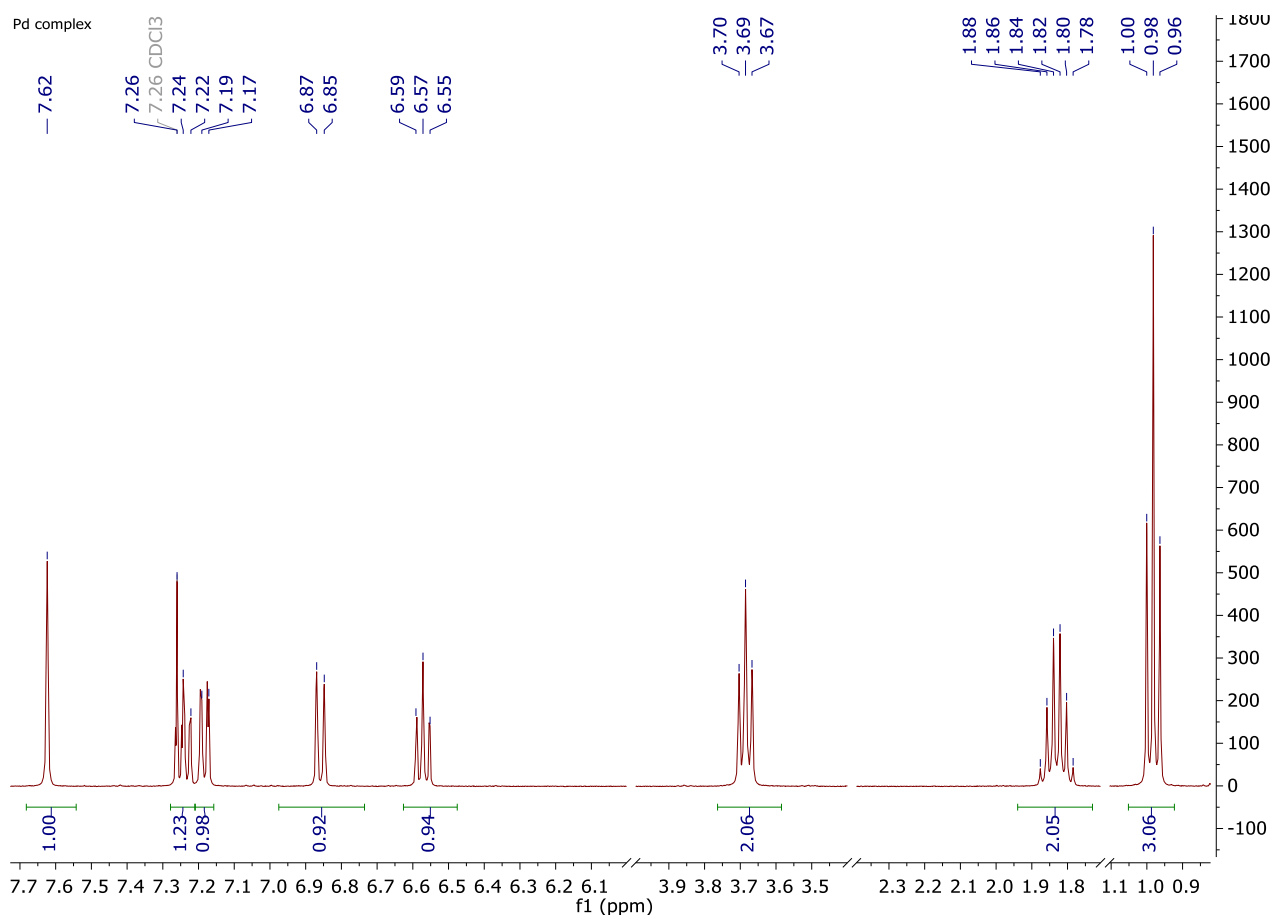


Figure 2.8: ^1H NMR Spectrum of the bis(salicylaldiminato)Pd(II) complex (**MC3**) recorded in CDCl_3 .

2.5.1.3 Characterization of bis(salicylaldiminato)palladium(II) complex **MC3** via single crystal XRD analysis

Single crystals suitable for XRD analysis were obtained for **MC3** by slow diffusion of diethylether into a concentrated solution of the complex in dichloromethane at room temperature, which resulted in yellow-square shape crystals. All crystallographic data as well as selected bond lengths, bond angles and torsion angles are shown in **Table 2.9** and **Table 2.10** respectively.

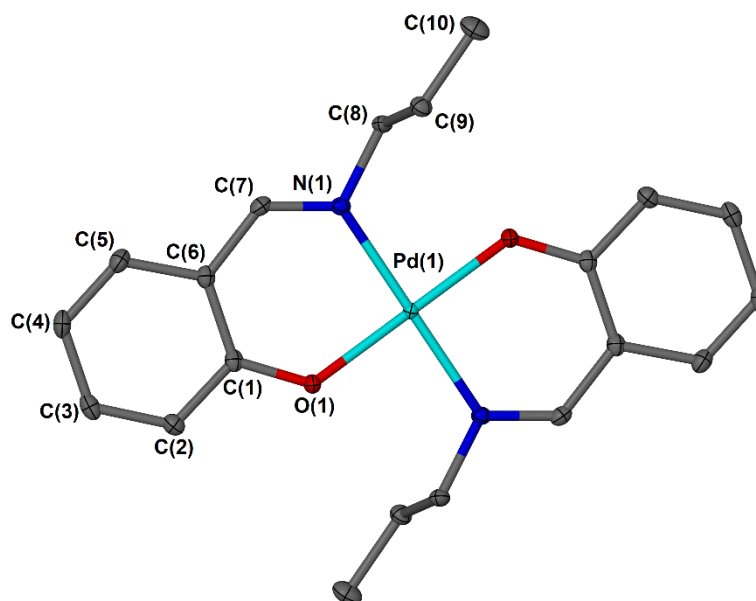


Figure 2.9: Molecular structure of bis(salicylaldiminato)palladium (II) (**MC3**) complex with atomic numbering, drawn at 50% probability ellipsoids. Hydrogen atoms are omitted for clarity.

The complex **MC3** consists of a square-planar geometry (**Figure 2.9**) with a phenolato bound bidentate ligand (N[∧]O). The 2-((propylimino)methyl)phenol ligand **L1**, is coordinated in a trans fashion relative to the imine functionality bound to a propyl chain. The metal-ligand bond lengths for the complex **MC3** are displayed as Pd(1)-N(1) and Pd(1)-O(1) which are in the range of 2.0292(13) and 1.9816(12) Å respectively (**Table 2.10**). This confirms that the Pd(1)-O(1) bond is shorter, which confirms that the bond is stronger compared to the Pd(1)-N(1) bond. From the single crystal XRD it is found that the metallo-ring is flat, while the alkyl chains are protruding from the metallocycle (**Figure 2.10**). There are however electromagnetic interactions present in the crystal lattice. These intramolecular hydrogen bonding include, C(9)-H(9A)---O(1) with the distance of the H.....O being 2.57 Å at an angle of 112°. These bond lengths are similar to structures of salicylaldimine complexes previously reported in literature.²⁹⁻³⁰

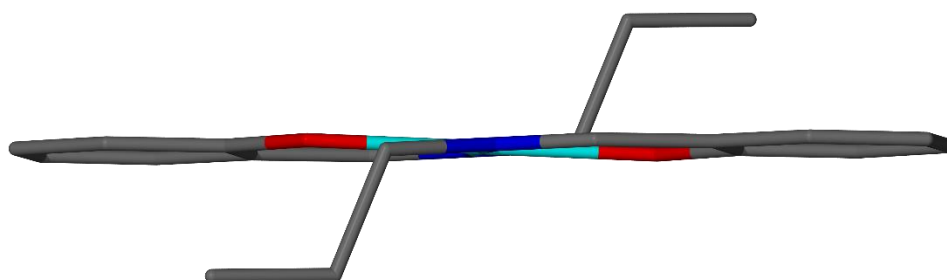


Figure 2.10: Palladium complex (**MC3**) with alkylchain protruding from metalloring.

Chapter 2: Preparation and Characterization of Schiff-base ligands and complexes**Table 2.9:** Crystallographic data pertaining complex **MC3**.

Parameters	Complex (MC3)
Empirical formula	C ₂₀ H ₂₄ N ₂ O ₂ Pd
Mr (g/mol)	430.81
Crystal system	monoclinic
Space group	P21/c
<i>a</i> (Å)	10.0259(7)
<i>b</i> (Å)	10.0747(7)
<i>c</i> (Å)	8.9809(7)
α (deg)	90
β (deg)	102.453(1)
γ (deg)	90
Volume (Å ³)	885.80(11)
Z	2
D _{calc} (g/cm ³)	1.615
F(000)	440
λ (MoK α) (Å)	0.71073
Crystal size (mm)	0.08 x 0.08 x 0.11
Temperature (K)	100
2 θ max (deg)	27.2
absorption corrections applied (mm ⁻¹)	1.063
Goodness-of-fit on F ²	1.07
Final <i>R</i> ₁ indices [<i>I</i> > 2 σ (<i>I</i>)]	0.0169
<i>wR</i> ₂ (all reflections)	0.0463

Table 2.10: Relevant bond lengths, bond angles and torsion angles for complex MC3.

Complex (MC3)	
Bond lengths (Å)	
Pd(1)-N(1)	2.0292(13)
Pd(1)-O(1)	1.9816(12)
Bond angles (°)	
O(1) – Pd(1) – N(1)	92.16(5)
Torsion angle (°)	
C(9) – C(8) – N(1) – C(7)	102.80(16)

2.5.1.4 Characterization of bis(salicylaldiminato)palladium(II) complex **MC3** using mass spectrometry

The structure of the model palladium complex (**MC3**) was further elucidated by ESI mass spectrometry. It is found that the molecular ion of **MC3** $[M + H]^+$ appeared at m/z 431.1. This also proves that the complex is mononuclear and stable. The theoretical measurements correspond to the experimental measurements as depicted in **Figure 2.11**.

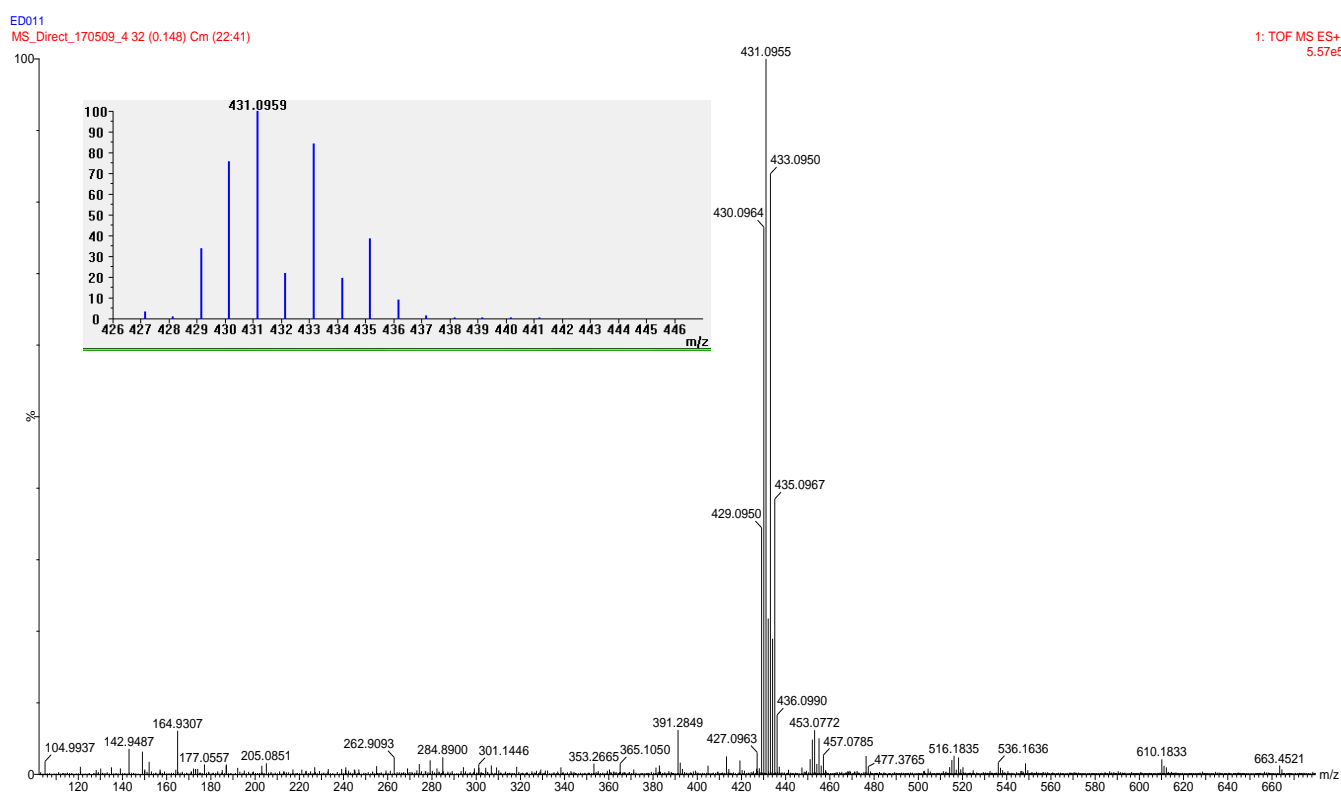


Figure 2.11: Mass Spectrum of the bis(salicylaldiminato)Pd(II) complex **MC3**.

2.6 Concluding remarks

This chapter contains a range of model and siloxane-functionalized salicylaldimine complexes which were prepared via Schiff base condensation reactions. All the model complexes exhibited stability in solution and in air, while the functionalized complexes were stored under inert conditions since the siloxane tail-end tend to hydrolyse over a given time when exposed to air. The model complexes (**MC1-MC3**) were fully characterized by a range of analytical techniques, which include EPR spectroscopy (**MC1**), UV/vis spectroscopy, FT-IR spectroscopy, ^1H NMR spectroscopy, mass spectrometry and single crystal diffraction. The siloxane functionalized complexes (**FC1-FC3**) were fully characterized by EPR spectroscopy (**FC1**), UV/vis spectroscopy, FT-IR spectroscopy, ^1H NMR spectroscopy (**FC3**), mass spectrometry and single crystal diffraction (**MC3**). An attempt was made

Chapter 2: Preparation and Characterization of Schiff-base ligands and complexes

to characterize the cobalt complexes (**MC2** and **FC2**) by EPR spectroscopy but were unable to obtain suitable spectra. The molecular structure of **MC3** was determined by single crystal X-ray diffraction, which showcased a square planar molecular geometry.

2.7 Experimental section

2.7.1 General remarks and instrumentation

All syntheses were carried out under inert conditions using dry nitrogen and utilization of standard Schlenk techniques. Microwave assisted reactions were done in a CEM Microwave reactor. All FT-IR spectra were recorded as neat samples using a Nicolet Avatar 330 FT-IR spectrometer fitted with an ATR accessory. Varian VNMRS 300, 400 and 600 MHz spectrometers were used to measure the ^1H NMR spectra. Melting points were measured using a Stuart scientific SMP3 melting point apparatus. A Waters API Quattro Micro and Water API Q-TOF Ultima instruments were used to measure ESI-MS in the positive mode by means of direct injections. UV-Vis analyses were recorded on a GBC 920 UV-Vis spectrophotometer. A Bruker SMART Apex 2 diffractometer containing a CCD area detector was used to collect all single X-ray diffraction data.³¹ Structure elucidation was achieved by Direct Methods using SHELXL-2014 and SHELXS-97 for structure refinements.³² The program X-Seed was used as a graphical interface for the SHELX program.³³ All non-hydrogen atoms were refined anisotropically. POV-Ray was used to generate high resolution molecular diagrams.³⁴ Elemental analyses were performed on a Vario EL Cube Elemental Analyser CHNS instrument at Stellenbosch University. All air sensitive compounds were stored in a nitrogen purged glovebox.

2.7.2 Materials

All Reagents were obtained from Sigma-Aldrich/Merck and used without further purifications. Solvents were purchased from Sigma-Aldrich/ Merck and Kimix, and were purified using a Pure Solv™ micro solvent purifier fitted with activated alumina columns. Other solvents such as, methanol, acetone and ethanol, were purified by distillation over magnesium fillings and iodine. Acetonitrile was purified by distillation over phosphorous pentoxide.

2.7.3 Synthesis of salicylaldimine model and functionalized Schiff base ligands

2.7.3.1 Model 2-Propyliminomethyl-phenol ligand (L1)

Salicylaldehyde (5.00 mmol, 0.611 g) and propylamine (5.00 mmol, 0.296 g) were dissolved in dry THF (6 ml) in a 10 ml microwave reactor tube. A small amount of MgSO_4 was added to this tube. This was allowed to react in a microwave reactor for 10 minutes under nitrogen atmosphere at 100 W while maintaining a constant temperature of 80 °C. After the allotted time, a bright yellow solution

Chapter 2: Preparation and Characterization of Schiff-base ligands and complexes

was obtained and filtered to remove the MgSO_4 . The solvent was removed under reduced pressures and a yellow oil was obtained (0.791 g, 96.0 %). Characterization was achieved by ^1H NMR and FT-IR (ATR) spectroscopy.

Model ligand **L1**: Yellow oil, yield 96.0 %. IR: FT-IR, ν/cm^{-1} : 1630 (Imine, $\text{HC}=\text{N}$), ^1H NMR (600 MHz, CDCl_3): δ (ppm) = 13.65 ($\text{H}_{\text{Ar-OH}}$, s, 1H), 8.33 (H_{imine} , s, 1H), 7.31-7.28 ($\text{H}_{\text{Ar-H}}$, m, 1H), 7.25 ($\text{H}_{\text{Ar-H}}$, dd, 1H, $^3J_{\text{H-H}} = 7.6$ Hz, $^4J_{\text{H-H}} = 1.7$ Hz), 6.96 ($\text{H}_{\text{Ar-H}}$, d, 1H, $^3J_{\text{H-H}} = 8.3$ Hz), 6.86 ($\text{H}_{\text{Ar-H}}$, m, 1H, $^3J_{\text{H-H}} = 7.4$ Hz, $^4J_{\text{H-H}} = 1.1$ Hz), 3.56 (propyl N-CH_2 , td, 2H, $^3J_{\text{H-H}} = 6.8$ Hz, $^4J_{\text{H-H}} = 1.2$ Hz), 1.73 (propyl $\text{CH}_2\text{-CH}_2\text{-CH}_3$, sextet, 2H, $^3J_{\text{H-H}} = 7.2$ Hz), 0.99 (propyl $\text{CH}_2\text{-CH}_2\text{-CH}_3$, t, 3H, $^3J_{\text{H-H}} = 7.4$ Hz).

2.7.3.2 Functionalized 2-(3-triethoxysilanepropyliminomethyl)-phenol ligand (L2)

Salicylaldehyde (5.00 mmol, 0.611 g) and 3-aminopropyl-triethoxysilane (5.00 mmol, 1.10 g) were dissolved in dry THF (6 ml) in a 10 ml microwave reactor tube. A small amount of MgSO_4 was added to this tube. This was allowed to react in a microwave reactor for 10 minutes under a nitrogen atmosphere at 100 W while maintaining a constant temperature of 80 °C. After the allotted time, a bright yellow solution was obtained and filtered to remove the MgSO_4 . Excess salicylaldehyde was removed by vacuum distillation and product was redissolved in diethyl ether. The solvent was removed under reduced pressure and a yellow oil was obtained (1.66 g, 78.2 %). Characterization was achieved by ^1H NMR and FT-IR (ATR) spectroscopy.

Functionalized ligand **L2**: Yellow oil, yield 78.2 %. IR: FT-IR, ν/cm^{-1} : 1631 (Imine, $\text{HC}=\text{N}$), 1077 (Si-O), 755 (Si-O). ^1H NMR (400 MHz, CDCl_3): δ (ppm) = 13.97 ($\text{H}_{\text{Ar-OH}}$, s, 1H), 8.67 (H_{imine} , s, 1H), 7.66-7.61 ($\text{H}_{\text{Ar-H}}$, m, 1H), 7.58 ($\text{H}_{\text{Ar-H}}$, dd, 1H, $^3J_{\text{H-H}} = 7.6$ Hz, $^4J_{\text{H-H}} = 1.7$ Hz), 7.29 ($\text{H}_{\text{Ar-H}}$, d, 1H, $^3J_{\text{H-H}} = 8.3$ Hz), 7.20 ($\text{H}_{\text{Ar-H}}$, td, 1H, $^3J_{\text{H-H}} = 7.6$ Hz, $^4J_{\text{H-H}} = 1.1$ Hz), 3.93 (propyl N-CH_2 , td, 2H, $^3J_{\text{H-H}} = 6.8$ Hz, $^4J_{\text{H-H}} = 1.1$ Hz), 2.21-2.12 (propyl $\text{CH}_2\text{-CH}_2\text{-CH}_3\text{-Si}$, m, $^3J_{\text{H-H}} = 8$ Hz, 2H), 1.05-1.01 (propyl $\text{CH}_2\text{-CH}_2\text{-CH}_2\text{-Si}$, m, 2H), 4.17 ($\text{Si-O-CH}_2\text{-CH}_3$, q, 6H, $^3J_{\text{H-H}} = 7.0$ Hz), 1.57 ($\text{Si-O-CH}_2\text{-CH}_3$, t, 9H, $^3J_{\text{H-H}} = 7.0$ Hz).

2.7.4 Synthesis of model and functionalized Cu(II) complexes

2.7.4.1 Model bis(salicylaldiminato)Cu(II) complex MC1

2-Propyliminomethyl-phenol **L1** (5.17 mmol, 0.843 g) was dissolved in dry ethanol (5 ml), which resulted in a yellow solution. $\text{Cu}(\text{OAc})_2\text{H}_2\text{O}$ (2.59 mmol, 0.515 g) was added to the solution containing **L1**, which then resulted in a green solution. The reaction mixture was stirred for 6 hours under nitrogen at 80 °C. The solvent was removed *in vacuo* and a green crude powder was obtained. The green crude was purified by simply redissolving it in dry DCM (5 ml) then syringe filtered. The DCM

Chapter 2: Preparation and Characterization of Schiff-base ligands and complexes

solution containing the complex was subjected to slow evaporation of the solvent to obtain green crystals (0.812 g, 81.2 %).

Model complex **MC1**: Green solid, yield 81.2 %. IR: FT-IR, ν/cm^{-1} : 1613 (C=N). Elemental Analysis (%): Calc. For $\text{C}_{20}\text{H}_{24}\text{N}_2\text{O}_2\text{Cu}$ (387.96 g/mol): C, 61.91; H, 6.24; N, 7.22; Found: C, 61.69; H, 6.86; N, 7.17. MS (ESI, m/z): 388.1 $[\text{M}]^+$. Melting Point: 124-126 °C.

2.7.4.2 Functionalized 2-(3-triethoxysilanepropyliminomethyl)-phenolate Cu (II) complex FC1

2-(3-Triethoxysilanepropyliminomethyl)-phenol **L2** (1.00 mmol, 0.326 g) was dissolved in dry ethanol (5 ml), which resulted in a yellow solution. $\text{Cu}(\text{OAc})_2\cdot\text{H}_2\text{O}$ (0.501 mmol, 0.100 g) was added to the solution containing **L2**, which resulted in a green solution. The reaction mixture was stirred for 3 hours under nitrogen at 80 °C. The solvent was removed *in vacuo* and a green crude powder was obtained. The green crude was purified by simply redissolving it in dry DCM (5 ml) after which it was syringe filtered. The solvent was removed from the filtrate *in vacuo* and a green powder was obtained (0.211 g, 60.4 %).

Functionalized complex **FC1**: Green solid, yield 60.4 %. IR: FT-IR, ν/cm^{-1} : 1620 (C=N), 1047 (Si-O), 755 (Si-O). Elemental Analysis (%): Calc. For $\text{C}_{32}\text{H}_{52}\text{N}_2\text{O}_8\text{Si}_2\text{Cu}$ (712.48 g/mol): C, 53.29; H, 7.36; N, 3.93; Found: C, 53.71; H, 6.99; N, 3.91. Melting Point: 236-239 °C.

2.7.5 Synthesis of model and functionalized Co(II) complexes**2.7.5.1 Model bis(salicylaldiminato)Co(II) complex MC2**

2-Propyliminomethyl-phenol **L1** (4.02 mmol, 0.655 g) was dissolved in dry ethanol (5 ml), which resulted in a yellow solution. $\text{Co}(\text{OAc})_2\cdot 4\text{H}_2\text{O}$ (2.01 mmol, 0.500 g) was added to the solution containing **L1**, which then resulted in a pink-orange solution. The reaction mixture was stirred for 4 hours under nitrogen at 80 °C. The solvent was removed *in vacuo* and a green crude powder was obtained. The green crude material was purified by simply redissolving it in dry DCM (5 ml) and then syringe filtered. The DCM solution containing the complex was allowed to evaporate slowly to obtain green crystals (0.686 g, 74.0 %).

Model complex **MC2**: Green solid, yield 74.0 %. IR: FT-IR, ν/cm^{-1} : 1612 (C=N). Elemental Analysis (%): Calc. For $\text{C}_{20}\text{H}_{24}\text{N}_2\text{O}_2\text{Co}$ (383.35 g/mol): C, 62.66; H, 6.31; N, 7.31; Found: C, 60.30; H, 6.27; N, 6.67. MS (ESI, m/z): 383.1 $[\text{M}]^+$. Melting Point: 214.1-216.2 °C.

2.7.5.2 Functionalized 2-(3-triethoxysilanepropyliminomethyl)-phenolate Co (II) complex FC2

2-(3-Triethoxysilanepropyliminomethyl)-phenol **L2** (1.41 mmol, 0.470 g) was dissolved in dry ethanol (5 ml), which resulted in a yellow solution. $\text{Co}(\text{OAc})_2 \cdot 4\text{H}_2\text{O}$ (0.706 mmol, 0.180 g) was added to the solution containing **L2**, which then resulted in a pink-orange solution. The reaction mixture was stirred for 3 hours under nitrogen at 80 °C. After the allotted time, a green-brown precipitate formed. The solid was filtered and washed with dry methanol (2 x 5 ml). The solid was dried for 6 hours under vacuum and a green-brown powder was obtained (0.379 g, 74.4 %).

Functionalized complex **FC2**: Green solid, yield 74.4 %. IR: FT-IR, ν/cm^{-1} : 1622 (C=N), 1047 (Si-O), 755 (Si-O). Elemental Analysis (%): Calc. For $\text{C}_{32}\text{H}_{52}\text{N}_2\text{O}_8\text{Si}_2\text{Co}$ (707.87 g/mol): C, 54.29; H, 7.40; N, 3.96; Found: C, 53.97; H, 6.93; N, 3.78. Melting Point: >300 °C.

2.7.6 Synthesis of model and functionalized Pd(II) complexes

2.7.6.1 Model bis(salicylaldiminato)Pd(II) complex MC3

2-Propyliminomethyl-phenol **L1** (1.34 mmol, 0.218 g) was dissolved in dry acetone (10 ml), which resulted in a yellow solution. $\text{Pd}(\text{OAc})_2$ (0.668 mmol, 0.150 g) was suspended in this yellow solution, which then resulted in a brown-orange suspension. The reaction mixture was refluxed for 3 hours under nitrogen at 55 °C. The solvent was removed *in vacuo* and an orange-yellow powder was obtained. The orange-yellow crude material was recrystallized from dichloromethane and ethanol at a relatively low temperature (-4 °C) which resulted in orange crystals (0.183 g, 77.0 %).

Model complex **MC3**: IR: FT-IR, ν/cm^{-1} : 1612 (Imine, HC=N). ^1H NMR (400 MHz, CDCl_3): δ (ppm) = 7.62 (H_{imine} , s, 1H), 7.27-7.22 (H_{Ar} , m, 1H), 7.18 (H_{Ar} , dd, 1H, $^3J_{\text{H-H}} = 7.9$ Hz, $^4J_{\text{H-H}} = 1.9$ Hz), 6.86 (H_{Ar} , d, 1H, $^3J_{\text{H-H}} = 8.4$ Hz), 6.54-6.50 (H_{Ar} , m, 1H), 3.97 (propyl N- $\text{CH}_2\text{-CH}_2\text{-CH}_3$, t, 2H, $^3J_{\text{H-H}} = 7.3$ Hz), 1.83 (propyl $\text{CH}_2\text{-CH}_2\text{-CH}_3$, sextet, 2H, $^3J_{\text{H-H}} = 7.5$ Hz), 0.98 (propyl N- $\text{CH}_2\text{-CH}_2\text{-CH}_3$, t, 3H, $^3J_{\text{H-H}} = 7.4$ Hz). Elemental Analysis (%): Calc. For $\text{C}_{20}\text{H}_{24}\text{N}_2\text{O}_2\text{Pd}$ (430.1 g/mol): C, 55.76; H, 5.62; N, 6.50; Found: C, 55.03; H, 6.13; N, 6.40. MS (ESI, m/z): 431.1 $[\text{M}+\text{H}]^+$. Melting Point: 192-194 °C.

2.7.6.2 Functionalized 2-(3-triethoxysilanepropyliminomethyl)-phenolate Pd (II) complex FC3

2-(3-Triethoxysilanepropyliminomethyl)-phenol **L2** (1.34 mmol, 0.218 g) was dissolved in dry acetone (10 ml), which resulted in a yellow solution. $\text{Pd}(\text{OAc})_2$ (0.668 mmol, 0.150 g) was suspended in this yellow solution, which then resulted in a brown-orange suspension. The reaction mixture was refluxed for 3 hours under nitrogen at 55 °C. The solvent was removed *in vacuo* and an orange-

Chapter 2: Preparation and Characterization of Schiff-base ligands and complexes

yellow powder was obtained. The orange-yellow crude material was recrystallized from dichloromethane and ethanol at a relatively low temperature (-4 °C) which resulted in a yellow powder (0.262 g, 52.4 %).

Functionalized complex **FC3**: IR: FT-IR, ν/cm^{-1} : 1619 (Imine, HC=N), 1047 (Si-O), 755 (Si-O). ^1H NMR (600 MHz, CDCl_3): δ (ppm) = 7.64 (H_{imine} , s, 1H), 7.23-7.20 (H_{Ar} , m, 1H), 7.16 (H_{Ar} , dd, 1H, $^3J_{\text{H-H}} = 7.9$ Hz, $^4J_{\text{H-H}} = 1.8$ Hz), 6.86 (H_{Ar} , d, 1H, $^3J_{\text{H-H}} = 8.4$ Hz), 6.57-6.54 (H_{Ar} , m, 1H), 3.71 (propyl N- $\text{CH}_2\text{-CH}_2\text{-CH}_3\text{-Si}$, m, 2H), 1.92 (propyl N- $\text{CH}_2\text{-CH}_2\text{-CH}_3\text{-Si}$, m, 2H), 0.69 (propyl $\text{CH}_2\text{-CH}_2\text{-CH}_2\text{-Si}$, m, 2H), 3.80 (Si-O- $\text{CH}_2\text{-CH}_3$, q, 6H, $^3J_{\text{H-H}} = 7.0$ Hz), 1.19 (Si-O- $\text{CH}_2\text{-CH}_3$, t, 9H, $^3J_{\text{H-H}} = 7.0$ Hz). Elemental Analysis (%): Calc. For $\text{C}_{32}\text{H}_{52}\text{N}_2\text{O}_8\text{Si}_2\text{Pd} \cdot (755.3 \text{ g/mol})$: C, 50.88; H, 6.94; N, 3.71; Found: C, 50.58; H, 6.23; N, 3.63. Melting Point: >300 °C, colour change from yellow to brown-black 257-260 °C.

2.8 References

- 1 P. Bruijninx, G.-J. Gruter, A. Westenbroek and E. Engelen-Smeets, *Lignin Valorisation The importance of a full value chain approach*, 2016.
- 2 A. Das, A. Rahimi, A. Ulbrich, M. Alherech, A. H. Motagamwala, A. Bhalla, L. Da Costa Sousa, V. Balan, J. A. Dumesic, E. L. Hegg, B. E. Dale, J. Ralph, J. J. Coon and S. S. Stahl, *ACS Sustain. Chem. Eng.*, 2018, **6**, 3367–3374.
- 3 S. K. Hanson and R. T. Baker, *Acc. Chem. Res.*, 2015, **48**, 2037–2048.
- 4 M. M. Gupta, M. M. Gupta, Rajnikant, V. K. Gupta, P. A. Gale and C.-H. Lee, *New J. Chem.*, 2015, **39**, 3578–3587.
- 5 V. O. Sippola and A. O. I. Krause, *Catal. Today*, 2005, **100**, 237–242.
- 6 Y. Salman, F. B. Barlas, M. Yavuz, K. Kaya, S. Timur and F. Ç. Telli, *Inorganica Chim. Acta*, 2018, **483**, 98–105.
- 7 M. Sebastian, V. Arun, P. P. Robinson, A. A. Varghese, R. Abraham, E. Suresh and K. K. M. Yusuff, *Polyhedron*, 2010, **29**, 3014–3020.
- 8 A. K. Meher and Y. C. Chen, *Anal. Chim. Acta*, 2016, **937**, 106–112.
- 9 C. R. Nayar and R. Ravikumar, *J. Coord. Chem.*, 2014, **67**, 1–16.
- 10 M. T. . Tarafder, K.-B. Chew, K. A. Crouse, A. . Ali, B. . Yamin and H.-K. Fun, *Polyhedron*,

Chapter 2: Preparation and Characterization of Schiff-base ligands and complexes

- 2002, **21**, 2683–2690.
- 11 P. U. Naik, G. J. McManus, M. J. Zaworotko and R. D. Singer, *J. Chem. Soc. Dalt. Trans.*, 2008, 4834–4836.
- 12 P. Arthi, D. Mahendiran, S. Shobana, P. Srinivasan and A. K. Rahiman, *J. Mol. Struct.*, 2018, **1161**, 306–319.
- 13 R. A. Festa and D. J. Thiele, *Curr. Biol.*, 2011, **21**, R877–R883.
- 14 K. Czarnek, S. Terpilowska and A. K. Siwicki, *Cent. Eur. J. Immunol.*, 2015, **40**, 236–242.
- 15 V. Sippola, O. Krause and T. Vuorinen, *J. Wood Chem. Technol.*, 2004, **24**, 323–340.
- 16 K. Kervinen, H. Korpi, M. Leskelä and T. Repo, *J. Mol. Catal. A Chem.*, 2003, **203**, 9–19.
- 17 D. X. Martíneza Vargas, J. Rivera De La Rosa, S. Arif Iyoob, C. J. Lucio-Ortiz, F. J. Cerino Córdoba and C. D. Garcia, *Appl. Catal. A Gen.*, 2015, **506**, 44–56.
- 18 V. D. Chaube, S. Shylesh and A. P. Singh, *J. Mol. Catal. A Chem.*, 2005, **241**, 79–87.
- 19 S. Guieu, F. Cardona, J. Rocha and A. M. S. Silva, *New J. Chem.*, 2014, **38**, 5411–5414.
- 20 S. Uzman, *Spectrosc. Lett.*, 2000, **4**, 445–455.
- 21 A. D. Garnovskii, A. S. Burlov, K. A. Lysenko, D. A. Garnovskii, I. G. Borodkina, A. G. Ponomarenko, G. G. Chigareno, S. A. Nikolaevskii and V. I. Minkin, *Russ. J. Coord. Chem.*, 2009, **35**, 122–129.
- 22 H. Oshita, T. Yoshimura, S. Mori, F. Tani, Y. Shimazaki and O. Yamauchi, *J. Biol. Inorg. Chem.*, 2018, **23**, 51–59.
- 23 A. D. Naik, S. Bourbigot, S. Bellayer, N. Touati, K. Ben Tayeb, H. Vezin and G. Fontaine, *ACS Appl. Mater. Interfaces*, 2018, **12**, 24860–24875.
- 24 M. S. Bukharov, V. G. Shtyrlin, A. S. Mukhtarov, G. V. Mamin, S. Stapf, C. Mattea, A. A. Krutikov, A. N. Il'in and N. Y. Serov, *Phys. Chem. Chem. Phys.*, 2014, **16**, 9411–9421.
- 25 S. Bhatt and B. Trivedi, *Polyhedron*, 2012, **35**, 15–22.
- 26 K. M. Raj, B. Vivekanand, G. Y. Nagesh and B. H. M. Mruthyunjayaswamy, *J. Mol. Struct.*, 2014, **1059**, 280–293.

Chapter 2: Preparation and Characterization of Schiff-base ligands and complexes

- 27 M. T. Räsänen, H. Korpi, M. R. Sundberg, A. Savin, M. Leskelä and T. Repo, *Inorganica Chim. Acta*, 2013, **394**, 203–209.
- 28 W. Fu, L. Yue, X. Duan, J. Li and G. Lu, *Green Chem.*, 2016, **18**, 6136–6142.
- 29 C. E. Satheesh, P. Raghavendra Kumar, P. Sharma, K. Lingaraju, B. S. Palakshamurthy and H. Raja Naika, *Inorganica Chim. Acta*, 2016, **442**, 1–9.
- 30 T. Naota and H. Koori, *J. Am. Chem. Soc.*, 2005, **127**, 9324–9325.
- 31 Apex2, *Data Collect. Softw.*, Bruker AXS, 2010.
- 32 G. M. Sheldrick, *Acta Crystallogr. Sect. A Found. Crystallogr.*, 2008, **64**, 112–122.
- 33 L. J. Barbour, *J. Supramol. Chem.*, 2001, **1**, 189–191.
- 34 POV-Ray, *Version 3.6*, Williamstown, Australia, Persistence of vision ray.

Chapter 3

Preparation and Characterization of immobilized catalysts IC1-IC6.

3.1 Introduction

The pursuit to employ heterogeneous catalysts in catalytic reactions for valorization of lignin has gained much attention in recent years. Although homogeneous catalysis offers higher activity and better selectivity. Heterogeneous catalyst can be important especially given the increasing emphasis on developing greener technologies. This is because heterogeneous systems allow for recyclability and reusability of these type of catalysts.¹ To accomplish heterogeneity, suitable support materials need to be developed and evaluated. In addition, these materials need to be able to withstand very harsh reaction conditions. Since the discovery of mesoporous silica, it has found use in a variety of applications. Some of these include separation science, heterogeneous catalysis, drug delivery and optics.²⁻⁵

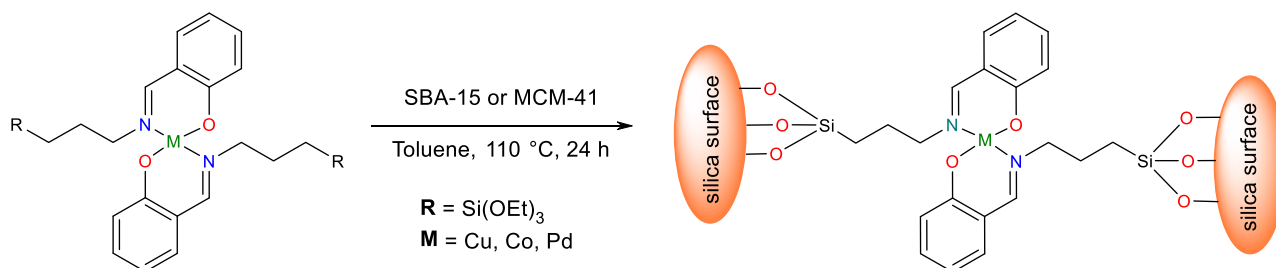
Recently, numerous salen based transition metal complexes have been immobilized onto organic/inorganic support materials. These support materials include, polymers such as Merrifield (chloromethylstyrene–divinylbenzene cross-linked co-polymer) resin beads, zeolites, magnetic nanoparticles, activated carbon, porous silica, MCM-41 and SBA-15.^{3,6-8} These supports usually exhibit high stability and can therefore be employed under harsh reaction conditions.⁹ The preparation of these support materials has extensively been explored using a range of solid-state analytical techniques for heterogeneous catalysis. One of the main objectives in this project is to “heterogenize” homogeneous catalysts, which could potentially allow separation of the catalyst from a reaction mixture.

Mirzaee et al. designed vanadium and molybdenum catalysts using Schiff base-functionalized boehmite nanoparticles as supports. These catalysts showed promising results in the epoxidation of alkenes in the presence of tert-butyl hydrogen peroxide. Furthermore, the catalysts could be recovered and showed moderate recyclability attributes.⁹

Another immobilization example using mesoporous silica was reported by Ayala et al. who used MCM-41 as a support material in the oxidation of sulfides to sulfoxides. The catalyst showed promising results during the recyclability tests (up to five times) with no significant changes in the activity and selectivity of these oxidation reactions.⁸

3.1 Chapter 3: Preparation and Characterization of immobilized catalysts IC1-IC6.

Another example reported by Melián-Rodríguez et al. used a ruthenium metal/metal-oxide heterogenous catalyst in the oxidation of veratryl alcohol to veratraldehyde. This catalyst was recycled up to three times however, the activity changed significantly (about 30 % drop) and the selectivity remained above 50 % towards veratraldehyde, while veratric acid was about 5 %.¹⁰



Scheme 3.1: Immobilization process.

The preparation and characterization of the “heterogenized” complexes (**IC1-IC6**) as well as the native silica, MCM-41 and SBA-15, are discussed in the sections to follow. All materials prepared including the silica native material as well as immobilized complexes were characterized by a range of solid-state analytical techniques. These analytical techniques include, infrared spectroscopy, solid-state ²⁹Si NMR, low angle powder X-ray diffraction, transmission electron microscopy (TEM), scanning electron microscopy (SEM), adsorption/ desorption surface analysis (BET), Thermal gravimetric analysis and inductively coupled plasma - optical emission spectrometry (ICP-OES).

3.2 Results and discussion

3.2.1 Synthesis and characterization of mesoporous silica, MCM-41 and SBA-15

The preparation of the native silica materials, MCM-41 and SBA-15 followed a literature procedure reported by Karandikar et al. and Martínez-Vargas et al.¹¹⁻¹² These materials were simply prepared by reacting tetraethyl orthosilicate (TEOS) with an appropriate surfactant. In the case of MCM-41, cetyltrimethylammonium bromide (CTAB) was used as the surfactant under basic conditions, whereas an acidic medium together with poly(ethyleneglycol)-blockpoly(propyleneglycol)-block-poly(ethyleneglycol) (PEG-PPG copolymer) was used to prepare SBA-15. Both native silica materials were isolated as white powders which were calcined for 8 hours at 550 °C. This was done to remove the residual organic template. Characterization of the native silica material MCM-41 and SBA-15 was achieved by FT-IR(ATR) spectroscopy, (BET) surface analysis, thermal gravimetric analysis (TGA). low-angle powder X-ray diffraction, transmission electron microscopy (TEM) and scanning electron microscopy (SEM).

3.1 Chapter 3: Preparation and Characterization of immobilized catalysts IC1-IC6.**3.3.1.1 Characterization of the native material SBA-15 and MCM-41 by FT-IR spectroscopy.**

The synthesis of the native material was confirmed by FT-IR spectroscopy. Both spectra showed absorbances that is characteristic of these materials and which are reported in the literature. In the FT-IR spectra (**Figure 3.1**), one notable dissimilarity can be observed with respect to the Si-O-Si asymmetric stretching around 1244 cm^{-1} which can only be observed for MCM-41. Strong bands can be observed around $1055/1057\text{ cm}^{-1}$ and $799/808\text{ cm}^{-1}$ which can be assigned to the Si-O and O-Si-O stretching vibrations respectively. ¹³

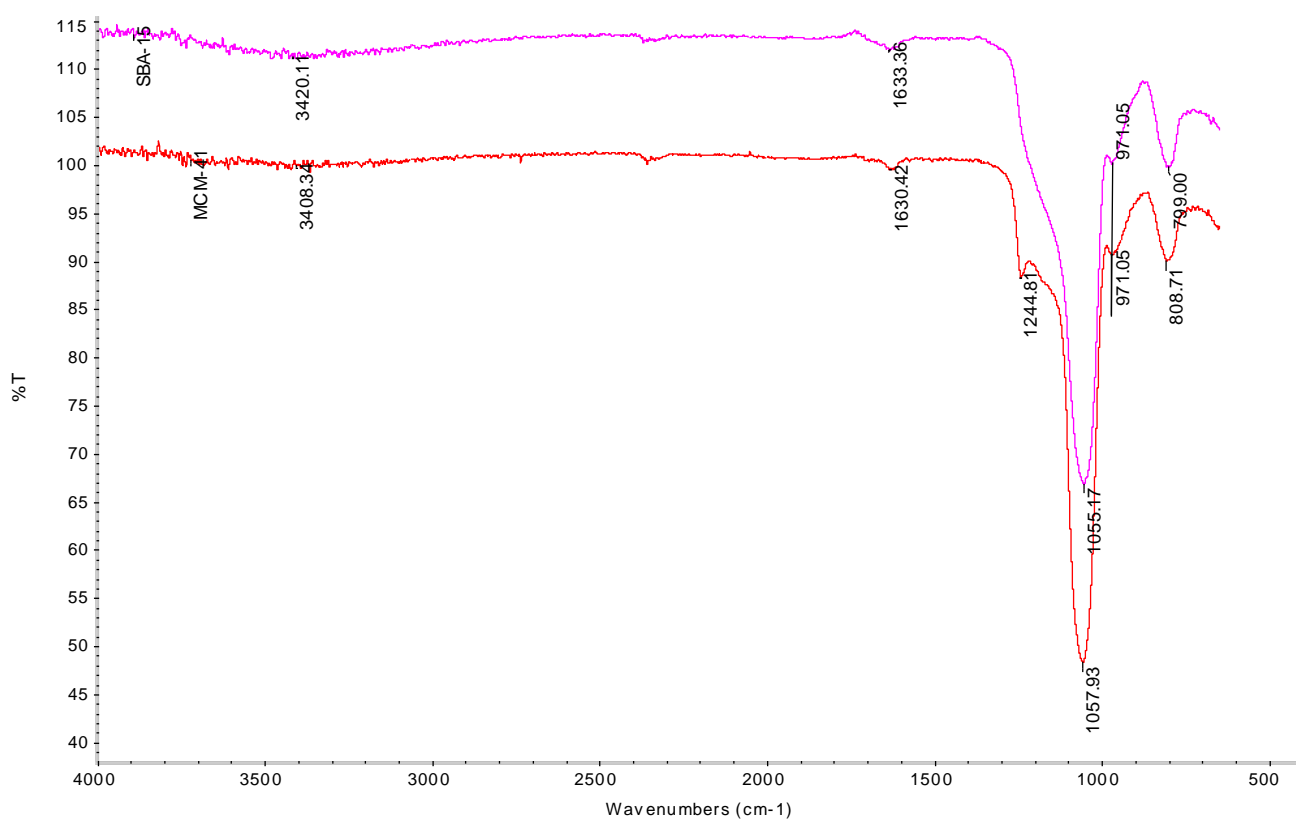


Figure 3.1: FT-IR (ATR) of the native silica materials (SBA-15 & MCM-41).

3.1 Chapter 3: Preparation and Characterization of immobilized catalysts IC1-IC6.**3.3.1.2 Characterization of MCM-41 and SBA-15 via BET analysis.**

BET (Brunauer–Emmett–Teller) surface analysis demonstrated to be a useful technique to determine the surface area (m^2/g), average pore diameter (\AA) and total pore volume (cm^3/g) of the native silica materials. Pre-degassing in the range of 150-230 °C was employed for 18 hours to maintain sample dryness during analysis. Six types of nitrogen adsorption isotherms can arise from BET analysis. These isotherms are categorized based on the adsorption profile that they display.¹⁴ The six isotherms (type I-VI) are shown in **Figure 3.2**. Type I isotherm is considered as the Langmuir isotherm, which is typical for microporous structures whereas type II and III are for non-porous structures. Isotherms type IV and V are characteristic of mesoporous structures.¹⁴

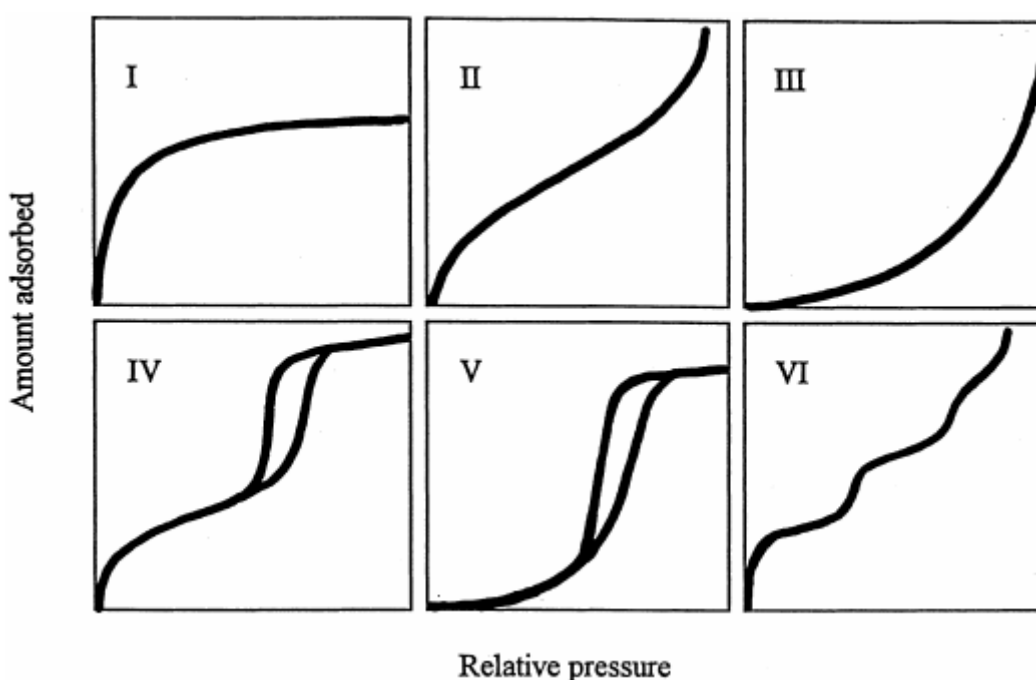


Figure 3.2: Type of BET isotherms.¹⁴

Both MCM-41 and SBA-15 prepared in this project, displayed type IV isotherms, which is characteristic of a mesoporous structure (**Figure 3.3**). The SBA-15 material exhibited a distinct H1 hysteresis loop which is indicative for large pore materials (**Figure 3.3**). MCM-41 exhibited no H1 hysteresis loop which is due to the pore size of the material. An average pore diameter of greater than 40 \AA as well as a temperature lower than 70 K is required for the formation of the H1 hysteresis loop.¹⁵ As such, a smaller average pore diameter was obtained for MCM-41 and a temperature of 77.4 K was used for the BET measurements. Even though both SBA-15 and MCM-41 were measured at 77.4 K, only SBA-15 exhibited this loop which is indicative of the average pore diameter being 55 \AA while MCM-41 exhibited an average pore diameter of 31 \AA which corroborates the abovementioned observation (**Table 3.1**).

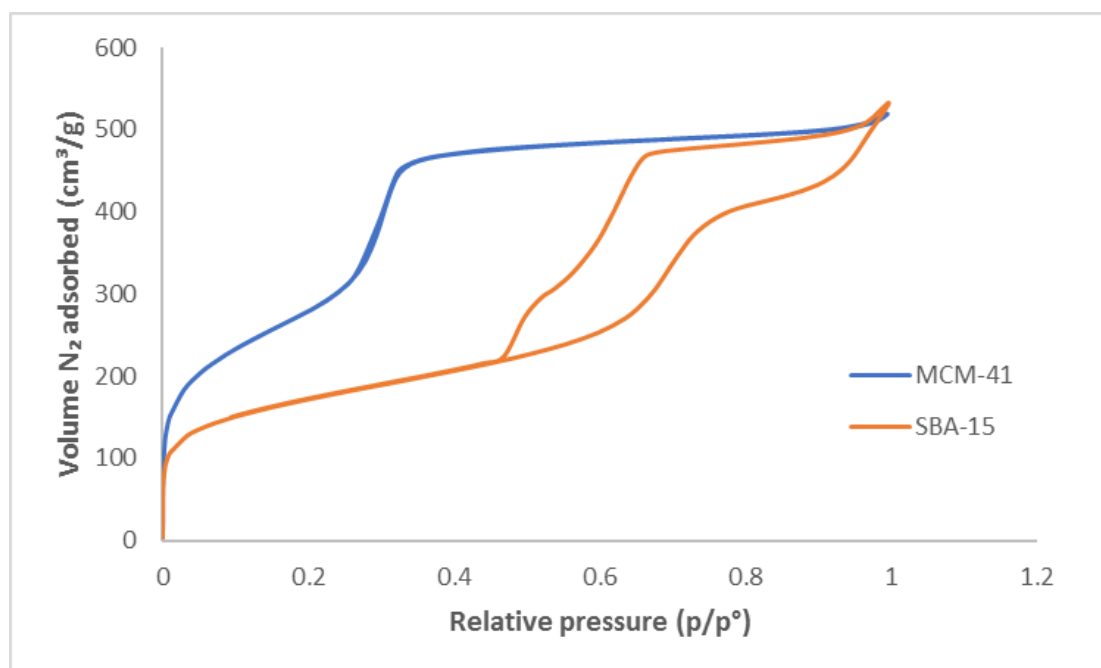
3.1 Chapter 3: Preparation and Characterization of immobilized catalysts IC1-IC6.

Figure 3.3: N₂ adsorption-desorption isotherms of native materials.

The native silica materials, MCM-41 and SBA-15 exhibited surface areas of 1026 m²/g and 601.81 m²/g respectively (**Table 3.1**). It is known that larger surface area is usually inversely proportional to wall thickness.¹⁶ From the BET analysis, MCM-41 showed a larger surface area, which imply that a larger volume of nitrogen gas can be adsorbed. A summary of the total pore volume, surface area and average pore diameter obtained from BET analysis is given in **Table 3.1**.

Table 3.1: Summary of pore volume, surface area and average pore diameter for the native silica materials.

Material	BET Surface area (m ² /g)	Pore Volume (cm ³ /g)	Average Pore diameter (Å)
MCM-41	1026.97	0.81	31.41
SBA-15	601.81	0.83	54.98

All BET measurements were done at 77.4 K.

3.1 Chapter 3: Preparation and Characterization of immobilized catalysts IC1-IC6.**3.3.1.3 Characterization of MCM-41 and SBA-15 via thermal gravimetric analysis (TGA)**

The thermal stability of the native silica materials was investigated by thermal gravimetric analysis (TGA) measurements. Both SBA-15 and MCM-41 underwent weight losses between 75 °C - 100 °C and 200 °C - 600 °C (**Figure 3.4** and **Figure 3.5**). This first weight loss is due to water that is physically adsorbed onto the materials. Further weight loss can be observed at about 340 °C which is due to the decomposition of the surfactant that was partially removed during the calcination process. The TGA results confirmed that the native silica materials are good candidates for the use as a catalyst since it can withstand elevated temperatures.¹⁷

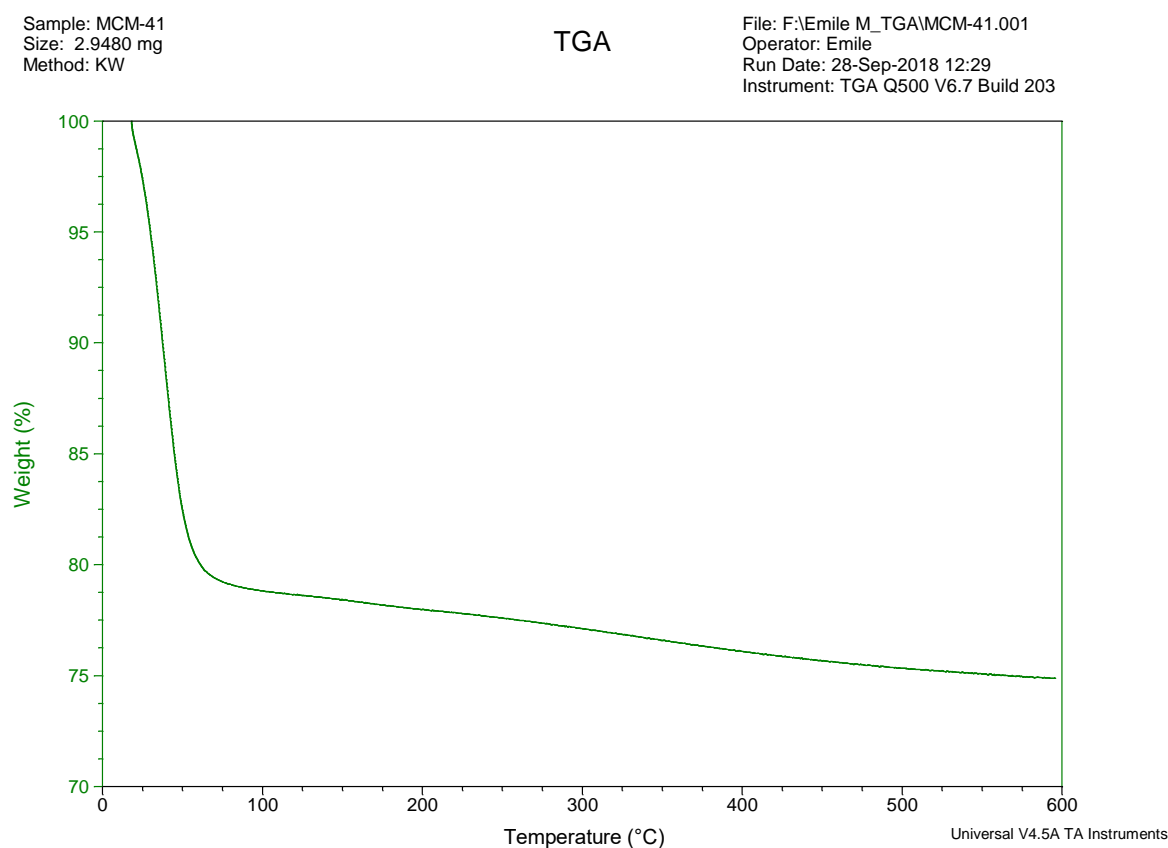


Figure 3.4: TGA analysis of MCM-41.

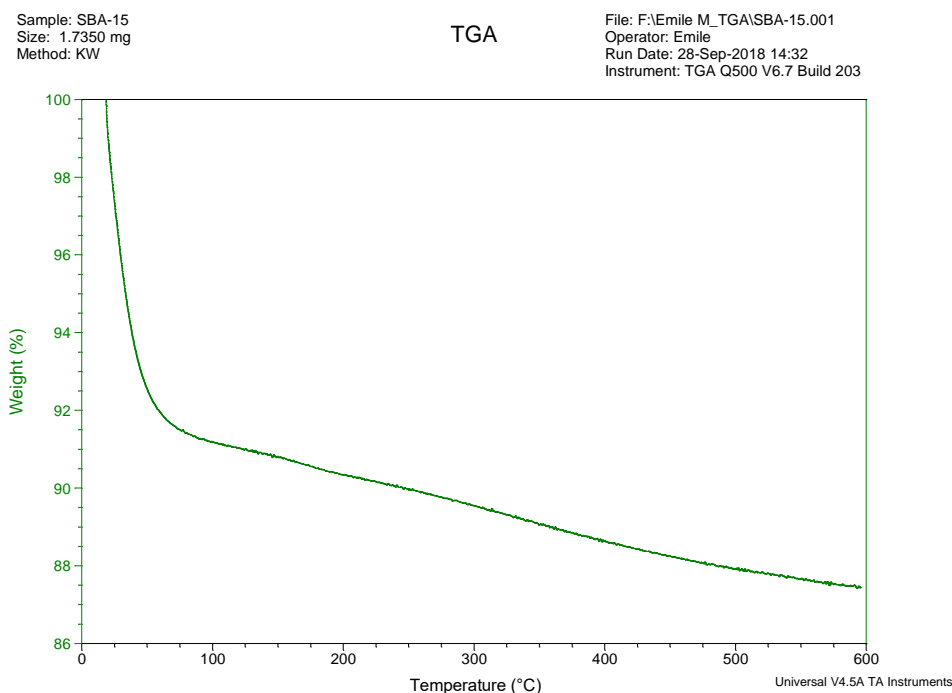
3.1 Chapter 3: Preparation and Characterization of immobilized catalysts IC1-IC6.

Figure 3.5: TGA analysis of SBA-15.

3.3.1.4 Characterization of MCM-41 and SBA-15 by means of ^{29}Si nuclear magnetic resonance (NMR) spectroscopy.

The presence of siloxane moieties in the native silica material, **SBA-15** and **MCM-41** was confirmed by ^{29}Si NMR spectroscopy (**Figure 3.6**). The spectra for both materials showed characteristic peaks which can be attributed to the silanol signals Q^2 (92.31 ppm) and Q^3 (101.84 ppm) (**Figure 3.6**). These distinct resonances are typical for the siloxane functionality [$\text{Q}^n = \text{Si}(\text{OSi})_n - (\text{OH})_{4-n}$]. The NMR spectra, confirm the presence of the siloxanes.¹⁸

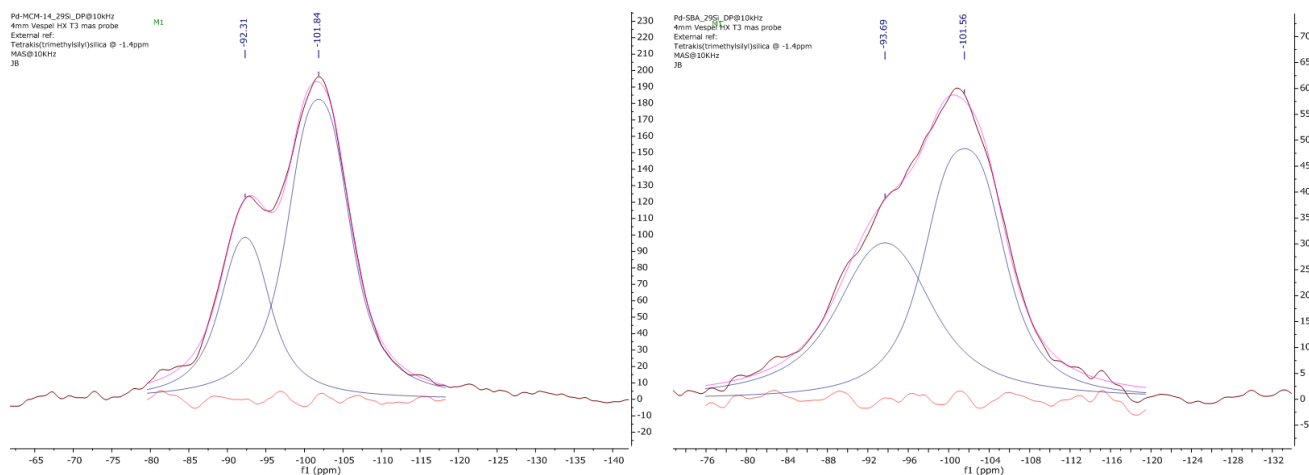


Figure 3.6: Deconvoluted ^{29}Si Nuclear Magnetic resonance spectrum of native silica material MCM-41(left) and SBA-15(right).

3.1 Chapter 3: Preparation and Characterization of immobilized catalysts IC1-IC6.**3.3.1.5 Characterization of MCM-41 and SBA-15 by means of Powder X-Ray Diffraction (XRD)**

A powder X-ray diffraction plot was obtained for the native silica materials (**MCM-41** and **SBA-15**). Four diffraction peaks at 100 ($2\theta = 2.32^\circ$), 110 ($2\theta = 4.04^\circ$), 200 ($2\theta = 4.94^\circ$) and 210 ($2\theta = 6.09^\circ$) can be observed for **MCM-41**, whereas only three diffraction peaks can be observed for **SBA-15** (**Figure 3.7**). Diffraction peaks 110, 200 and 210 were detected at $2\theta = 1.72^\circ$, 1.94° and 2.34° respectively and confirms a highly ordered structure, whereas the reflection peak 100 ($2\theta = 0.88^\circ$) is related to a typical mesoporous structure which can also be associated with a hexagonal symmetry. The diffraction peak (210) with low intensity is evidence that the material has a high degree of crystallinity.¹⁹

The X-ray diffraction peaks are summarized in **Table 3.2**.

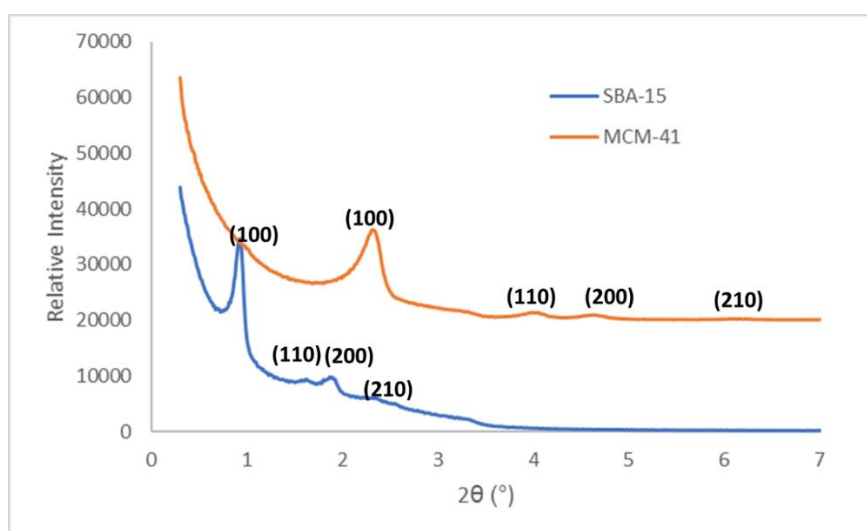


Figure 3.7: Powder X-ray diffraction of the native silica materials.

Table 3.2: Powder X-ray diffraction data for native silica.

Material	Diffraction peaks (2θ)			
	100	110	200	210
SBA-15	0.88	1.72	1.94	2.34
MCM-41	2.32	4.04	4.94	6.09

3.1 Chapter 3: Preparation and Characterization of immobilized catalysts IC1-IC6.**3.3.1.6 Characterization of MCM-41 and SBA-15 by means scanning electron microscopy (SEM) and transmission electron microscopy (TEM).**

Surface morphology analysis of the native silica was performed using scanning electron microscopy (SEM). The SEM images clearly confirm hexagonal structures, which correlates well with **MCM-41** characteristics reported in literature. **SBA-15**, displays particles with a more spherical morphology. (**Figure 3.8**).

A high-resolution micrograph was obtained from TEM analysis. The TEM micrograph for the native material SBA-15, displays the expected arrays of the mesoporous channels. In the image below, a top view clearly shows the pores (**Figure 3.9**, green circle) and a side confirms the array of mesoporous channels (**Figure 3.9**, red circle). This is similar for **MCM-41**, however we could only obtain a side view for this native material. (**Figure 3.9**)

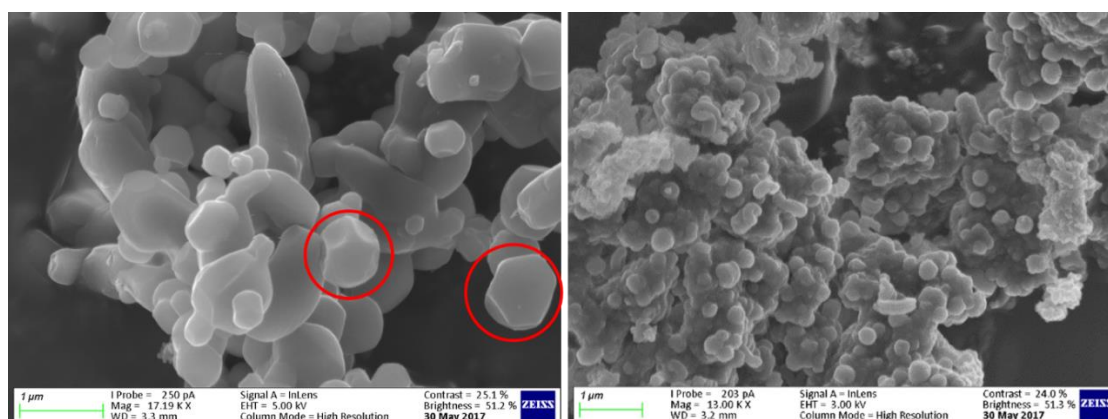


Figure 3.8: SEM micrographs of native silica materials, **MCM-41**(left) and **SBA-15**(right).

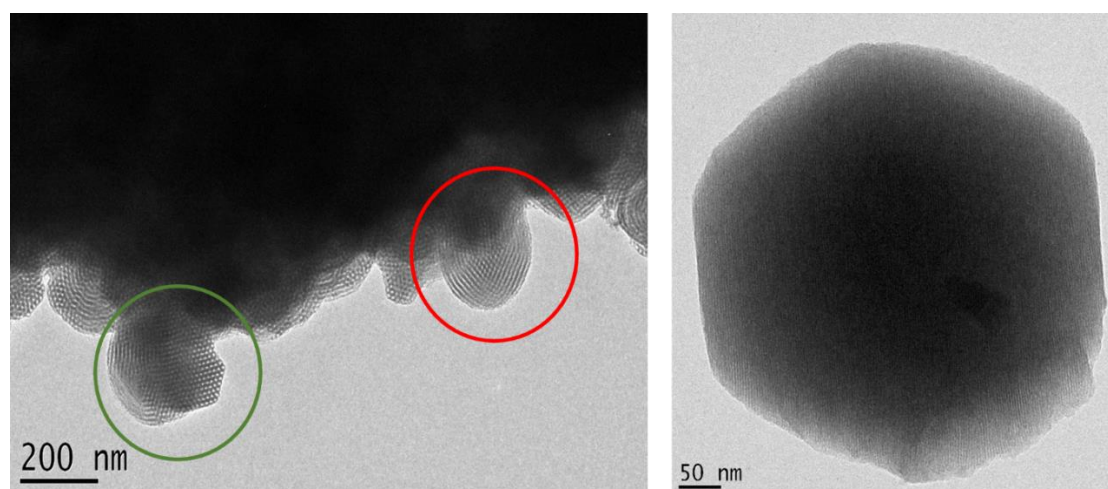
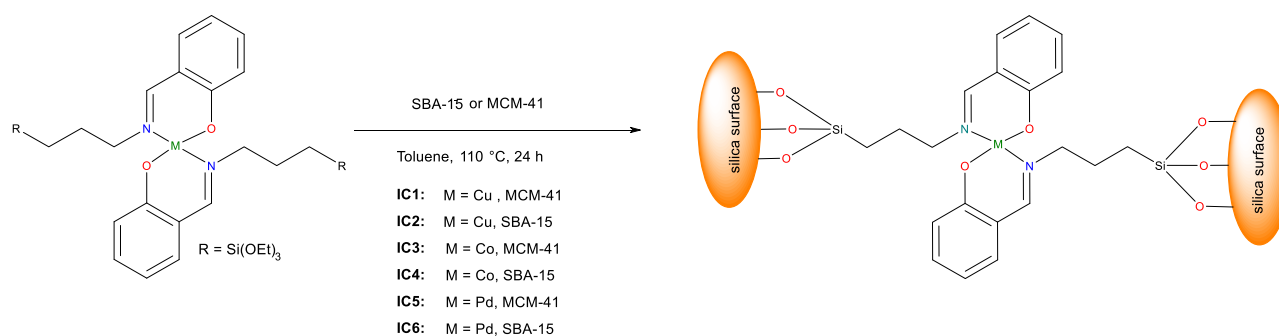


Figure 3.9: TEM micrographs of native silica materials, **SBA-15**(left) and **MCM-41**(right).

3.1 Chapter 3: Preparation and Characterization of immobilized catalysts IC1-IC6.**3.3 Synthesis and characterization of immobilized catalysts**

The immobilization of the complexes comprised the reaction of a functionalized salicylaldimine complex via condensation with surface hydroxy groups of an inorganic support material such as silica. This allows the functionalized complex to bond covalently to the silica. The preparation of the immobilized complexes are shown in **Scheme 3.2**.



Scheme 3.2: Preparation of immobilized catalysts **IC1-IC6**.

In the current work, 10 % of the functionalized complex was reacted with the native silica material. This was done by simply partially dissolving the complex in an appropriate amount of dry dichloromethane and then adding it to a slurry containing toluene and the respective support material. The insoluble cobalt complex (**FC2**) were added to the respective support as a powder. This was then allowed to react for 24 hours at 110 °C. After the allotted time, the reaction mixtures were filtered, washed with methanol or dichloromethane and dried *in vacuo* for 18 hours at 70 °C. After drying, light green powders were obtained for **IC1-IC4**, whereas **IC5-IC6** yielded light yellow powders.

3.3.1 Characterization of immobilized catalysts, IC1-IC6.

All the immobilized catalysts were characterized by inductively coupled plasma - optical emission spectrometry analysis (ICP-OES), FT-IR (ATR) spectroscopy, BET surface analysis, powder X-ray diffraction, scanning electron microscopy (SEM), transmission electron microscopy (TEM) and thermal gravimetric analysis (TGA).

3.1 Chapter 3: Preparation and Characterization of immobilized catalysts IC1-IC6.**3.3.1.1 Characterization of immobilized catalysts, IC1-IC6, by means of FT-IR (ATR) spectroscopy.**

The FT-IR spectra of the respective SBA-15 and MCM-41 immobilized catalysts are shown in **Figures 3.10** and **3.11** respectively. Both spectra display no distinct differences in the IR spectra, which is due to the relatively low loading of the functionalized complex onto the silica surfaces. This is confirmed by the intense bands of the siloxane moiety that can be seen on the spectra since the organometallic region is not visible.

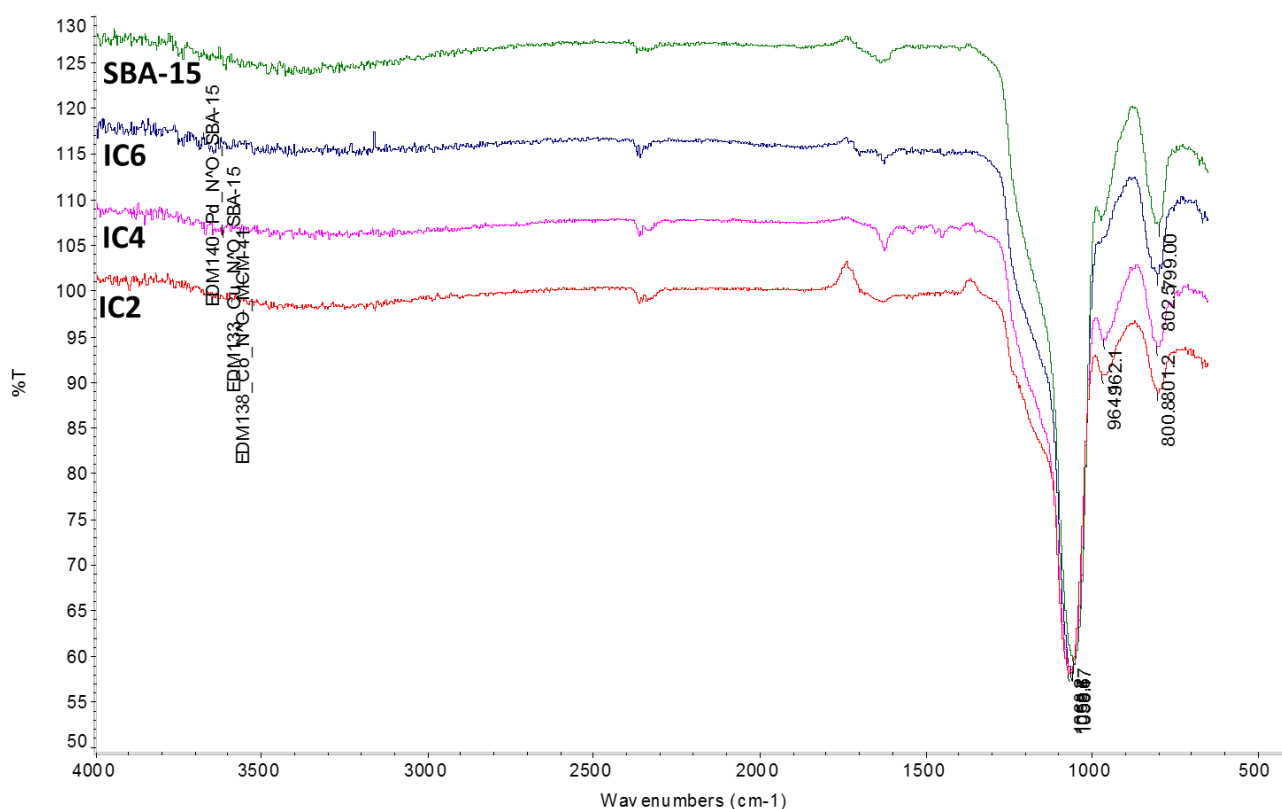


Figure 3.10: FT-IR(ATR) spectra of immobilized catalysts based on material SBA-15.

3.1 Chapter 3: Preparation and Characterization of immobilized catalysts IC1-IC6.

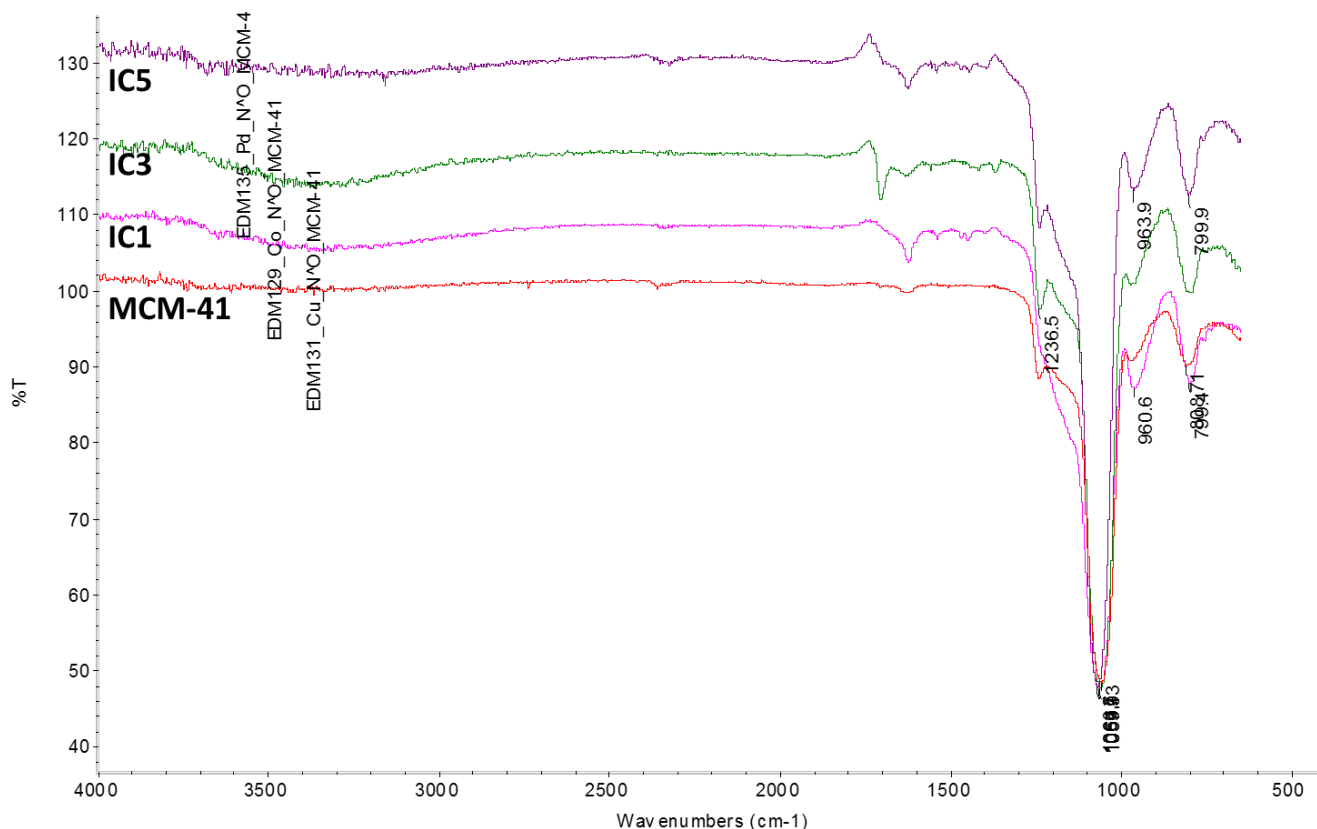


Figure 3.11: FT-IR(ATR) spectra of immobilized catalysts containing silica native material MCM-41.

3.3.1.2 Characterization of immobilized catalysts, IC1-IC6, by means of ICP-OES spectroscopy.

Inductively coupled plasma - optical emission spectrometry (ICP-OES) analysis proved to be a useful technique to determine the metal loading on the support material. The immobilized catalysts (**IC1-IC4**) were pre-digested in concentrated nitric acid, whereas aqua-regia was used to digest catalysts (**IC5-IC6**). After the digestion, any residual material was filtered off and the mother liquor was analysed.

The low loading for **IC2** and **IC3** could possibly be due to the functionalized complex having low solubility in the solvent system used for the immobilization.

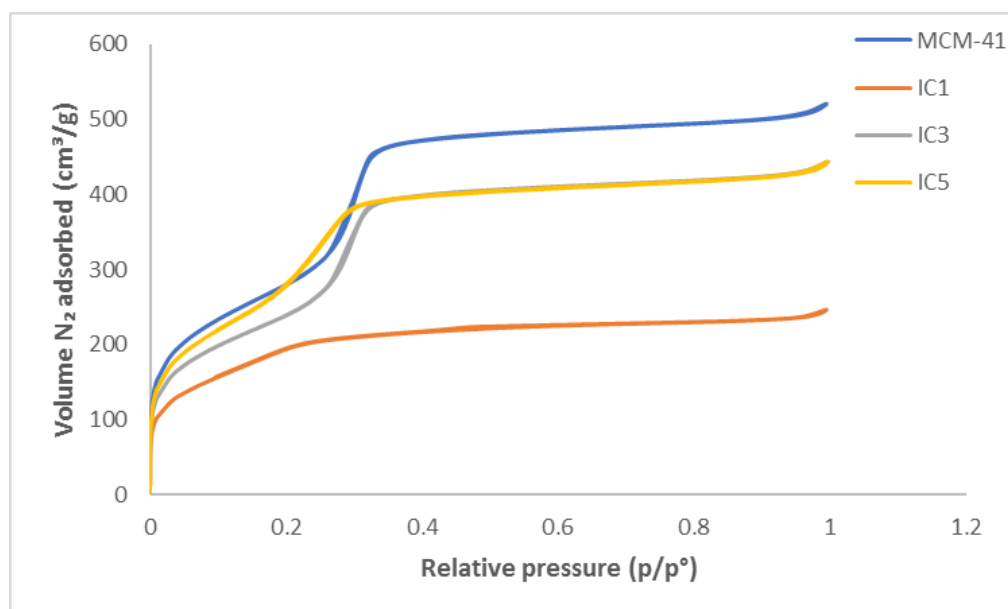
3.1 Chapter 3: Preparation and Characterization of immobilized catalysts IC1-IC6.**Table 3.3:** A summary of the metal loading determined by ICP-OES for the immobilized catalysts IC1-IC6.^a

Material	Metal loading % (w/w)
IC1 (MCM-41)	0.978
IC2 (SBA-15)	0.280
IC3 (MCM-41)	0.369
IC4 (SBA-15)	1.03
IC5 (MCM-41)	0.885
IC6 (SBA-15)	0.860

^a 100 mg of functionalized complex immobilized onto 1.00 gram of silica.

3.3.1.3 Characterization of MCM-41 and SBA-15 via BET surface analysis.

BET surface analysis was used to determine whether the surface area of the material changed after immobilization. A decrease in nitrogen volume adsorption can be anticipated as a result of immobilization. This trend is distinctly seen for immobilized catalysts consisting of MCM-41 (Figure 3.12) and SBA-15 (Figure 3.13) derivatives, which displayed type IV isotherms.

**Figure 3.12:** BET measurements of immobilized catalysts containing silica native material MCM-41.

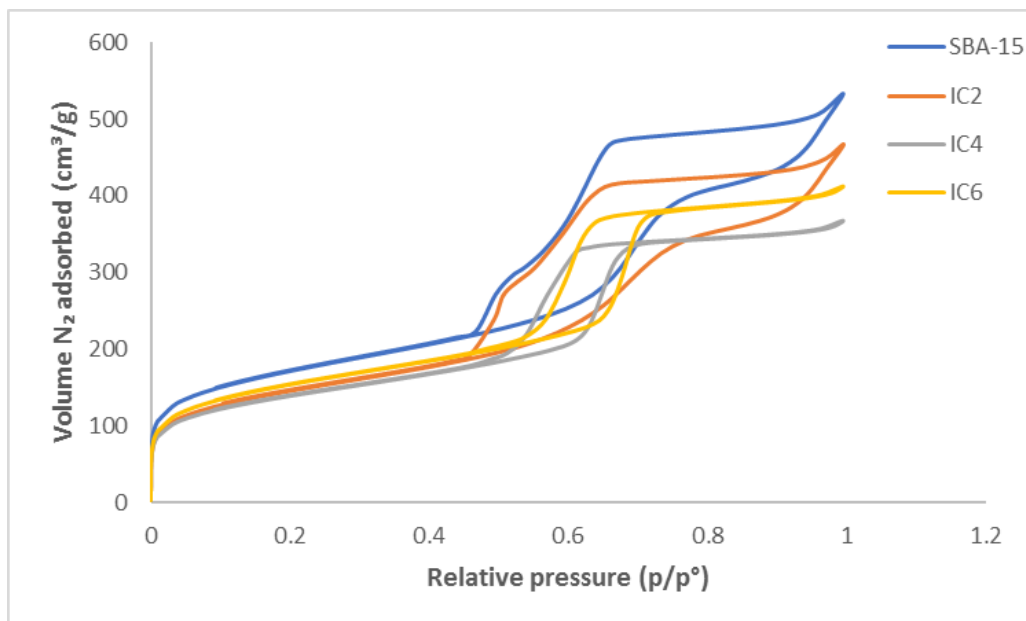
3.1 Chapter 3: Preparation and Characterization of immobilized catalysts IC1-IC6.

Figure 3.13: BET measurements of immobilized catalysts containing silica native material SBA-15.

The BET surface analysis displays a decrease in surface area, average pore diameter and total pore volume for all immobilized catalysts in comparison to the native material, MCM-41 and SBA-15. This is conclusive evidence that the functionalized complexes are immobilized onto the supports. These results are summarized in **Table 3.4**.

Table 3.4: A summary of surface area, pore volume and average pore diameter of immobilized catalysts as well as their respective support material.

Material	BET Surface area (m ² /g)	Pore Volume (cm ³ /g)	Average Pore diameter (Å)
MCM-41	1027	0.81	31.41
IC1 (MCM-41)	677	0.38	22.61
IC3 (MCM-41)	865	0.69	22.79
IC5 (MCM-41)	1017	0.69	27.03
SBA-15	602	0.83	54.98
IC2 (SBA-15)	509	0.73	46.97
IC4 (SBA-15)	491	0.57	46.54
IC6 (SBA-15)	541	0.64	47.28

3.1 Chapter 3: Preparation and Characterization of immobilized catalysts IC1-IC6.**3.3.1.4 Characterization of immobilized catalysts (IC1-IC6) via thermal gravimetric analysis (TGA).**

The thermal stability of the immobilized catalysts (**IC1-IC6**) were investigated using thermal gravimetric analysis (TGA) measurements. The TGA plots for immobilized catalysts, **IC1** and **IC2** are shown below in **Figure 3.14** and **Figure 3.15** respectively. Both **IC1** and **IC2** exhibit weight losses below 100 °C. This weight loss of 2-10 % can be attributed to residual water that physically adsorbed onto the surface of the materials as well as residual toluene starting to volatilize at 110 °C. Further weight loss of 2-3 % for **IC1** can be observed between 300 °C and 400 °C as well as constant weight loss for **IC2**, which is due to the decomposition of the ligand scaffold of the functionalized complex. The TGA analysis confirmed that the immobilized catalysts are good candidates as precursors that could potentially be used in catalysis since it withstands elevated temperatures.

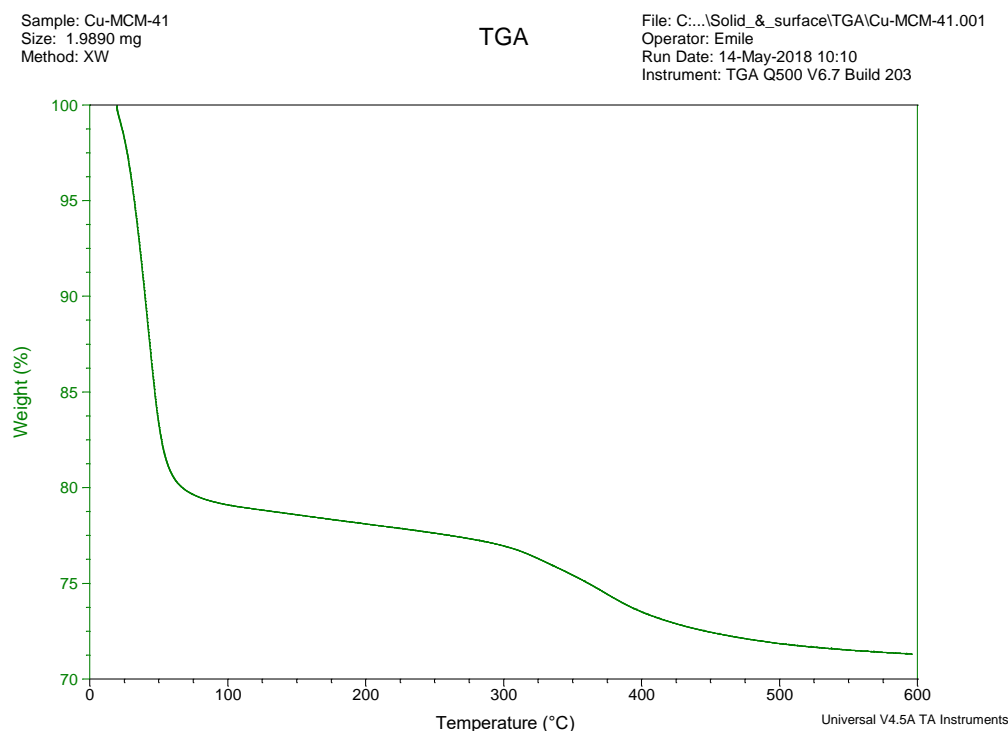


Figure 3.14: TGA analysis of immobilized catalyst **IC1** supported on MCM-41.

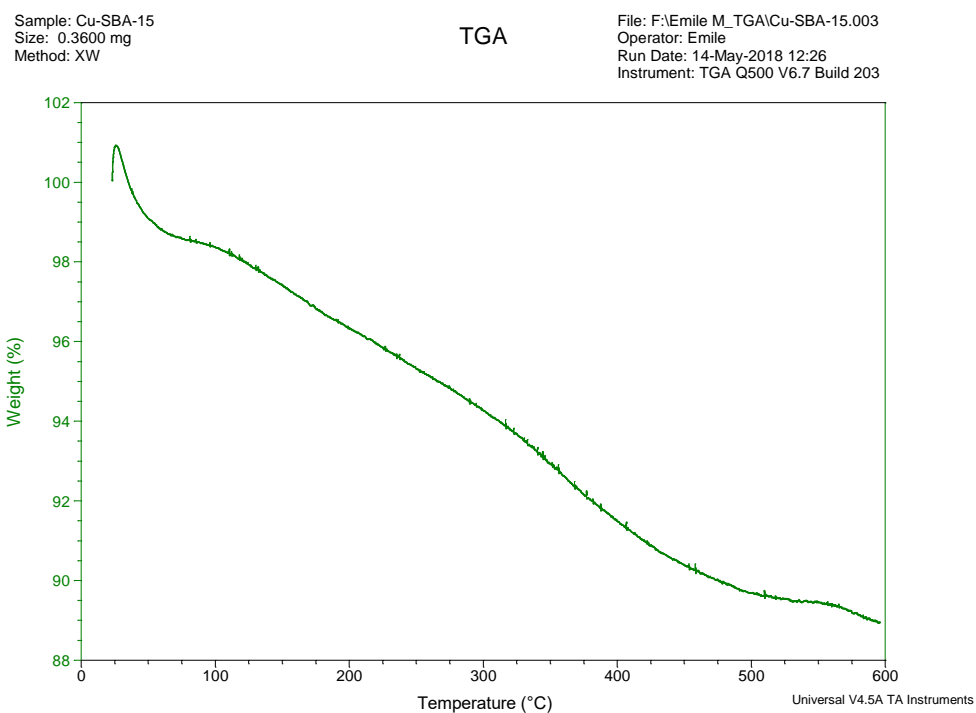
3.1 Chapter 3: Preparation and Characterization of immobilized catalysts IC1-IC6.

Figure 3.15: TGA analysis of immobilized catalyst **IC2** containing support material SBA-15.

3.3.1.5 Characterization of immobilized catalyst IC1-IC6 by means of Powder X-Ray Diffraction (XRD).

Powder X-ray diffraction was also employed to study the immobilized catalysts **IC1-IC6**. No significant changes were observed for the immobilized catalysts compared to the native supports. Four diffraction peaks at 100, 110, 200, 210 were observed for the **MCM-41** derivatives (**Figure 3.16**), whereas only three diffraction peaks at 100, 110 and 200 were observed for the **SBA-15** derivatives (**Figure 3.17**). There were also no changes in the 2 theta values. However, the intensity of some of the immobilized catalyst decreased which is indicative of the functionalized complex occupying pores in the materials. The materials obtained after immobilization preserved the characteristics of the mesoporous structures **MCM-41** and **SBA-15**.

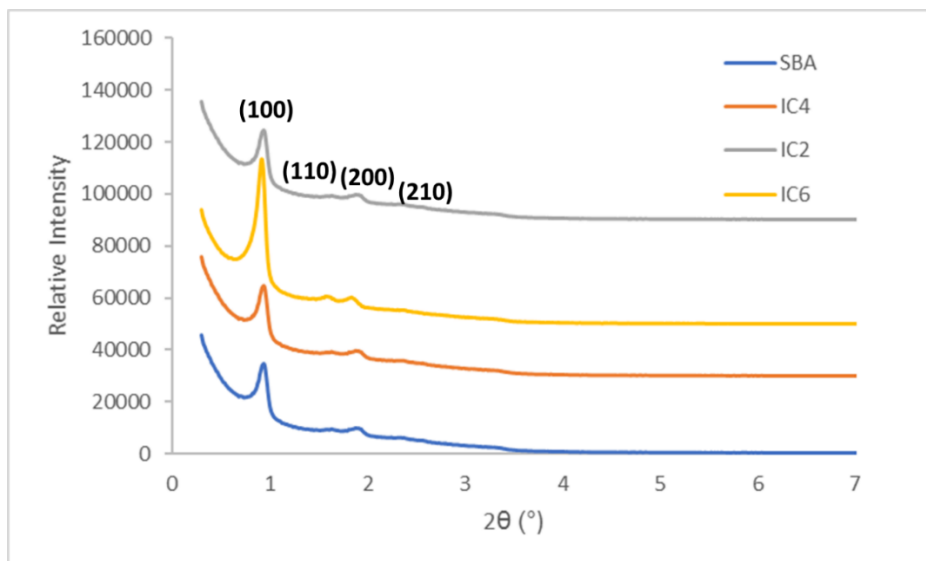
3.1 Chapter 3: Preparation and Characterization of immobilized catalysts IC1-IC6.

Figure 3.16: Powder X-ray diffraction plots of the immobilized catalyst containing native silica support SBA-15.

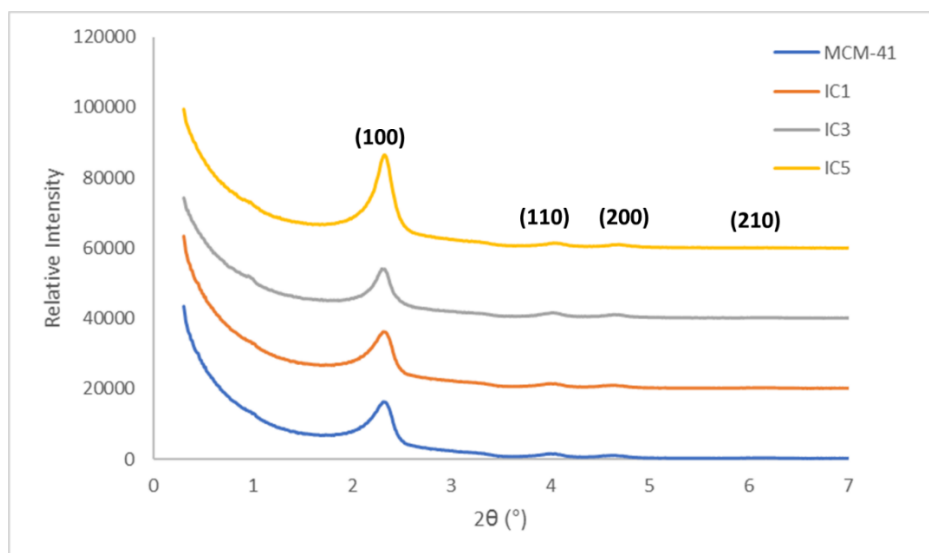


Figure 3.17: Powder X-ray diffraction plots of the immobilized catalyst containing native silica support MCM-41.

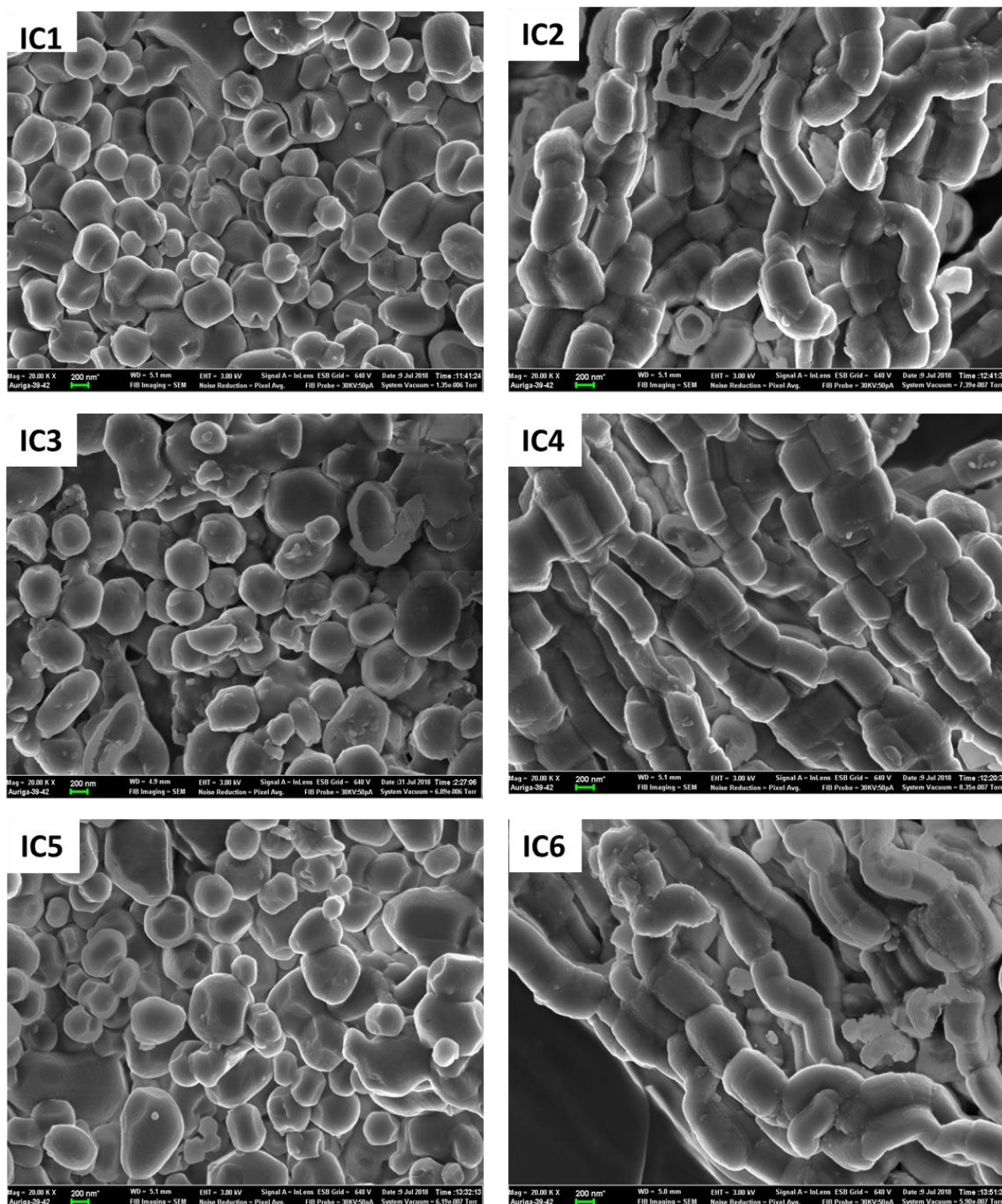
3.1 Chapter 3: Preparation and Characterization of immobilized catalysts IC1-IC6.**3.3.1.6 Characterization of immobilized catalysts, IC1-IC6, by means of scanning electron microscopy (SEM) and transmission electron microscopy (TEM).**

Figure 3.18: SEM micrographs of the immobilized catalysts IC1-IC6.

3.1 Chapter 3: Preparation and Characterization of immobilized catalysts IC1-IC6.

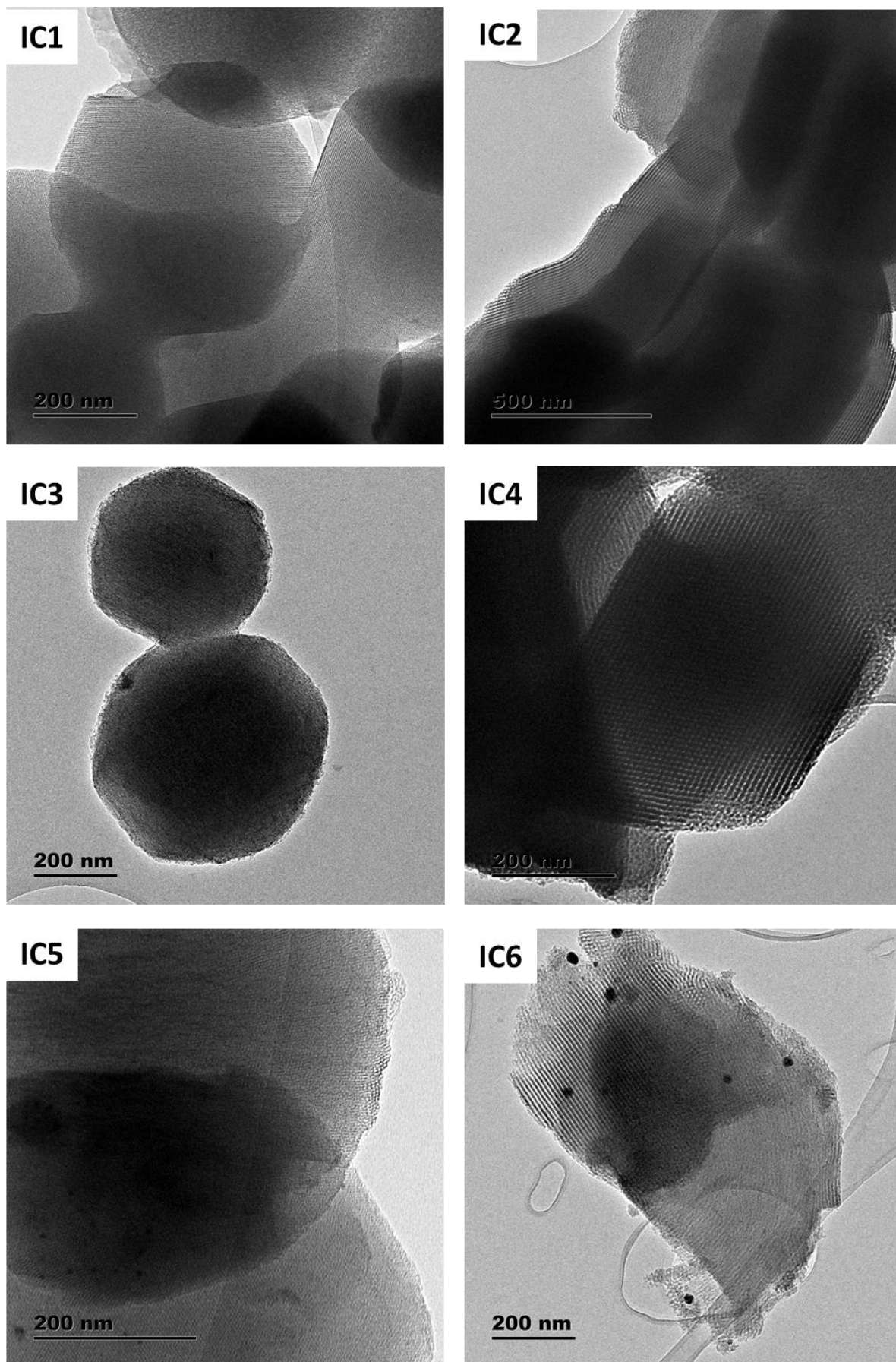


Figure 3.19: TEM micrographs of the immobilized catalysts IC1-IC6.

3.1 Chapter 3: Preparation and Characterization of immobilized catalysts IC1-IC6.

Surface morphology analysis of the immobilized catalysts were investigated using scanning electron microscopy (SEM). **Figure 3.18** displays hexagonal structures for **IC1**, **IC3** and **IC5** which is characteristic of native material MCM-41. A more cylindrical structure can be observed for **IC2**, **IC4** and **IC6** that is characteristic of the native material SBA-15.

The TEM micrographs of the immobilized catalysts **IC1-IC6** are shown in **Figure 3.19**. The TEM micrographs confirmed that the support material retained it's structure after immobilization as can be seen by the array of mesoporous channels. Energy-dispersive X-ray spectroscopy (EDS) was used to determine the elemental composition of the immobilized catalysts (**IC1-IC6**). Confirmation of the silica, copper, cobalt and palladium metal was achieved by TEM-EDS analysis (**Figure 3.20**).

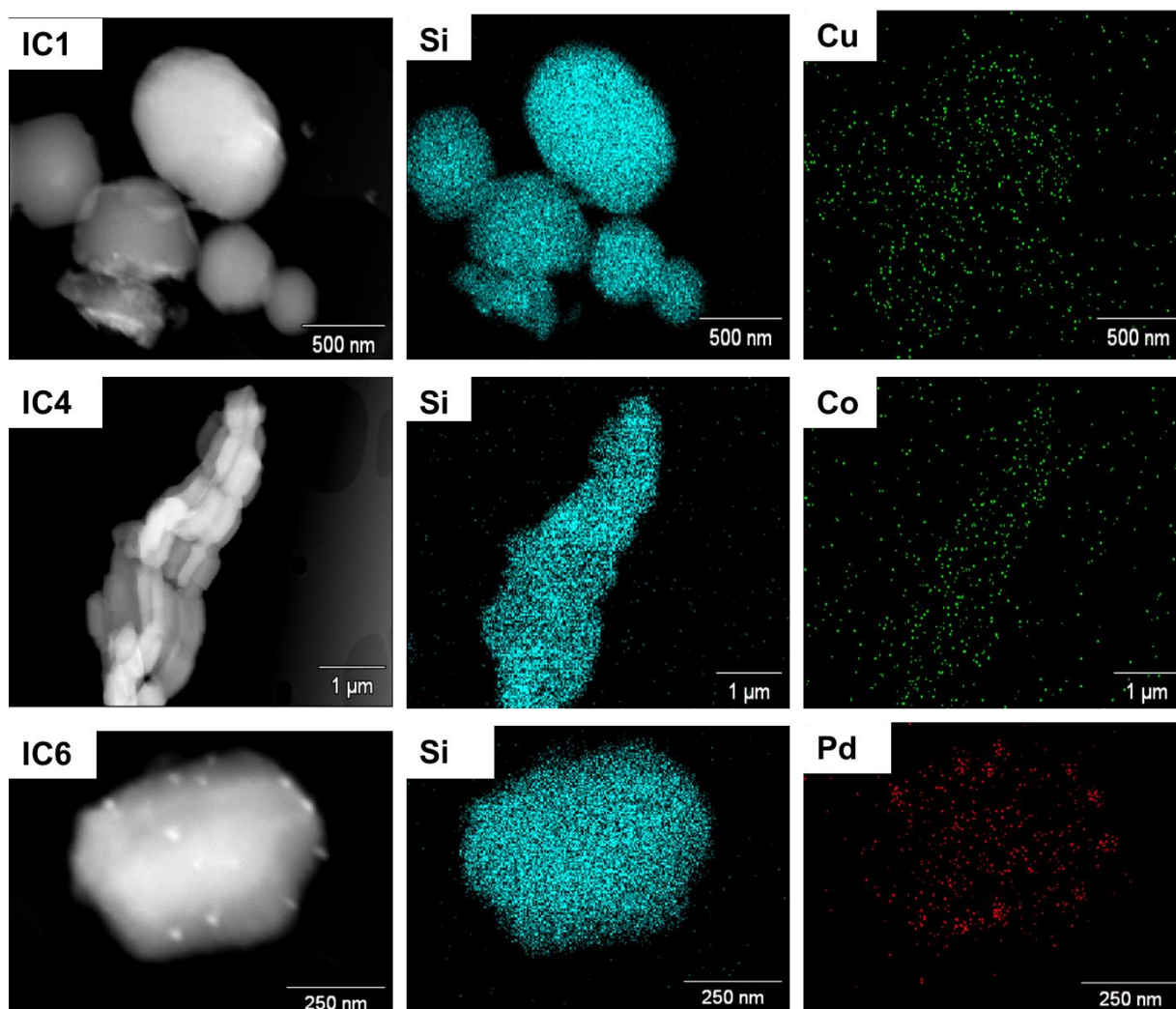


Figure 3.20: Selected TEM EDS images of immobilized complexes **IC1**, **IC4** and **IC6**

3.1 Chapter 3: Preparation and Characterization of immobilized catalysts IC1-IC6.

3.4 Concluding Remarks

In this project, two types of native material (MCM-41 and SBA-15) were prepared which were good candidates as support materials for immobilized catalysts. Copper, cobalt and palladium functionalized complexes were successfully immobilized onto their respective support material. The native silica material as well as the immobilized catalysts (**IC1-IC6**) were characterized by a range of solid-state analytical techniques including FT-IR (ATR) spectroscopy, BET surface analysis, ICP-OES spectroscopy, powder X-ray diffraction, scanning electron microscopy (SEM) and transmission electron microscopy (TEM). These techniques confirmed that the immobilization process was successful.

3.5 Experimental section**3.5.1 General remarks and instrumentation**

All syntheses were carried out under inert conditions using dry nitrogen and utilization of standard Schlenk techniques.

All FT-IR spectra were recorded as neat samples using a Nicolet Avatar 330 FT-IR spectrometer fitted with an ATR accessory. Varian VNMRS 500 MHz Solid State NMR spectrometer was used to measure the ^{29}Si NMR spectra. Field-emission scanning electron microscopy (FESEM) was carried out using a Zeiss Auriga Cobra Field Emission scanning electron microscope (Zeiss, Germany) with a GEMINI column operating at an accelerating voltage of 3 kV, to study the morphology of the materials. Samples were carbon-coated before analysis to minimize their possible charging. SEM-Energy dispersive X-ray spectroscopy (SEM-EDS) was performed on the same SEM instrument coupled with an Oxford Instruments X-Max^N detector operating at an accelerating voltage of 15kV and a sample working distance of 5 mm, to determine elemental composition and mapping. Electron micrographs and selected area diffraction patterns (SAED) were collected using a JEOL JEM-2100 (JEOL, Japan) HR-transmission electron microscope (HR-TEM), operated at an accelerating voltage of 200 kV. The powder samples were sonicated for 15 min, dissolved in ethanol and dispersed on a copper grid for TEM analysis. The Carl Zeiss "SmartSEM" software was used to collect SEM images. The Oxford Instruments NanoAnalysis "AZtec" software (version 2.2, SP1) was used to acquire the EDS data. TEM images and particle size were determined by ImageJ^(R) software. Thermogravimetric analysis was determined by a TA Instruments Q500 thermogravimetric analyser. A Thermo iCAP 6000 series supplied by Thermo Scientific was used to perform ICP-OES analysis. An appropriate amount of immobilized catalyst (40 mg) was digested in nitric acid (15 ml) for 24 hours at 100 °C. The solution was evaporated and then redissolved in aqueous hydrochloric acid (10 %, 10 ml). This solution was then syringe filtered and analyzed. All air sensitive compounds were stored in a nitrogen purged glovebox.

3.1 Chapter 3: Preparation and Characterization of immobilized catalysts IC1-IC6.

3.5.2 Materials

All Reagents were obtained from Sigma-Aldrich/Merck and used without further purifications. Solvents were purchased from Sigma-Aldrich/ Merck and Kimix, which were purified using a Pure Solv™ micro solvent purifier fitted with activated alumina columns. Other solvents such as, methanol, acetone and ethanol, were purified by distillation over magnesium fillings and iodine. Acetonitrile was purified by distillation over phosphorous pentoxide.

3.5.3 Synthesis of silica native material (MCM-41)

To a stirring solution containing an ammonia solution (410 mL, 25 % wt) distilled water was added (540 ml). Whilst stirring the solution, cetyltrimethylammonium bromide (CTAB) (3.994 g) was added and the mixture heated to 50 °C. Tetraethoxysilane (TEOS) (20 ml) was added after the solution became homogeneous. A white slurry formed, and the mixture was stirred for a further 2 hours at 50 °C. The solution was cooled to room temperature, filtered and washed with 1300 ml distilled water. The white solid obtained was calcined at 550 °C for 8 hours giving 4.274 g of MCM-41.

3.5.4 Synthesis of silica native material (SBA-15)

Poly(ethylene)-block-poly(propylene)-block-poly(ethylene) (8.050 g) was dissolved in (60 mL) distilled water and 2 M HCl solution (360 ml). Tetraethoxysilane (TEOS) (18.2 ml) was added to the stirring solution and the mixture was heated at 35 °C for 20 hours. The temperature of the mixture was then increased to 80 °C and aged for 24 hours without being stirred. A solid product formed, and it was filtered off and washed with 2000 ml of distilled water and dried at room temperature overnight. The white powder was then calcined at 550 °C for 8 hours. 5.586 g of SBA-15 was obtained.

3.5.5 Synthesis of immobilized catalysts**3.5.5.1 Synthesis of immobilized catalysts IC1-IC6**

General procedure for immobilization: The native silica material, MCM-41 or SBA-15 (1.00 g), was added to a stirring hot toluene (20 ml) solution, which formed a white slurry. The appropriate amount of functionalized complex (0.1 g), e.g. **FC1**, was added to the white slurry which resulted in a green reaction mixture. This green mixture was stirred for 24 hours at 110 °C under nitrogen. After the allotted time, the solid was filtered and continuously washed with dry methanol (5 x 5 ml) until no colour change was observed in the mother liquor. This solid was allowed to dry at room temperature and then dried in vacuo at 80 °C. A green powder was obtained for **IC1-IC4** and a yellow powder for **IC5-IC6**. These immobilized complexes were stored in a nitrogen purged glovebox. [3-4]

3.6 References

- 1 S. Sabater, J. A. Mata and E. Peris, *ACS Catal.*, 2014, **4**, 2038–2047.
- 2 R. Brady, B. Woonton, M. L. Gee and A. J. O'Connor, *Innov. Food Sci. Emerg. Technol.*, 2008, **9**, 243–248.
- 3 J. Liang, Z. Liang, R. Zou and Y. Zhao, *Adv. Mater.*, 2017, **29**, 1–21.
- 4 A. Watermann, *Nanomaterials*, 2017, **7**, 189–205.
- 5 M. Laskowska, I. Kityk, M. Dulski, J. Jędryka, A. Wojciechowski, J. Jelonkiewicz, M. Wojtyniak and Ł. Laskowski, *Nanoscale*, 2017, **9**, 12110–12123.
- 6 R. Castaldo, R. Avolio, M. Cocca, G. Gentile, M. E. Errico, M. Avella, C. Carfagna and V. Ambrogi, *Macromolecules*, 2017, **50**, 4132–4143.
- 7 M. A. Schwegler, P. Vinke, M. van der Eijk and H. van Bekkum, *Appl. Catal. A, Gen.*, 1992, **80**, 41–57.
- 8 V. Ayala, A. Corma, M. Iglesias and F. Sánchez, *J. Mol. Catal. A Chem.*, 2004, **221**, 201–208.
- 9 M. Mirzaee, B. Bahramian and M. Mirebrahimi, *Cuihua Xuebao/Chinese J. Catal.*, 2016, **37**, 1263–1274.
- 10 M. Melián-Rodríguez, S. Saravanamurugan, S. Kegnaes and A. Riisager, *Top. Catal.*, 2015, **58**, 1036–1042.
- 11 P. Karandikar, K. C. Dhanya, S. Deshpande, A. J. Chandwadkar, S. Sivasanker and M. Agashe, *Catal. Commun.*, 2004, **5**, 69–74.
- 12 D. X. Martínez-Vargas, J. Rivera De La Rosa, L. Sandoval-Rangel, J. L. Guzmán-Mar, M. A. Garza-Navarro, C. J. Lucio-Ortiz and D. A. De Haro-Del Río, *Appl. Catal. A Gen.*, 2017, **547**, 132–145.
- 13 M. Esmaeilpour, A. R. Sardarian and J. Javidi, *J. Organomet. Chem.*, 2014, **749**, 233–240.
- 14 M. D. Donohue and G. L. Aranovich, *Adv. Colloid Interface Sci.*, 1998, **76–77**, 137–152.
- 15 V. B. Fenelonov, V. N. Romannikov and A. Y. Derevyankin, *Microporous Mesoporous Mater.*, 1999, **28**, 57–72.
- 16 B. Lefèvre, A. Galarneau, J. Iapichella, C. Petitto, F. Di Renzo, F. Fajula, Z. Bayram-Hahn, R. Skudas and K. Unger, *Chem. Mater.*, 2005, **17**, 601–607.
- 17 W. Fu, L. Yue, X. Duan, J. Li and G. Lu, *Green Chem.*, 2016, **18**, 6136–6142.
- 18 M. Gago, Sandra Bruno, Sofia M. Queiro's, Diogo C. Valente, Anabela A. Gonçalves, Isabel S. Pillinger, *Catal. Letters*, 2011, **141**, 1009–1017.
- 19 H. Zhang, J. Sun, D. Ma, X. Bao, A. Klein-Hoffmann, G. Weinberg, D. Su and R. Schlögl, *J. Am. Chem. Soc.*, 2004, **126**, 7440–7441.

Chapter 4:

Model and immobilized catalysts as precursors in the oxidation of veratryl alcohol.

4.1 Introduction

Conventional methods employed in the oxidation of aromatic alcohols to aldehydes or acids consists of many synthetic steps. Traditionally, many catalytic processes in the flavour industry make use of a glyoxylic method together with highly toxic oxidants such as manganese oxide and potassium dichromate to name a few.¹ These oxidants are usually employed in the production of vanillin and veratrylaldehyde which are often produced in high yield reactions.^{2,3} The production of these products usually suffer from major drawbacks, one of which is the formation of by-products as well as separation thereof from the target products.⁴ Thus, there is a need to develop a more sustainable chemical process which will alleviate the formation of waste.

The utilization of first row transition metals as catalysts has become a viable route to oxidize lignin model compounds due to their relative abundance in nature. Currently, extensive research is being conducted on the oxidation of lignin model compounds using Schiff base complexes. These complexes are relatively cheap and easy to synthesize.⁵ In comparison to traditional methods, the use of first row transition metals employed as catalyst provides potential advantages. These advantages include highly selective synthesis of aromatic oxygenates and low production of waste. Introducing oxidants such as air, molecular oxygen, and other oxidants such as hydrogen peroxide and *tert*-butyl hydroperoxide in oxidation reactions contribute to greener chemical processes.^{1,6}

Multiphase catalysis has become of interest to many researchers due to its potential to allow for the separation of the catalyst from reaction mixtures. Various support systems can be employed to facilitate these multiphase chemical processes. These systems include metal complexes supported on mesoporous silica, ionic liquids and nanoparticles.⁷⁻⁹

In a report by Hu et al. it was illustrated that 4-methyl guaiacol can be oxidized to vanillin using an N,N'-ethylenebis(acetylacetoniminato)-cobalt(II) pyridinehexafluorophosphate (Co-[Salen-Py][PF₆]₂). This catalyst displayed good activity with yields up to 90%. The use of simple crystallization of the salt by addition of NaOH led to the recovery of the catalyst and the isolation of vanillin. The catalyst was recycled and reused for up to three runs without losing activity. Therefore, this catalyst can be considered as a green alternative to conventional catalysts in the production of vanillin.² Another example of a catalyst based on an ionic liquid reported by Fan et al., consisting of a ruthenium zeolitic imidazolate framework (ZIF) together with copper oxide that was employed in

Chapter 4: Model and immobilized catalysts as precursors in the oxidation of veratryl alcohol.

the oxidation of veratryl alcohol (VA) to veratrylaldehyde (VAD). In their study the Ru@ZIF + CuO system showed the ability to be highly active with substrate conversion close to 100%. During the formation of VAD, the product underwent subsequent aldol-condensation with acetone to form a new compound with high yields.¹⁰

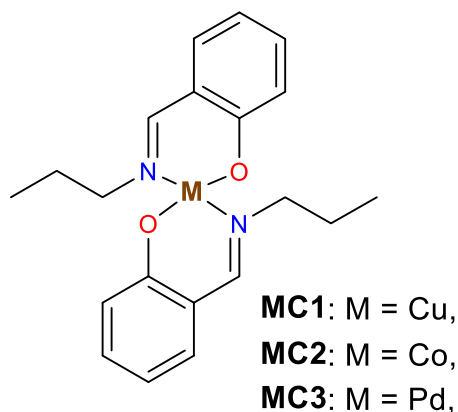
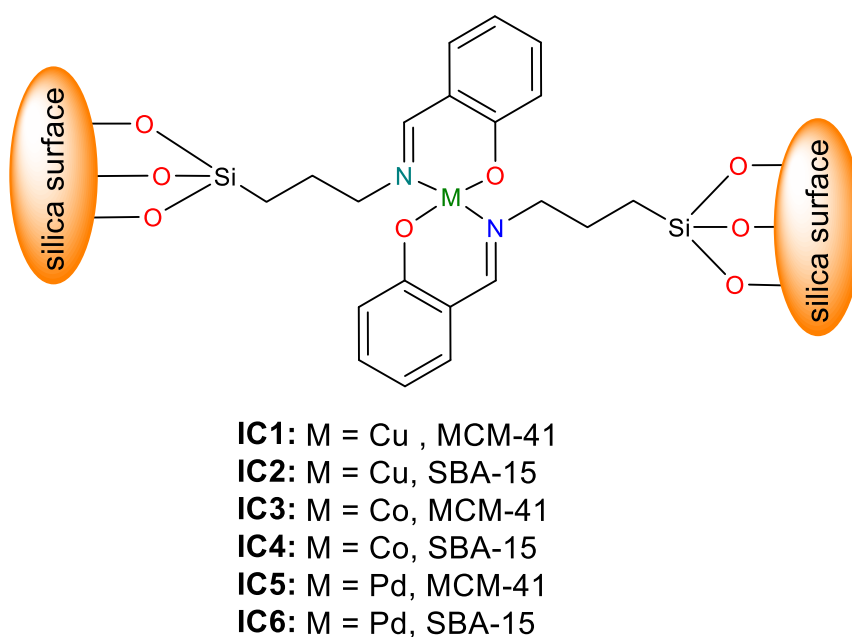
The use of biomass as chemical feedstock has the potential to replace fossil-based chemicals. Veratrylaldehyde (VAD), obtained from the biomass source, lignin, is one of the most widely used aromatic compounds used in the flavourant and pharmaceutical industry. The production thereof however suffers from a few challenges, especially with regards to separating the products as well as the catalyst from reaction mixtures. Overcoming these challenges was illustrated by Melián-Rodríguez et al. when they supported a ruthenium catalyst onto γ -alumina and silica respectively. Both supported catalysts displayed excellent activity of 99% substrate conversion with VAD forming predominantly (67% VAD yield). Recyclability of the catalyst was achieved for up to three runs without a dramatic drop in activity. However, the reuse of the catalyst resulted in a significant drop in selectivity VAD yield.¹¹

In light of the above, we embarked on an investigation in which we evaluated some of the immobilized catalysts reported in **Chapter 3** in the oxidation of lignin model compounds. The focus was essentially on veratryl alcohol as model compound.

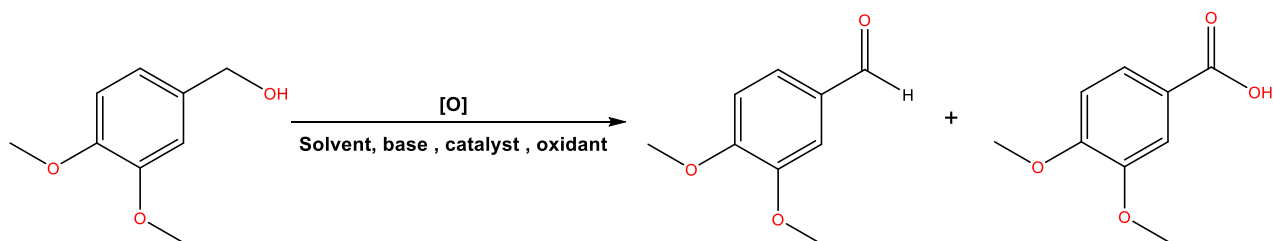
4.2 Preliminary reaction conditions employed in the oxidation of veratryl alcohol.

Preliminary catalytic studies were conducted using modified conditions reported by Kervinen et al. These researchers demonstrated that cobalt Schiff base complexes are active in the oxidation of veratryl alcohol. Furthermore, these catalytic reactions were performed in alkaline media (pH = 12) at 80 °C in the presence of molecular oxygen for 24 hours. The catalyst systems exhibited good selectivity towards veratraldehyde.¹²

In our study, reported here, we employed immobilized Cu, Co and Pd complexes in the oxidation of veratryl alcohol. Supports such as SBA-15 and MCM-41 were employed as catalyst carriers. The model catalysts (**MC1-MC3**) as well as their immobilized analogues (**IC1-IC6**) were evaluated in the oxidation reactions. These catalysts are based on Schiff base complexes of copper, cobalt and palladium respectively (**Figure 4.1** and **Figure 4.2**). The copper Schiff base complex **MC1** was employed to optimize reaction conditions. The results of the optimization process are described in **Section 4.3**.

Chapter 4: Model and immobilized catalysts as precursors in the oxidation of veratryl alcohol.**Figure 4.1:** Model complexes, **MC1-MC3**.**Figure 4.2:** Representation of immobilized catalysts, **IC1-IC6**.**4.3 Optimizing catalytic conditions for the oxidation of veratryl alcohol**

In a typical oxidation reaction of veratryl alcohol, **MC1** was used to optimize reaction conditions. An adapted procedure was followed based on a report by Kervinen and co-workers.¹³ During the optimization process the catalyst concentration, base concentration, reaction time, reaction temperature and the nature of the oxidant was varied. A schematic representation of the oxidation of veratryl alcohol to veratrylaldehyde is shown below (**Scheme 4.1**).

Chapter 4: Model and immobilized catalysts as precursors in the oxidation of veratryl alcohol.

Scheme 4.1: Typical oxidation reaction of veratryl alcohol to veratrylaldehyde.

4.3.1 Typical oxidation reaction conditions

Initially, the conditions employed based on literature protocols were 0.595 mmol veratryl alcohol followed by the addition of 0.750 mmol NaOH, 2.5 mol % catalyst (**MC1**) and acetonitrile as solvent (3 ml). The reaction was conducted under 1 bar oxygen pressure for 24 hours at 60 °C. The choice of temperature was selected due to acetonitrile having a boiling point of 82 °C. The substrate concentration was 0.297 mol/L in an acetonitrile solution. Prior to the reaction, oxygen gas was used to purge the reaction mixtures. In a typical reaction, the substrate was added to the reactor tube followed by the catalyst after which it was heated to the appropriate temperature. Once the appropriate temperature was reached, sodium hydroxide was added, and 1 bar of oxygen maintained. The reaction was then allowed to stir for 24 hours at the set temperature.

4.3.1.1 Control reactions

The main parameters influencing the conversion of veratryl alcohol to veratrylaldehyde were the nature of the oxidant, base concentration and catalyst concentration. The influence of these parameters on conversion were studied by systematically omitting one of the parameters at a time. In the absence of the catalyst, a conversion of only 2 % was obtained after 6 hours reaction time. In the absence of oxidant, but under nitrogen atmosphere moderate conversion was obtained of up to 33 % with aldehyde yields up to 92 %. However, in the absence of the base, NaOH less than 2 % conversion was obtained with only aldehyde being detected. It can thus be seen from **Figure 4.3** that both the base and catalyst is needed for the transformation to occur.

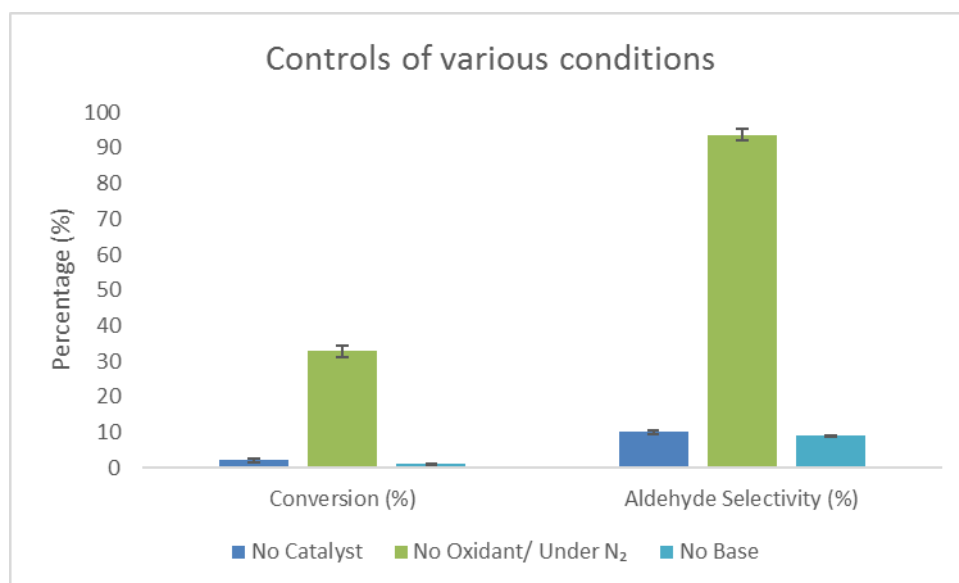


Figure 4.3: Influence of main parameters. Reaction conditions: 1.) No catalyst: 1.0 mmol veratryl alcohol, 0.2 mmol NaOH, 25 °C, 6 hours, 10 ml acetonitrile. 2.) No oxidant: 1.0 mmol veratryl alcohol, 0.2 mmol NaOH, 2 mol% catalyst loading, 25 °C, 6 hours, 10 ml acetonitrile, nitrogen atmosphere. 3.) No base (NaOH): 1.0 mmol veratryl alcohol, 2 mol% catalyst loading, 25 °C, 6 hours, 10 ml acetonitrile, 1 atm oxygen pressure.

4.3.1.2 Catalyst concentration

The first parameter to be varied was the catalyst concentration. Four experiments were conducted using 1 mol %, 2 mol %, 2.5 mol % and 3 mol % of catalyst respectively. The remaining reaction conditions were 0.20 mmol NaOH under 1 atm oxygen pressure for 24 hours at 60 °C. From these experiments, it was found that the activity was higher at the lower catalyst loading. Increasing the catalyst loading above 2 mol% leads to a slight decrease in conversion. This lack of increased activity at higher catalyst loading could potentially be a result of the fact that catalyst deactivation is faster at the higher catalyst concentration, which eventually results in the catalyst activity reaching a plateau.

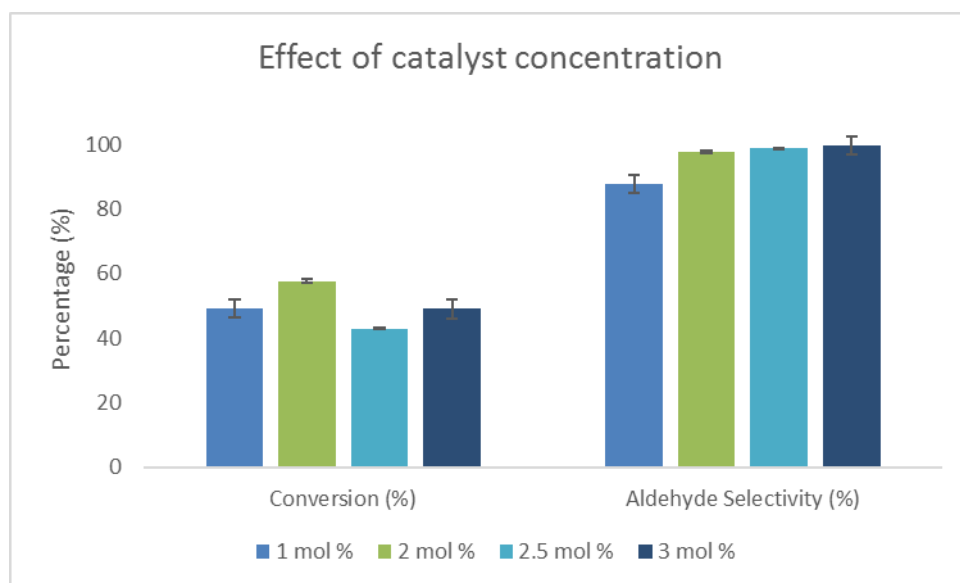
Chapter 4: Model and immobilized catalysts as precursors in the oxidation of veratryl alcohol.

Figure 4.4: Influence of catalyst (**MC1**) concentration on conversion and selectivity. Reaction conditions: 1.0 mmol veratryl alcohol, 0.20 mmol NaOH, 1 atm oxygen pressure, 60 °C, 24 hours, 10 ml acetonitrile.

In our experiments, we observed with an increase in catalyst loading, the respective turnover numbers (TON's) decreased (**Table 4.1**). A comparison between catalyst loading 1 mol% and 2 mol% illustrated the fact that 2 mol% produced a low TON's even though it exhibited higher activity and selectivity compared to 1 mol%. Therefore, catalyst loading of 2 mol% was chosen, since it exhibited more activity and selectivity towards aldehyde close to 100%.

Table 4.1: Conversion, aldehyde yield and turnover numbers at different catalyst loadings using **MC1** as catalyst.^a

Catalyst loading (mol%)	Conversion (%)	Aldehyde yield (%) ^b	TON ^c
1.0	49 ± 3.0	88	36
2.0	58 ± 2.0	98	29
2.5	43 ± 0.5	99	12
3.0	49 ± 2.5	100	17

^a Reaction conditions: 1.0 mmol veratryl alcohol, 0.20 mmol NaOH, 1 atm oxygen pressure, 60 °C, 24 hours, 10 ml MeCN. ^b Aldehyde yields based total product obtained. ^c TON = mmol substrate converted/mmol catalyst.

4.3.1.3 Effect of base concentration

It has been previously found that the role of the base in the transformation of veratryl alcohol to veratrylaldehyde is to deprotonate the alcohol.¹³ Here we report on our investigation into the influence of the base on the catalytic reaction system (**Figure 4.5**). This was done by varying the

Chapter 4: Model and immobilized catalysts as precursors in the oxidation of veratryl alcohol.

NaOH concentration. Initially, 0.05 mmol base was used which resulted in 28 % substrate conversion. Thereafter, the base concentration was systematically increased between 0.1 mmol and 0.4 mmol. This resulted in an increased conversion with selective formation of the desired aldehyde. It was found that at 0.2 mmol base, the reaction operated at an optimum level. A dramatic drop in activity was observed when using 0.4 mmol of base. At the higher base concentration, the formation of a solid residue is observed. This solid residue is possibly a dimeric hydroxy or peroxy bridged copper species, which is probably insoluble and inactive. This potentially points to catalyst deactivation under these reaction conditions.^{13,14}

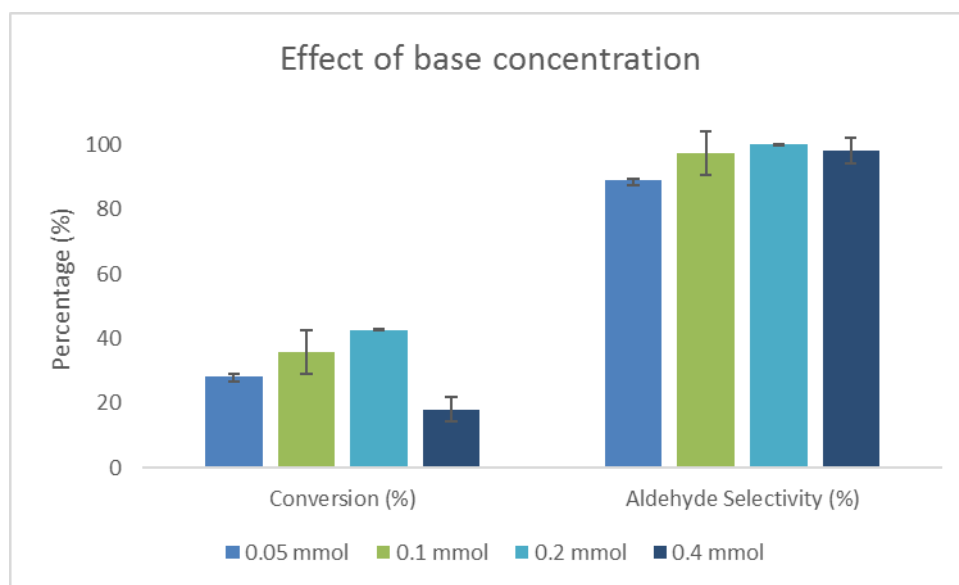


Figure 4.5: Effect of base concentration on conversion and selectivity. Reaction conditions: 1.0 mmol veratryl alcohol, 2 mol% catalyst (**MC1**), 1 atm oxygen pressure, 60 °C, 24 hours, 10 ml acetonitrile.

4.3.1.4 Effect of temperature

The activity of **MC1** is relatively low at 80 °C with the conversion only reaching around 20 %. A trend can be observed when reducing the temperature. The activity gradually increased when reducing the temperature from 80 to 25 °C except for extremely low temperatures (**Figure 4.6**). The highest activity was achieved at room temperature with conversions up to 58 %. At this temperature, 100 % selectivity towards veratrylaldehyde was obtained. At 60 °C and 40 °C, substrate conversion at both temperatures were between 40 – 43 % respectively, with 97 – 98 % selectivity to veratrylaldehyde. After establishing an optimum temperature, an experiment was conducted to investigate if the activity is altered by reducing the temperature to extremely low temperature of 0 °C. The conversion obtained at this temperature was below 2 %. Therefore, presumably the active species for the oxidation reaction only forms at temperatures between 25 °C and 60 °C, while temperatures of 80 °C and higher the catalyst decomposes. Another problem is

Chapter 4: Model and immobilized catalysts as precursors in the oxidation of veratryl alcohol.

that at this temperature the solvent, acetonitrile starts to volatilize (b.p. 82 °C). Therefore, In the light of the above, it was decided to use 25 °C as the optimum temperature.

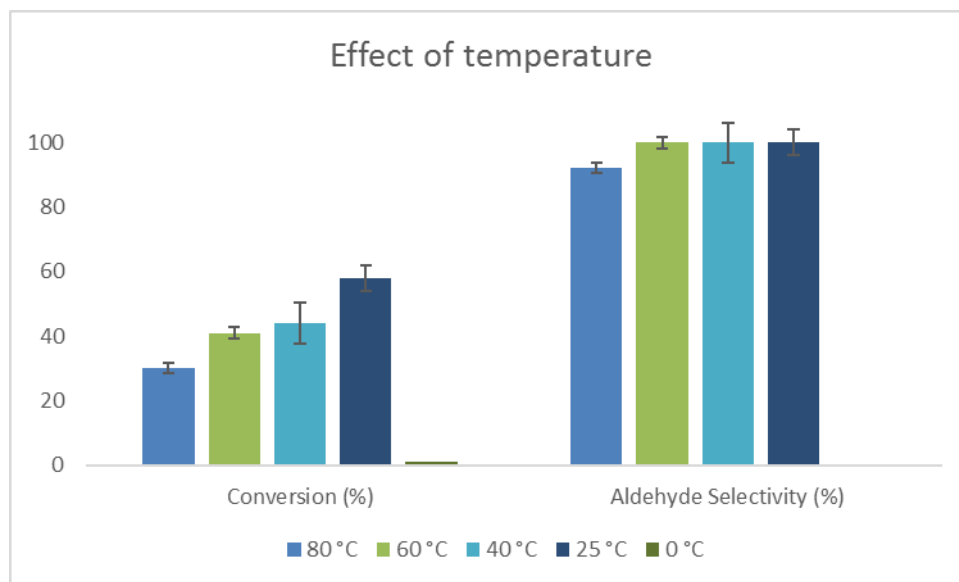


Figure 4.6: Influence of temperature on conversion and selectivity. Reaction conditions: 1.0 mmol veratryl alcohol, 2 mol% catalyst loading (**MC1**), 0.2 mmol NaOH, 1 atm oxygen pressure, 24 hours, 10 ml acetonitrile.

4.3.1.5 Effect of reaction time

Another parameter investigated was the influence of reaction time on conversion. Four different reactions were carried out at optimum catalyst loading of 2 mol %. After a three hour period, it is clear that some of the veratryl alcohol was converted to veratryl aldehyde. However, the activity at this time is below 20 % with an aldehyde yield of 100 %. The conversion is roughly doubled when the reaction time is increased to 6 hours. Gradually increasing reaction times between 6 and 24 hours essentially showed no significant increase in conversion. The unchanged activity over extended time is due to catalyst deactivation.¹³ Over this time interval the amount of veratrylaldehyde decreases slightly with a concomitant increase in veratric acid (**Figure 4.7**). This is a result of the overoxidation of the aldehyde. From the reactions conducted, the optimum conditions of the catalytic system were established. These conditions are 2 mol % catalyst, 0.2 mmol NaOH at 25 °C under 1 atm oxygen pressure for 6 hours.

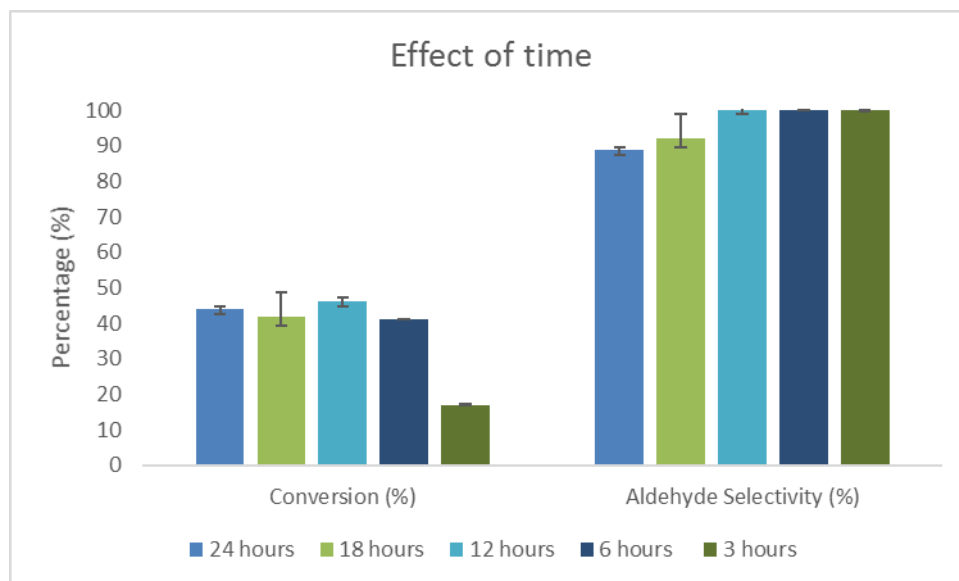


Figure 4.7: Influence of time on conversion and selectivity. Reaction conditions: 1.0 mmol veratryl alcohol, 2 mol% catalyst loading (**MC1**), 0.2 mmol NaOH, 1 atm oxygen pressure, 25°C, 10 ml acetonitrile.

4.3.1.6 Effect of oxidant

In literature examples, the most common oxidant used in the oxidation of lignin model compounds is oxygen. A comparative study was conducted to establish the effect of different oxidants on the activity as well as selectivity in the oxidation of veratryl alcohol. A few experiments were carried using different amounts of oxidant relative to substrate (**Figure 4.8**). In the case of H₂O₂, as the substrate to oxidant ratio increased, only a slight increase in activity was observed. Although hydrogen peroxide mediated the formation of only veratrylaldehyde, it exhibited low activity with substrate conversions below 20 %. *tert*-Butyl hydrogen peroxide was able to oxidize veratryl alcohol to veratrylaldehyde with various oxidant to substrate ratios. As the ratio increases, an increase in activity can be observed. However, simultaneously as the ratio increases greater quantities of aldehydes are converted to the carboxylic acid, veratric acid.

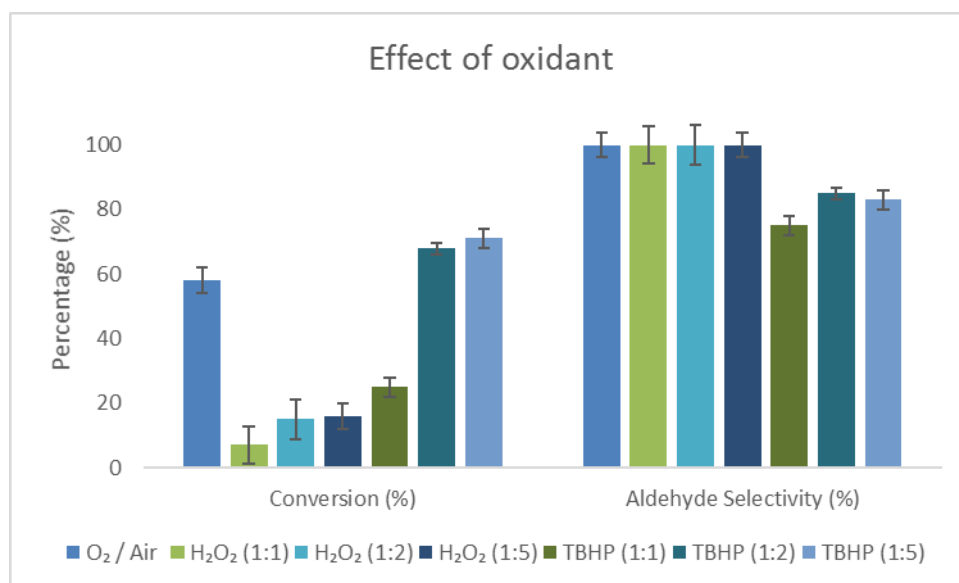
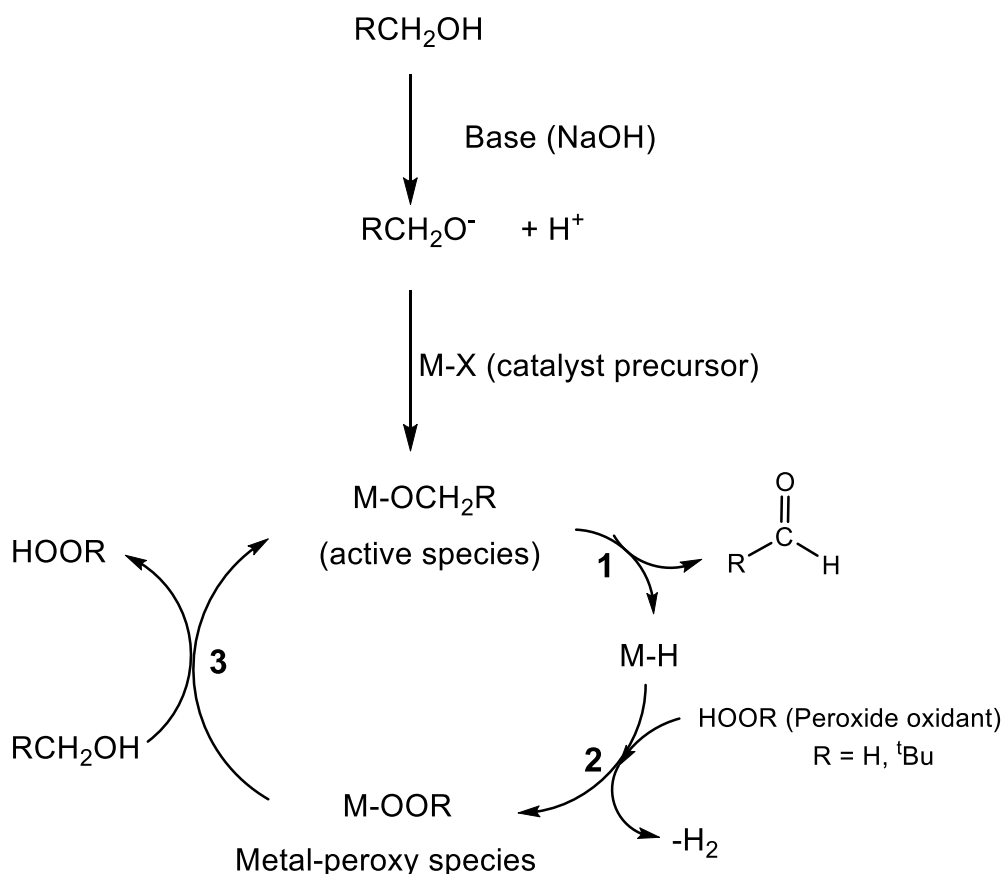
Chapter 4: Model and immobilized catalysts as precursors in the oxidation of veratryl alcohol.

Figure 4.8: Influence of oxidant on conversion and selectivity. Reaction conditions: 1.0 mmol veratryl alcohol, 2 mol% catalyst loading (**MC1**), 0.2 mmol NaOH, 25 °C, 6 hours, 10 ml acetonitrile.

In this study, oxygen still remained the best oxidant when compared with hydrogen peroxide (H₂O₂) and *tert*-butyl hydrogen peroxide (TBHP). Hydrogen peroxide prefers to be in an acidic medium since the low pH inhibits the decomposition of H₂O₂.¹⁵ Therefore, the ineffectiveness of hydrogen peroxide as an oxidant in the catalytic reaction can be attributed to its rapid decomposition in alkaline media. The decomposition of hydrogen peroxide is very rapid, resulting in low concentrations of the species being present in solutions. The depletion of H₂O₂ could potentially hinder the formation of the metal-hydroperoxy species which is formed in step 2, **Scheme 4.2**. This ultimately prevents the regeneration of the active species, viz the metal-alkoxide, leading to a retardation of the overall process.

TBHP is often preferred over hydrogen peroxide in oxidation reactions since firstly it is more stable than H₂O₂ and secondly its able to form a stable intermediates such as metal-peroxo species due to the bulky *tert*-butyl substituent it possesses. The reasonable activity observed when using TBHP is due to the fact that this metal-peroxo species forms rapidly. This in turn favours the formation of the metal-alkoxide and ultimately the target aldehyde (**Scheme 4.2**).

Chapter 4: Model and immobilized catalysts as precursors in the oxidation of veratryl alcohol.**Scheme 4.2:** Metal-hydride pathway for the oxidation of alcohols with peroxides, ROOH as oxidant

The use of TBHP is also preferred over molecular oxygen since the former being in solution allows catalysis to take place in a homogeneous solution. This facilitates interaction between the oxidant and the metal centre.^{2,12,14,16,17} Even though TBHP exhibits higher activity than oxygen and H₂O₂, oxygen was used thereafter as the main oxidant since it is a much greener oxidant than the peroxides as well as the fact that veratrylaldehyde formed selectively.

4.3.1.7 Model complex (MC1) in the absence of oxygen

In our system, control reactions were conducted as mentioned previously. The influence on activity and selectivity in the absence of oxygen was studied. Only the model catalyst **MC1** was used in these experiments. The reaction conditions consisted of 2 mol % of **MC1** catalyst, 0.2 mmol base, 1 mmol veratryl alcohol at 25 °C for 6 hours and 12 hours.

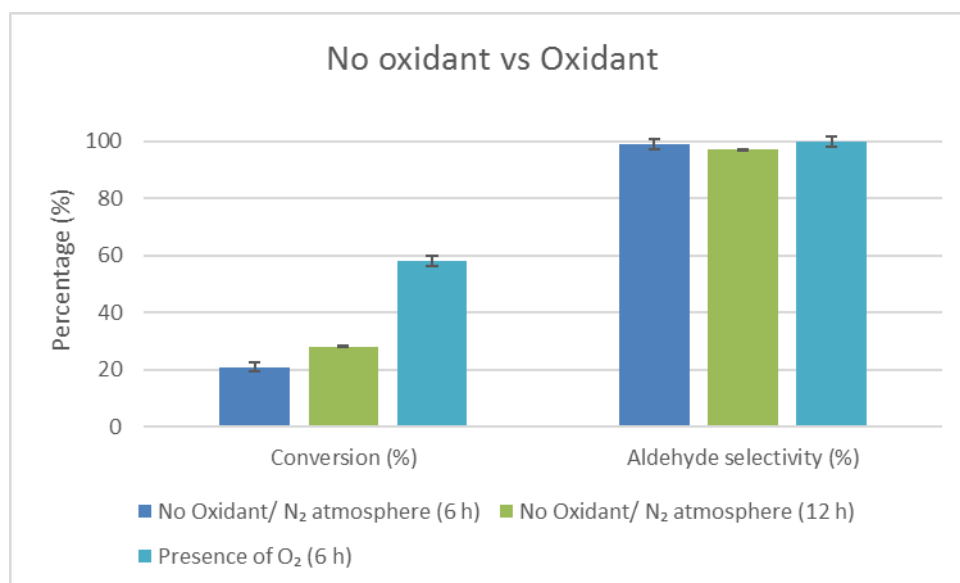
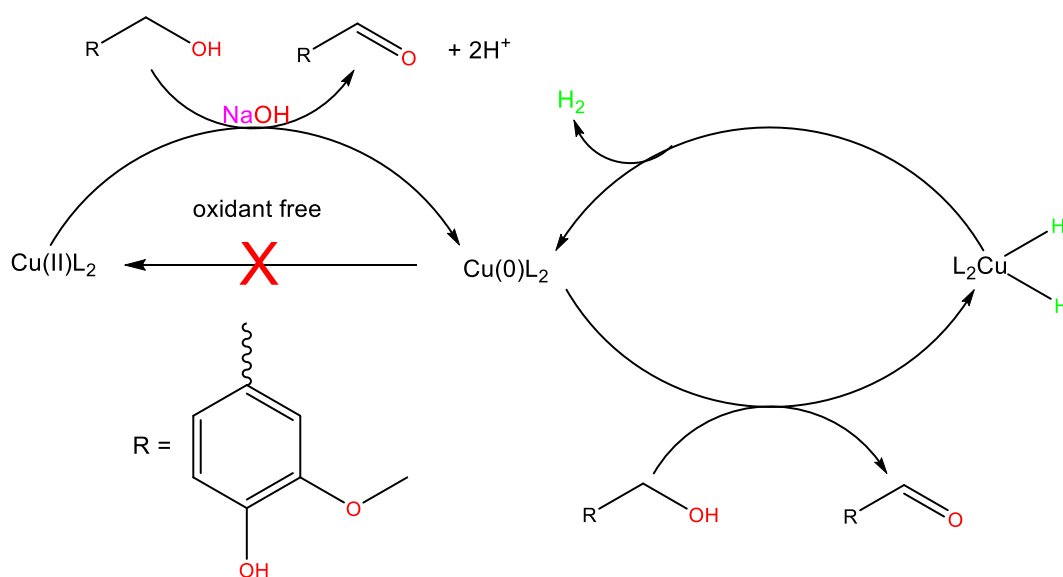
Chapter 4: Model and immobilized catalysts as precursors in the oxidation of veratryl alcohol.

Figure 4.9: Influence on conversion and selectivity over time in the absence of oxidant. Reaction conditions: 1.0 mmol veratryl alcohol, 2 mol% catalyst loading (**MC1**), 0.2 mmol NaOH, 25 °C, 6 hours and 12 hours, 10 ml acetonitrile.

In our study we found that the catalyst was active in the oxidation of veratryl alcohol to veratrylaldehyde in the absence of oxygen with reactions being conducted under nitrogen atmosphere (**Figure 4.9**). In comparison with the proposed mechanistic pathway for an oxidant free transformation of alcohols to aldehydes reported by Fu et al., it appears that our system has characteristics similar to what is proposed by these authors. This mechanism could potentially involve two distinct chemical pathways (**Scheme 4.3**).



Scheme 4.3: Currently accepted mechanism for dehydrogenation reactions.¹⁸

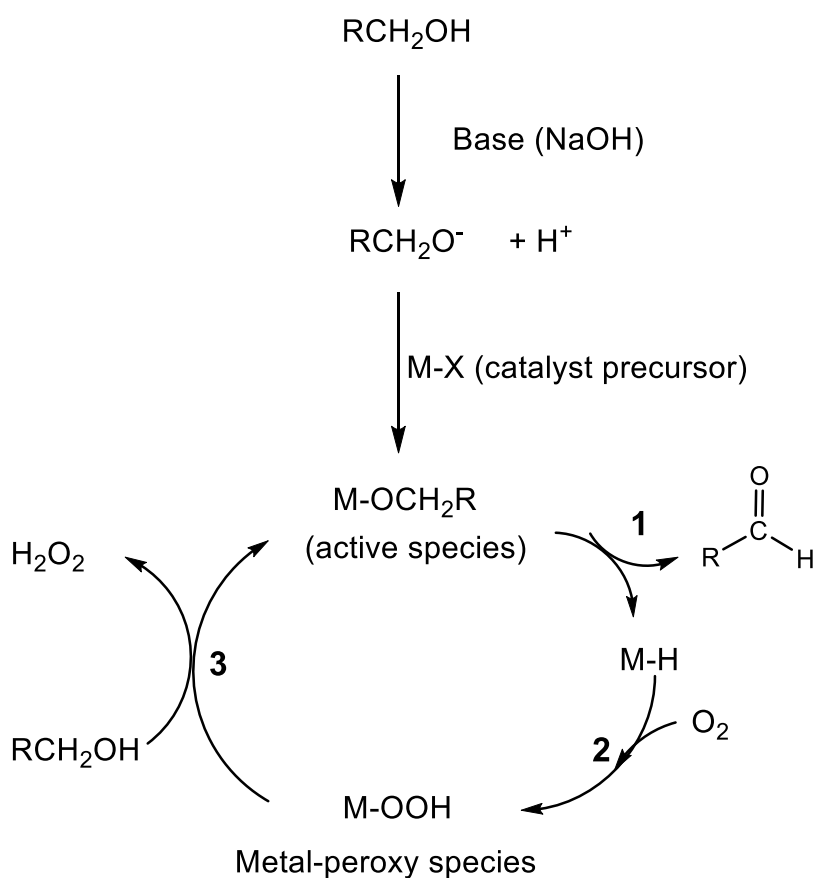
One of the pathways involves a β -hydrogen transfer from a metal-alkoxide intermediate and this leads to the generation of a metal(0) species and the aldehyde. The metal (0) species undergoes

Chapter 4: Model and immobilized catalysts as precursors in the oxidation of veratryl alcohol.

oxidative addition of the alcohol by activation of the O-H bond to form a metal alkoxy-hydride species. This is followed by β -hydrogen transfer from the alkoxy ligand to form a new dihydrido metal species and the elimination of the target aldehyde.

Finally, molecular hydrogen is released from the metal to generate the active metal(0) species. It is highly likely that our catalytic system follows a similar pathway to that proposed by Fu et al. Further experiments were conducted by increasing the reaction time to 12 hours in the absence of oxidant. After the allotted time, it was observed that the activity slightly increased with selectivity to the aldehyde up to 97 %.

Reactions were subsequently repeated in the presence of oxygen. In this case we note a dramatic increase in conversion. For example, the conversion doubles when carried out under aerobic conditions. Clearly oxygen has a crucial role in the reaction pathway. Previous work reported in the literature established that oxygen facilitates the formation of an active metal-hydroperoxy intermediate thus ultimately increasing the rate of the overall reaction. This is shown in **Scheme 4.4**.¹²



Scheme 4.4: Metal-hydride pathway for the oxidation of alcohols with oxygen as oxidant

4.4 Comparative study of model catalysts (MC1-MC3) against immobilized catalysts (IC1-IC6)

4.4.1 Model catalysts in presence of oxygen

After using the copper model complex, **MC1** to establish optimum reaction conditions, the remaining model catalysts (**MC2-MC3**) were also evaluated in the oxidation of veratryl alcohol (**Figure 4.10**).

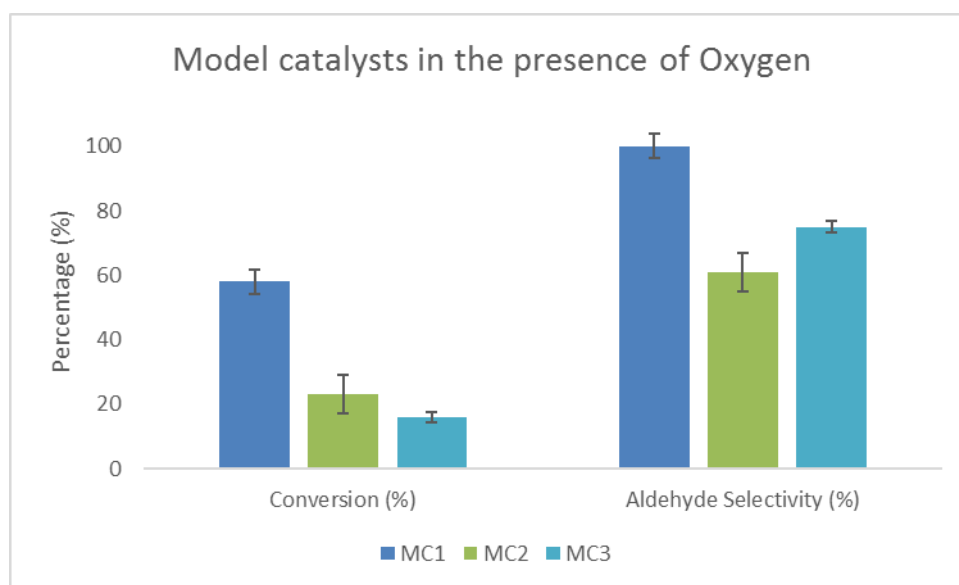
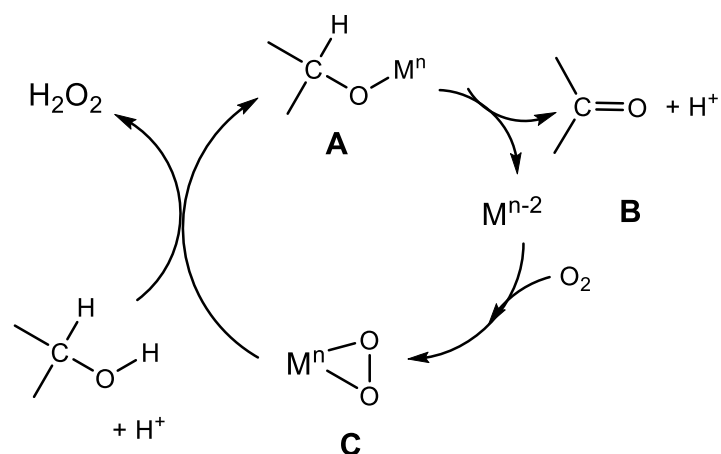


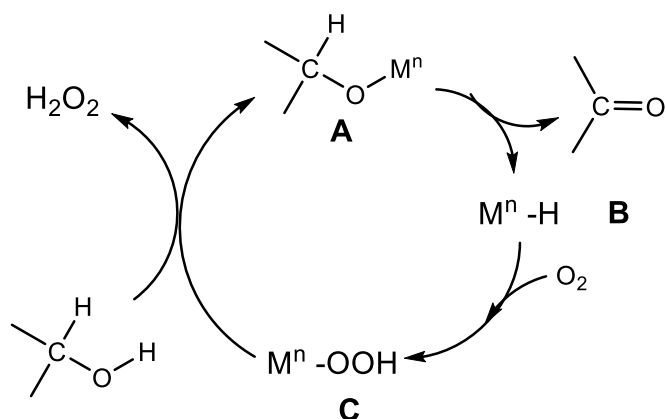
Figure 4.10: Activity and selectivity of different model catalysts in the presence of oxygen. Reaction conditions: 1.0 mmol veratryl alcohol, 2 mol% catalyst loading (**MC1-MC3**), 0.2 mmol NaOH, 1 atm oxygen pressure, 25 °C, 6 hours, 10 ml acetonitrile.

Amongst all the model catalysts, **MC1** exhibited the best activity in the presence of oxygen with conversions up to 58 % with veratrylaldehyde formed predominantly. In nature, enzymes contain metal centres such as copper which has the ability to activate molecular oxygen. The activity that the copper catalyst, **MC1**, displayed in the presence of oxygen could be a result of a peroxo-copper species forming which is highly reactive in the oxidation of veratryl alcohol.¹⁹ It was previously thought that oxygen mediates the formation of this peroxo-copper species (C, **Scheme 4.5**). The latter is required to generate the metal-alkoxy (active species, A, **Scheme 4.5**).

Chapter 4: Model and immobilized catalysts as precursors in the oxidation of veratryl alcohol.**Scheme 4.5:** Metal-peroxy pathway for the oxidation of alcohols.

It can therefore be concluded that the role of oxygen is most likely to form the metal-peroxy species which then allows the formation of the active metal-alkoxy species.

The cobalt catalyst, **MC2**, on the other hand exhibited substrate conversion of only about 20 % with selectivity towards aldehyde being moderate around 61 % with the rest being veratric acid. These reactions were conducted at 25 °C, which could potentially contribute to the low activity. In literature, these types of cobalt catalysts are usually employed at elevated temperatures above 70 °C, which suggests that the active species only forms at elevated temperatures. Increased amount of base is often required to deprotonate the substrate, which results in the formation of free alkoxide ions which subsequently coordinate to the metal centre. The M-alkoxide bond involves pi-donation from the alkoxide ligand into the empty d-orbital on the metal.^{12,13,20,21} This subsequently undergoes β -hydrogen transfer to produce a metal hydride (B, **Scheme 4.6**)

**Scheme 4.6:** Metal-hydride pathway for the oxidation of alcohols

Similar results as for the cobalt catalyst were obtained for the palladium precursor, **MC3**, with a relatively low conversion of 16 %. Softer metals such as palladium often catalyze reactions which are usually initiated by metal-hydride intermediates (**Scheme 4.6**). However the metal-hydride

Chapter 4: Model and immobilized catalysts as precursors in the oxidation of veratryl alcohol.

pathway often requires higher temperature to form palladium(0).²² It is likely that the degree of oxygen diffusion through the solution to get to the substrate is rate limiting. This could possibly be the fact that copper catalyst (**MC1**) forms the peroxy-species faster than the other catalyst (**MC2** & **MC3**) at ambient temperature.^{23,24}

4.4.2 Model catalysts in presence of TBHP

The activity of different complexes (Cu (**MC1**), Co (**MC2**), Pd (**MC3**)) were evaluated using TBHP as oxidant. *tert*-Butyl hydroperoxide is normally preferred over hydrogen peroxide since it is more thermally stable and the fact that it forms stable radicals. Together with transition metals it rapidly mediates the oxidation of alcohols.²⁵

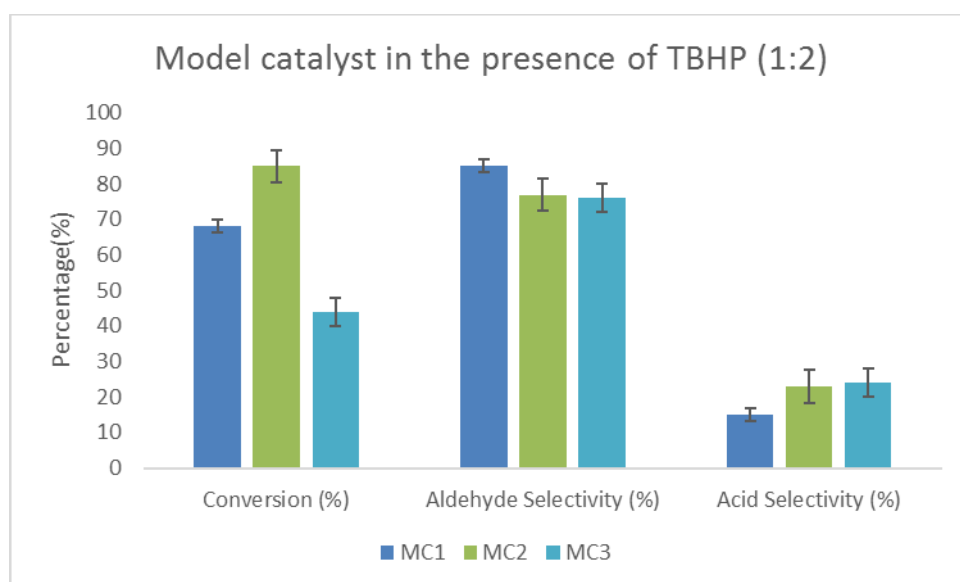


Figure 4.11: Activity of different catalysts on conversion and selectivity in the presence of TBHP. Reaction conditions: 1.0 mmol veratryl alcohol, 2 mol% catalyst loading (**MC1-MC3**), 0.2 mmol NaOH, 2 mmol TBHP, 25 °C, 6 hours, 10 ml acetonitrile.

In our reactions using TBHP as oxidant, the model cobalt catalyst **MC2** exhibited significantly higher substrate conversion compared to the complexes **MC1** (Cu) and **MC3** (Pd) (**Figure 4.11**). The strong and sterically bulky oxidant, *tert*-butyl hydrogen peroxide when used with the cobalt complex **MC2** gives a conversion of about 85 % with the aldehyde being the major product. However, TBHP favours overoxidation since it contains a high degree of oxygen, which resulted in some of the aldehyde being consumed to the acid.²⁶ The oxidant, TBHP together with the cobalt catalyst could possibly undergo rapid formation of the peroxy-species which resulted in the conversion being about 85%.

The mononuclear copper complex, **MC1**, exhibited reasonable conversion of about 68 % compared with that of the palladium complex **MC3** (44 %). The copper catalyst (**MC1**) predominantly formed

Chapter 4: Model and immobilized catalysts as precursors in the oxidation of veratryl alcohol.

veratrylaldehyde with selectivity up to 85 % with the by-product being veratric acid (15 %). The selectivity towards veratrylaldehyde can be attributed to the copper slowly generating peroxy-species which prevents over-oxidation to the acid.^{12,16}

The palladium catalyst (**MC3**) exhibited lower activity compared to **MC1** and **MC2**. Often palladium catalysts together with alcohols and appropriate amounts of base favours a β -hydride transfer pathway. This then results in the formation of palladium(0) and aldehydes. These processes are usually irreversible in the absence of oxidants. A crucial step in the catalytic process is the alcohol coordinating to the palladium centre to afford a metal-alkoxide species. This metal-alkoxide then undergoes β -hydride elimination leading to the formation of a palladium-dihydride species as well as the target aldehyde. The generation of hydrogen gas occurs which in turn regenerate a palladium(0) species.¹⁸ In our study, an oxidant such TBHP was present. The presence of oxidant would then allow for the oxidation of palladium(0) back to palladium(II) the reaction to be reversible (Pd(0) to Pd(II)) which removes the hydrides from the metal center. The moderate conversion of about 40% could possibly be the fact that palladium catalyst together with TBHP probably need higher reaction temperatures to transform palladium(II) to palladium(0) which is the driving force to generate the palladium-dihydride species.²⁷

4.4.3 Immobilized catalyst applied in the oxidation of veratryl alcohol

After establishing that oxygen exhibits low solubility in acetonitrile, it was decided to employ TBHP as oxidant from this point forward. An attempt was made to use oxygen as oxidant, however oxygen exhibited conversions below 10% when employing it in oxidation of veratryl alcohol together with the immobilized complexes (**IC1-IC6**). A possible explanation for the low activity is the reduced mass transfer of oxygen to the solid support.

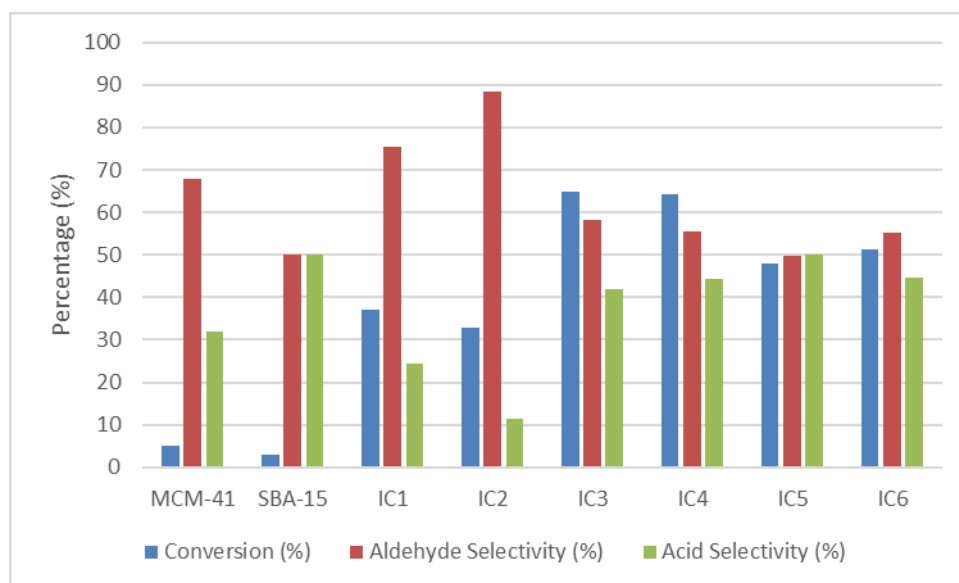
Chapter 4: Model and immobilized catalysts as precursors in the oxidation of veratryl alcohol.

Figure 4.12: Immobilized catalysts **IC1-IC6** and native silica material employed in the oxidation of veratryl alcohol. Reaction conditions: 1.0 mmol veratryl alcohol, 2 mol% catalyst loading, 0.2 mmol NaOH, 2 mmol TBHP, 25 °C, 6 hours, 10 ml acetonitrile.

Initially the native silica materials (MCM-41 and SBA-25) were tested as control experiments in the oxidation of veratryl alcohol (**Figure 4.12**). Both native silica materials gave conversions below 5%. This implies that the support materials do not influence the oxidation process significantly. As was the case for the model complexes, the immobilized complexes (**IC1-IC6**) also had the ability of oxidizing the veratryl alcohol to veratrylaldehyde and veratric acid. However, the use of a strong oxidant such as TBHP resulted in the selectivity being altered in such a way that some of the aldehyde is converted to the carboxylic acid. All the catalysts **IC1-IC6** employed in the oxidation reactions were used at metal loading of 2 mol % relative to substrate.

4.4.3.1 The nature of the support on activity and selectivity

The immobilized copper complexes (**IC1-IC2**) exhibited similar conversion of just over 30%. However, the SBA-15 immobilized catalyst, **IC2** displayed higher selectivity towards the aldehyde with yields up to 88 %. The model catalyst (**MC1**) exhibited a conversion of 70% with aldehyde yields of about 85%. A similar trend of selectivity towards the aldehyde can be observed for the copper analogues (**IC1** and **IC2**). The product selectivity of **IC2** is significantly better than **IC1** which can be the effect of the nature of the different supports. **IC1** being immobilized on MCM-41 has a larger surface area of 677 m²/g compared to **IC2** (509 m²/g). Usually larger surface areas tend to be more active in oxidation reactions since it contains more catalytic sites embedded on the silica surfaces.⁷

A comparison between the cobalt model complex **MC2** and the immobilized complexes **IC3-IC4** illustrated that both systems displayed better activity when compared to the Cu and Pd systems in

Chapter 4: Model and immobilized catalysts as precursors in the oxidation of veratryl alcohol.

the presence of TBHP as oxidant. The model cobalt catalyst (**MC2**) displayed substrate conversion of about 85% with aldehyde selectivity up to 78%. The immobilized counterparts, **IC3** and **IC4**, exhibited moderate conversion of about 65% with aldehyde selectivity between 55% to 59%. **IC3** and **IC4** showed no significant difference in activity with both producing promising results. Therefore, both immobilized counterparts undergo fast peroxo-cobalt formation which resulted in high activity.

It was also observed that the palladium model catalyst, **MC3**, displayed significantly less activity than its immobilized counterparts **IC5** and **IC6**. **IC5** displayed moderate activity of about 48 % while **IC6** exhibited conversion of 51%. No significant difference is observed in activity when comparing the two immobilized palladium catalysts with respect to the effect of the respective supports. There is, however, no difference in selectivity amongst the immobilized palladium catalysts.

Overall, for most of the immobilized catalysts **IC1-IC6** there is essentially no effect of the support on the selectivity. The slight changes in selectivity for immobilized catalysts **IC1-IC6** is essentially a catalyst effect rather than a support effect. The fact that the nature of the support has very little impact on the selectivity would seem to indicate that it is more likely that the catalyst is immobilized on the surface of the supports rather than in the pores. Surface localization of the catalyst on the surface would mean that the substrate would have easy access to the active sites. If the catalyst sites were localized inside the pores, then pore sizes would have controlled access to catalyst active sites. This would have an impact on selectivity, resulting in the different supports showing different selectivity. However, this is not the case, thus supporting the contention that the catalyst is largely on the support surface.

4.5 Recyclability of catalysts

Recycling experiments in the oxidation of veratryl alcohol were carried out with all the immobilized catalysts (**IC1-IC6**) in conjunction with TBHP as oxidant. After each catalytic run, the reaction mixture was centrifuged from which the supernatant was decanted, and the resulting catalyst was rinsed with methanol and further centrifuged. After this process, the catalyst was dried in *vacuo* for 2 hours and thereafter used in the next catalytic run.

The results displayed in **Table 4.2**, illustrate that the immobilized catalysts **IC3** and **IC4** could be recycled without significant loss of activity. These catalysts displayed only a slight decrease in conversion of about 7-10 % after the first round of recycling. After this it remained relatively stable. A significant increase in aldehyde yield was observed for catalysts **IC3** and **IC4** in subsequent cycles. Thereafter, the aldehyde yield remained above 60 % while experiencing a slight decrease in activity. This could potentially mean that the active species forms during the first cycle.

Chapter 4: Model and immobilized catalysts as precursors in the oxidation of veratryl alcohol.

From the results obtained from **Table 4.2**, moderate activity can be observed for immobilized Cu catalysts **IC1** and **IC2**. During the first catalytic runs, both catalysts exhibited high aldehyde yields between 76 and 89 % in addition to veratric acid. During the second run, **IC1** suffered a significant drop in activity of about 9 % which is potentially due to metal leaching into the solution. Visual detection of metal leaching was observed as seen by the solution adopting a slightly green colour. Further metal leaching was detected with ICP-OES with a concentration of about 10 ppm. The immobilized catalyst **IC2**, gave similar conversion compared to **IC1**. However, the activity for **IC1** dropped significantly whereas the activity **IC2** only dropped after the second run and then after that remained relatively unchanged. Catalysts with larger surface areas are prone to catalyst deactivation.²⁸

The MCM-41 immobilized palladium catalyst, **IC5** exhibited moderate conversion (48 %) which resulted in a 1:1 ratio product distribution of veratrylaldehyde and veratric acid. After recycling, catalyst **IC5**, showed a significant drop to 39% conversion. However, with the drop in activity, selectivity changed dramatically with yields reaching 72%, the other product being the carboxylic acid (28%). However, this catalyst could not be recycled due to mass loss during the catalytic runs. In addition, and the fact that metal leaching was observed visually with the formation of a bright yellow solution. The immobilized catalyst (**IC5**) changed colour from brown to black in solution after the first catalytic run. This suggests that the catalyst could possibly undergo a transformation in which Pd(II) is reduced to Pd(0). Constant activity throughout the four catalytic runs was observed for catalyst **IC6** from which veratrylaldehyde was obtained as the major product. After the second run, a larger percentage aldehyde yield was obtained compared to the first run. This could possibly indicate that the active species only forms after a certain time period. The constant activity could possibly be due to the rapid production of the peroxo-metallic species with TBHP from which oxygen gas is generated. The selectivity for **IC6** remained above 70% for the aldehyde. This however needs further investigation.

Chapter 4: Model and immobilized catalysts as precursors in the oxidation of veratryl alcohol.**Table 4.2:** Recyclability and reusability pertaining immobilized complexes **IC1-IC6.** ^a

IC1 in TBHP			IC3 in TBHP			IC5 in TBHP					
Conversion	Aldehyde	Acid yield	Conversion	Aldehyde	Acid yield	Conversion	Aldehyde	Acid yield			
(%)	yield (%)	(%)	(%)	yield (%)	(%)	(%)	yield (%)	(%)			
Run 1	37	76	24	Run 1	65	58	42	Run 1	48	50	50
Run 2	28	95	5	Run 2	58	71	29	Run 2	39	72	28
Run 3	26	88	12	Run 3	57	76	24	Run 3	-	-	-
Run 4	17	80	20	Run 4	58	62	38	Run 4	-	-	-
Run 5	10	82	18	Run 5	51	78	22	Run 5	-	-	-

IC2 in TBHP			IC4 in TBHP			IC6 in TBHP					
Conversion	Aldehyde	Acid yield	Conversion	Aldehyde	Acid yield	Conversion	Aldehyde	Acid yield			
(%)	yield (%)	(%)	(%)	yield (%)	(%)	(%)	yield (%)	(%)			
Run 1	33	89	11	Run 1	64	56	44	Run 1	48	55	45
Run 2	43	68	32	Run 2	54	60	40	Run 2	42	76	24
Run 3	32	82	18	Run 3	55	64	36	Run 3	41	79	21
Run 4	29	74	26	Run 4	52	68	32	Run 4	38	74	26
Run 5	28	88	12	Run 5	45	73	27	Run 5	-	-	-

^a Reaction conditions: veratryl alcohol (1 mmol), 2 mol % catalyst, temperature (25 °C), TBHP (2 mmol), acetonitrile (10 ml) and NaOH (0.2 mmol).

Chapter 4: Model and immobilized catalysts as precursors in the oxidation of veratryl alcohol.

4.6 Concluding remarks

In conclusion the copper model complex **MC1** in the presence of oxygen exhibited good activity as well as 100 % selectivity towards veratrylaldehyde compared to complexes **MC2** and **MC3**. The presence of base, NaOH, was required to deprotonate the substrate to most likely generate the alkoxide which subsequently coordinates to the metal. The model catalysts (**MC1-MC3**) displayed a significant increase in activity when TBHP was used as oxidant. However, the use of TBHP altered the selectivity and resulted in two products forming namely, veratrylaldehyde and veratric acid. The highest activity of 85 % was obtained for **MC2** (2 mol %) together with TBHP as oxidant for 6 hours.

The immobilized analogues (**IC1-IC6**) showed promising activity for the oxidation of veratryl alcohol in the presence of TBHP. The immobilized catalysts, **IC1-IC2** and **IC5-IC6** suffered from a dramatic drop in activity during recycling of the catalyst. This was attributed to the loss of catalyst during the recovery process as well as the leaching of the complex. The oxidation of veratryl alcohol using immobilized catalyst was not as effective when using oxygen and hydrogen peroxide as oxidants. In the case of oxygen as oxidant, slow diffusion of oxygen in acetonitrile could potentially be one of the major drawbacks. The use of hydrogen peroxide gave low activity which is possibly due to the fast decomposition thereof. The immobilized complexes **IC3** and **IC4** displayed the highest conversion of 65 % and 64 % respectively. Both these catalysts exhibit good recyclability with only a slight drop in activity after each recycle. Therefore, these catalysts applied in the oxidation of veratryl alcohol exhibited promising qualities and thus merit further investigation in order to fully ascertain its potential.

4.7 Experimental section

4.7.1 General remarks and instrumentation

All reagents were obtained from Sigma-Aldrich/Merck and used without further purification. Solvents were purchased from Sigma-Aldrich/ Merck and Kimix, which were purified using a Pure Solv™ micro solvent purifier fitted with activated alumina columns. Other solvents such as, methanol, acetone and ethanol, were purified by distillation over magnesium filings and iodine. Acetonitrile was purified by distillation over phosphorous pentoxide.

All catalytic reactions were conducted using a Radleys 12-stage carousel parallel reactor equipped with an oxygen gas distribution system. Quantitative and qualitative analysis were conducted on a Varian 3900 gas chromatograph containing a Cyclosil-β column (30 m x 0.25 mm x 0.25 μm) equipped with a flame ionisation detector (GC-FID) from which p-Xylene was

Chapter 4: Model and immobilized catalysts as precursors in the oxidation of veratryl alcohol.

used as internal standard. Additional quantitative analysis was done on a ThermoFischer scientific UltiMate 3000 ultra-high performance liquid chromatography (UHPLC) system containing BIO-RAD HPLC organic acid analysis column (aminex hpx-87, 300 x 7.8 mm 9 μm) equipped with a diode array detector (DAD) and an Agilent 1200 series high performance liquid chromatography containing a Phenomenex Luna C18 column (250 x 4.6 mm x 5 μm) equipped with a DAD detector.

4.7.2 General catalysis procedure using Oxygen

The general procedure for the oxidation of veratryl alcohol was carried out using model catalyst **MC1** as an example. Veratryl alcohol (0.168 g, 1.0 mmol) was dissolved in dry acetonitrile (10 ml) and transferred to a parallel reactor tube. The solution was saturated with oxygen gas. **MC1** catalyst (8.13 mg, 0.020 mmol, 2.0 mol %) was dissolved in the solution and sodium hydroxide (0.2 mmol, 2 M, 100 μl) was added to the tube. The tube was sealed and an oxygen blanket was maintained throughout the reaction. The reaction mixture was stirred for 6 hours at 25 $^{\circ}\text{C}$ and a green slurry was observed. After the allotted time, the reaction mixture was quenched in cold water and analyzed by GC-FID.

4.7.3 General catalysis procedure using Peroxides (H_2O_2 or TBHP) as oxidants

Veratryl alcohol (0.168 g, 1.0 mmol) was dissolved in dry acetonitrile (10 ml) using a parallel reactor tube. **MC1** (8.13 mg, 0.025 mmol, 2.0 mol %) was added to the solution and sodium hydroxide (0.2 mmol, 2 M, 100 μl) was added to the tube. Hydrogen peroxide (30 % solution) or *tert*-butyl hydrogen peroxide (70 % solution) was then added using appropriate ratios (substrate:oxidant). Gas evolution was observed when hydrogen peroxide was added. Addition of TBHP resulted in a white precipitate forming. The reaction mixture was stirred for 6 hours at 25 $^{\circ}\text{C}$ and a green solution was observed. After the allotted time, the reaction mixture was quenched in ice cold water followed by the addition of a small amount of MgSO_4 . Thereafter, the mixture was filtered, and quantitative analysis was performed using gas chromatography (GC-FID) and high-pressure liquid chromatography (HPLC). For GC analysis an internal standard, *p*-Xylene was used to quantify. HPLC quantifications employed the use of external calibration curve.

4.7.4 Recycling experiments

A typical recycling experiments was conducted simply by centrifuging the reaction mixture for 10 minutes at 6000 rpm. After the allotted time, the supernatant was transferred to a glass vial

Chapter 4: Model and immobilized catalysts as precursors in the oxidation of veratryl alcohol.

and dry methanol (5 ml) was added to the remaining catalyst which were further centrifuged for an additional 10 minutes at 6000 rpm. The resulting supernatant was discarded, and the catalyst was dried for 6 hours *in vacuo* for the next catalytic run.

4.8 References

- 1 K. Nagashima, T. Mitsudome, T. Mizugaki, K. Jitsukawa and K. Kaneda, *Green Chem.*, 2010, **12**, 2142–2144.
- 2 J. Hu, Y. Hu, J. Mao, J. Yao, Z. Chen and H. Li, *Green Chem.*, 2012, **14**, 2894–2898.
- 3 S. Ramachandra Rao and G. Ravishankar, *J. Sci. Food Agric.*, 2000, **80**, 289–304.
- 4 B. Barton, C. G. Logie, B. M. Schoonees and B. Zeelie, *Org. Process Res. Dev.*, 2005, **9**, 70–79.
- 5 K. C. Gupta, A. Kumar Sutar and C. C. Lin, *Coord. Chem. Rev.*, 2009, **253**, 1926–1946.
- 6 T. Mitsudome, A. Noujima, T. Mizugaki, K. Jitsukawa and K. Kaneda, *Green Chem.*, 2009, **11**, 793–797.
- 7 N. Malumbazo and S. F. Mapolie, *Mol. Catal. A*, 2009, **312**, 70–77.
- 8 K. Ambrose, B. B. Hurisso and R. D. Singer, *Can. J. Chem.*, 2013, **91**, 1258–1261.
- 9 I. B. Baguc, M. Celebi, K. Karakas, I. E. Ertas, M. N. Keles, M. Kaya and M. Zahmakiran, *ChemistrySelect*, 2017, **2**, 10191–10198.
- 10 H. Fan, Y. Yang, J. Song, G. Ding, C. Wu, G. Yang and B. Han, *Green Chem.*, 2014, **16**, 600–604.
- 11 M. Melián-Rodríguez, S. Saravanamurugan, S. Kegnæs and A. Riisager, *Top. Catal.*, 2015, **58**, 1036–1042.
- 12 K. Kervinen, Studies on veratryl alcohol oxidation catalyzed by Co(salen) type complexes and molecular oxygen in aqueous solution, PhD thesis, University of Helsinki, Helsinki, 2005.
- 13 K. Kervinen, H. Korpi, M. Leskelä and T. Repo, *J. Mol. Catal. A Chem.*, 2003, **203**, 9–19.
- 14 V. Sippola, *Transition metal-catalysed oxidation of lignin model compounds for oxygen delignification of pulp Väinö Sippola Distribution: Helsinki University of Technology Laboratory of Industrial Chemistry FIN-02015 TKK Otamedia Oy Espoo 2006*, 2006.
- 15 Z. Cheng, Benzyl Alcohol Oxidation Using In Situ Generated Hydrogen Peroxide from Hydrogen and Oxygen, MSc Thesis, Cardiff University, Cardiff, 2015.
- 16 S. M. Islam, P. Mondal, S. Mukherjee, A. S. Roy and A. Bhaumik, *Polym. Adv. Technol.*, 2011, **22**, 933–941.
- 17 V. Mahdavi and M. Mardani, *J. Chem. Sci.*, 2012, **124**, 1107–1115.

Chapter 4: Model and immobilized catalysts as precursors in the oxidation of veratryl alcohol.

- 18 W. Fu, L. Yue, X. Duan, J. Li and G. Lu, *Green Chem.*, 2016, **18**, 6136–6142.
- 19 M. M. Whittaker and J. W. Whittaker, *Biochemistry*, 2001, **40**, 7140–7148.
- 20 K. Kervinen, M. Allmendinger, M. Leskelä, T. Repo and B. Rieger, *Phys. Chem. Chem. Phys.*, 2003, **5**, 4450–4454.
- 21 K. Kervinen, H. Korpi, J. Gerbrand Mesu, F. Soulimani, T. Repo, B. Rieger, M. Leskelä and B. M. Weckhuysen, *Eur. J. Inorg. Chem.*, 2005, **2005**, 2591–2599.
- 22 R. A. Ten Brink, Gerd-Jan , Arends , Isabel W. C. E. and Sheldon, *Am. Assoc. Adv. Sci.*, 2000, **287**, 1636–1639.
- 23 T. Sato, Y. Hamada, M. Sumikawa, S. Araki and H. Yamamoto, *Ind. Eng. Chem. Res.*, 2014, **53**, 19331–19337.
- 24 C. Franco and J. Olmsted, *Talanta*, 1990, **37**, 905–909.
- 25 Y. Gao, J. Zhang, X. Chen, D. Ma and N. Yan, *Chempluschem*, 2014, **79**, 825–834.
- 26 J. Młochowski and H. Wójtowicz-Młochowska, *Molecules*, 2015, **20**, 10205–10243.
- 27 M. J. Beier, Heterogeneously Catalyzed Oxidation Reactions Using Molecular Oxygen, PhD thesis, Technical University of Denmark, Denmark, 2011.
- 28 S. Ray, S. F. Mapolie and J. Darkwa, *J. Mol. Catal. A Chem.*, 2007, **267**, 143–148.
- 29 H. Korpi, Copper di-imine complexes: Structures and catalytic activity in the oxidation of alcohols by dioxygen, PhD thesis, University of Helsinki, Helsinki, 2005.

Chapter 5:

Thesis summary and future recommendations.

5.1 Thesis summary

In this thesis, the synthesis, characterization and the evaluation of model bis-salicylaldiminato complexes and their immobilized counterparts in the oxidation of veratryl alcohol were investigated.

Chapter one covers a brief introduction of the valorization of biomass as a potential renewable resource. Various depolymerization processes of lignin were discussed in this chapter. An overview of various metal precursors employed in the oxidation of lignin model compounds ranging from first-row transition metals to platinum group metals is also given. In addition, this chapter provided some insight into the oxidation of lignin model compounds using heterogeneous catalyst systems. These heterogeneous catalysts include ionic liquids, metal-supported catalysts and metal-oxides.

In **Chapter two**, the preparation of a range of model and siloxane-functionalized salicylaldimine complexes are described. All the model complexes exhibited reasonable stability in solution and in air, while the siloxane-functionalized complexes were stored under inert conditions since the siloxane tail-end tends to hydrolyse over time when exposed to moist air. These complexes were fully characterized by a range of analytical techniques, which include EPR spectroscopy, UV/vis spectroscopy, FT-IR spectroscopy, ¹H NMR spectroscopy, mass spectrometry and single crystal diffraction. The structure of **MC3** was determined by single crystal X-ray diffraction. From this it was found that **MC3** had a square planar molecular geometry.

Chapter three describes a synthetic protocol for the preparation of two types of native silica material (MCM-41 and SBA-15) which were good candidates as support materials for immobilized catalysts. Copper, cobalt and palladium functionalized complexes were successfully immobilized onto their respective support materials. A comprehensive study on the characterization of the native silica material as well as the immobilized catalysts (**IC1-IC6**) was conducted and the results thereof described in this chapter. These materials were characterized by a range of solid-state analytical techniques including FT-IR (ATR) spectroscopy, BET surface analysis, ICP-OES spectroscopy, powder X-ray diffraction, scanning electron microscopy (SEM) and transmission electron microscopy (TEM).

Chapter 5: Thesis summary and future recommendations.

In **Chapter four** the evaluation of Schiff base complexes in the oxidation of veratryl alcohol to produce veratrylaldehyde is discussed. The catalytic experiments were carried out in acetonitrile in the presence of oxygen or TBHP as oxidant. All the model catalysts (**MC1-MC3**) were active in the presence of oxygen, with the copper catalyst (**MC1**) exhibiting the best activity and good selectivity towards veratrylaldehyde. In order to deprotonate the substrate, these reactions required the presence of base, NaOH. The use of TBHP as oxidant together with model catalysts (**MC1-MC3**), resulted in a dramatic increase in veratryl alcohol conversion. However, the selectivity of the products was altered by using TBHP. Thus, the use of TBHP resulted in two products forming namely, veratrylaldehyde and veratric acid. The highest conversion of 85 % was obtained for **MC2** (2 mol % catalyst loading) together with TBHP over 6 hours.

The immobilized analogues (**IC1-IC6**) showed promising activity for the oxidation of veratryl alcohol in the presence of TBHP. A dramatic decrease in activity was observed for immobilized catalysts **IC1-IC2** and **IC5-IC6** during the recycling of the catalysts. This could possibly be a result of metal leaching of the complex or due to the loss of catalyst during the recycling process. No activity was observed for the immobilized catalysts when using oxygen and hydrogen peroxide as oxidants. One of the potential limitations of using oxygen as oxidant in these heterogeneous systems is the low diffusion of oxygen from acetonitrile solvent to the encapsulated metal complex. Low activity was also observed when using hydrogen peroxide. This can be attributed to rapid decomposition of H₂O₂ under the reaction conditions used. The immobilized cobalt complexes **IC3** and **IC4** displayed the highest conversion of 65 % and 64 % respectively. Good recyclability was displayed with both catalysts and only a slight drop in activity was noted after each recycle. Thus, promising qualities were demonstrated with these catalysts when applied in the oxidation of veratryl alcohol and therefore, further investigation of these systems is warranted in order to fully ascertain their potential.

5.2 Recommendations for further studies

To advance this study, further understanding of the behaviour of our catalyst systems is needed given the promising results obtained in the oxidation of veratryl alcohol. Performing the catalytic reactions under more basic conditions could potentially increase activity and selectivity. The use of smaller chelating ring systems as ligands such as pyridine-imine or pyridine-triazole could increase electron density on the metal improving the oxidation potential of the metal. One of the main concerns is to understand the nature of the intermediates forming during the catalytic reactions. To gain more insight into this matter would require the use of in-situ analytical techniques which could potentially identify the types of intermediates. These intermediates include: i.) the existence of free alkoxide after proton abstraction in the substrate,

Chapter 5: Thesis summary and future recommendations.

ii.) the metal-alkoxide species (active species), iii.) the metal-hydride species (presence of oxidant) or metal-dihydride species (absence of oxidant), iv.) the peroxo-metal species. ¹H NMR, FT-IR and UV-Vis experiments would definitely be a viable route for detecting the metal-alkoxide, metal-hydride and metal-dihydride species. From our study, diffusion of oxygen is most likely to have an impact on catalyst activity, it would therefore be essential to do experiments at high oxygen pressures. Finally, some detail into the mechanism of these oxidation reactions can definitely be obtained by conducting kinetic studies.